Université de Lille

Doctoral School for Materials, Radiation and Environmental Sciences

Ph.D. THESIS

Novel Photomechanical Thin Films Combining Photochromic Dithienylethene and Thermoplastic Elastomer: Toward a Better Physical and Photochemical Understanding

To obtain the grade of

Doctor

Specialty: Theoretical Chemistry, Physics, Analytical

By

ARROYO DÍAZ Ismael

Presented May 11, 2023 in front of the following dissertation committee:

Aurélie PERRIER	Prof.	Université Paris Cité	Preesident
Moussa Naït-Abdelaziz	Prof.	Université de Lille	Examiner
Clémence ALLAIN	D.R.	Université Paris Saclay	Referee
Arnaud SPANGENBERG	C.R.	Université Haute Alsace	Referee
Michinori TAKESHITA	Prof.	Saga University	Examiner
Stéphane ALOISE	M.d.C.	Université de Lille	Supervisor

Université de Lille

Ecole Doctorale de Sciences de la Matière, du Rayonnement et de l'environnement

Thése de Doctorat

Nouveaux Films Minces Photomécaniques Combinant le Dithiényléthène Photochromique et L'élastomère Thermoplastique: Vers une Meilleure Compréhension Physique et Photochimique

En vue d'obtenir le grade de

Docteur

Spécialité: Chimie Théorique, Physique, Analytique

Présentée par

ARROYO DÍAZ Ismael

Soutenue le 11 Mai 2023 devant la commission d'examen:

Aurélie PERRIER	Prof.	Université Paris Cité	President
Moussa Naït-Abdelaziz	Prof.	Université de Lille	Examinateur
Clémence ALLAIN	D.R.	Université Paris Saclay	Rapportrice
Arnaud SPANGENBERG	C.R.	Université Haute Alsace	Rapporteur
Michinori TAKESHITA	Prof.	Saga University	Examinateur
Stéphane ALOISE	M.d.C.	Université de Lille	Supervisor

ABSTRACT:

This work presents a study on the development of a novel mixed system (photoactuator based on a supramolecular assembly) of photochromic dithienylethene A, and a thermoplastic elastomer poly(ethylene-co-butylene) B, both functionalized with UPy units. The study was conducted in the context of the ANR TACTIL project. The objective was to rationalize the processes involved in bending thin films irradiated with UV and visible light and find the ideal parameters to maximize the photomechanical effect and increase its performance. The study focused on the changes produced in the internal structure of the material, as well as in its morphology and photochemistry when it was subjected to alternating cycles of UV and visible light irradiation. The research combined several techniques to track the thin films' photochemistry, mechanics, and material science (WAXS, SAXS, AFM, SEM, UV-Vis spectrometry, and absorption analysis techniques.). The results showed that the system operates according to the DTE photochromic response, in combination with the mechanical relaxation of the elastomeric matrix. Furthermore, results rationalize the bending toward the light under UV irradiation which is explained in terms of the positive expansion coefficient inside the Timoshenko bimetallic model equation which is a model applied for DTE crystal photoactuators.

KEYSWORDS:

Photochromic, photoactuators, photoswitch, photomechanical effect, thermoplastic elastomer, dithienylethene, ureidopyriminone, supramolecular assembly, bending motion, deformation.

RESUMÉ:

Ce travail présente une étude sur le développement d'un nouveau système mixte (photoactionneur basé sur un assemblage supramoléculaire) de dithiényléthène photochromique A, et d'un élastomère thermoplastique poly(éthylène-co-butylène) B, tous deux fonctionnalisés avec des unités UPy. L'étude a été menée dans le cadre du projet ANR TACTIL. L'objectif était de rationaliser les processus impliqués dans la flexion de films minces irradiés par la lumière UV et visible et de trouver les paramètres idéaux pour maximiser l'effet photomécanique et augmenter ses performances. L'étude s'est concentrée sur les changements produits dans la structure interne du matériau, ainsi que dans sa morphologie et sa photochimie, lorsqu'il est exposé à des cycles alternés d'irradiation aux UV et à la lumière visible. La recherche a combiné plusieurs techniques pour suivre la photochimie, la mécanique et la science des matériaux des films minces (WAXS, SAXS, AFM, SEM, spectrométrie UV-Vis et techniques d'analyse d'absorption). Les résultats ont montré que le système fonctionne suivant la réponse photochromique DTE, en combinaison avec la relaxation mécanique de la matrice élastomère. En outre, les résultats rationalisent la déformation en direction de la lumière sous irradiation UV, qui est expliquée en termes de coefficient d'expansion positif dans l'équation du modèle bimétallique de Timoshenko, qui est un modèle appliqué aux photoactuateurs en cristaux DTE.

MOTS-CLÉS:

Photochromie, photoactuateurs, interrupteurs photosensibles, effet photomécanique, élastomère thermoplastique, dithiényléthène, uréidopyriminone, assemblage supramoléculaire, mouvement de flexion, déformation.

AGRADECIMIENTOS

Hoy, con profunda gratitud y emoción, quiero expresar mi más sincero agradecimiento al Dr Stephane Aloïse. por su invaluable apoyo y guía a lo largo de mi arduo camino hacia la finalización de esta tesis de doctorado. Su presencia como supervisor ha sido de una importancia significativa tanto en mi desarrollo profesional como personal.

Desde el primer día que nos conocimos, pude percibir su pasión inigualable por la investigación y su compromiso incansable para impulsar el conocimiento en nuestro campo. Su sabiduría, experiencia y dedicación me han inspirado a alcanzar altas metas y a superar desafíos en este viaje académico. Sus valiosos consejos, sus críticas constructivas y su capacidad para motivarme han sido fundamentales para la realización de este logro.

Además, quisiera extender mi agradecimiento al personal a los laboratorios LASIRE y UMET. Su colaboración y disposición para compartir conocimientos y recursos han enriquecido mi investigación y han contribuido al éxito de este proyecto. Su profesionalismo y amabilidad han creado un entorno de trabajo excepcional en el que he tenido la oportunidad de crecer como investigador.

No puedo pasar por alto el apoyo incondicional de mis padres, Maria del Rosario Diaz e Ildefonso Arroyo. Su amor, aliento y sacrificio han sido pilares fundamentales en mi vida. Gracias a su constante apoyo moral y emocional, he podido perseverar en los momentos más desafiantes de este viaje académico. Su confianza en mí y su ejemplo de perseverancia me han fortalecido y me han impulsado a dar lo mejor de mí en cada etapa de este proceso.

Además, me gustaría agradecer sinceramente a mis amigos, Angie y Clemente, Marco, Rebeca y Alejandro, así como todo al grupo de Mexicanos y Latinos que viven muy lejos de su país de origen y luchan cada día para alcanzar sus metas. Su apoyo inquebrantable, sus palabras de aliento y su comprensión durante los altibajos de este viaje académico han sido un bálsamo para mi espíritu. Su compañerismo y la capacidad de compartir tanto los triunfos como los desafíos han hecho que este camino sea más llevadero y significativo.

Finalmente, deseo expresar mi agradecimiento a ANR y Region Hauts de France por los recursos económicos otorgados, los cuales han sido cruciales para llevar a cabo mi investigación. Su inversión en la ciencia y la educación ha permitido que jóvenes investigadores como yo puedan perseguir sus sueños y contribuir al avance del conocimiento en nuestra sociedad.

En resumen, este logro no hubiera sido posible sin su apoyo, orientación y confianza en mí. Agradezco sinceramente a cada una de las personas que mencioné, ya que han dejado una huella imborrable en mi vida y en mi carrera académica. Este hito marca el inicio de una nueva etapa en mi vida, y me siento profundamente agradecido por haber tenido la oportunidad de contar con su valiosa presencia y respaldo.

Dr. Ismael Arroyo

ACKNOWLEDGMENTS

REMERCIEMENTS

Aujourd'hui, c'est avec une profonde gratitude et une grande émotion que je voudrais exprimer mes sincères remerciements au Dr Stéphane Aloïse pour son soutien et ses conseils inestimables tout au long de mon parcours ardu vers l'achèvement de cette thèse de doctorat. Sa présence en tant que superviseur a été d'une importance significative pour mon développement professionnel et personnel.

Dès le premier jour de notre rencontre, j'ai pu sentir sa passion inégalée pour la recherche et son engagement infatigable à faire progresser les connaissances dans notre domaine. Sa sagesse, son expérience et son dévouement m'ont incité à atteindre des objectifs élevés et à relever des défis au cours de mon parcours universitaire. Ses précieux conseils, ses critiques constructives et sa capacité à me motiver ont joué un rôle déterminant dans la réalisation de ce projet.

Je tiens également à remercier le personnel des laboratoires LASIRE et UMET. Leur collaboration et leur volonté de partager leurs connaissances et leurs ressources ont enrichi ma recherche et contribué à la réussite de ce projet. Leur professionnalisme et leur gentillesse ont créé un environnement de travail exceptionnel dans lequel j'ai eu l'occasion d'évoluer en tant que chercheur.

Je ne saurais passer sous silence le soutien inconditionnel de mes parents, Maria del Rosario Diaz et Ildefonso Arroyo. Leur amour, leurs encouragements et leurs sacrifices ont été des piliers fondamentaux dans ma vie. Grâce à leur soutien moral et émotionnel constant, j'ai pu persévérer dans les moments les plus difficiles de ce parcours académique. Votre confiance en moi et votre exemple de persévérance m'ont renforcé et m'ont poussé à faire de mon mieux à chaque étape de ce processus.

En outre, je voudrais remercier sincèrement mes amis, Angie et Clemente, Marco, Rebeca et Alejandro, ainsi que tout le groupe de Mexicains et de Latinos qui vivent loin de leur pays d'origine et luttent chaque jour pour atteindre leurs objectifs. Votre soutien indéfectible, vos mots d'encouragement et votre compréhension au cours des hauts et des bas de ce voyage universitaire ont été un baume pour mon esprit. Leur compagnie et leur capacité à partager les triomphes et les défis ont rendu ce voyage plus supportable et plus significatif.

Enfin, je voudrais remercier l'ANR et la Région Hauts de France pour les ressources financières qu'elles ont fournies et qui ont été cruciales pour ma recherche. Leur investissement dans la science et l'éducation a permis à de jeunes chercheurs comme moi de poursuivre leurs rêves et de contribuer à l'avancement des connaissances dans notre société.

En bref, cette réalisation n'aurait pas été possible sans leur soutien, leurs conseils et la confiance qu'ils m'ont accordée. Je remercie sincèrement chacune des personnes que j'ai mentionnées, car elles ont laissé une marque indélébile sur ma vie et ma carrière universitaire. Ce jalon marque le début d'une nouvelle étape dans ma vie, et je suis profondément reconnaissante d'avoir eu l'occasion de compter sur leur présence et leur soutien précieux.

Dr. Ismael Arroyo

ABREVIATIONS

Azo	Azobenzene
AZOs	Azobenzenes
CF	Closed Form
DAEs	Diarylethenes
DTE or DTEcore	1,2-bis(2,4-dimethyl-5-phenyl-3 thienyl) perfluorocyclopentane
DTEs	Dithienylethenes
DTE-UPy	1,2-bis(2,4-dimethyl-5-phenyl-3 thienyl) perfluorocyclopentane Functionalized UPy
LCE	Liquid crystal elastomer
NMR	Nuclear Magnetic Resonance
OF	Open Form
PEB	poly(ethylene-butylenes) diol
PEB-UPy	Telechelic poly(ethylene-butylenes) functionalized UPy
PME	Photomechanical Effect
PSS	Photo Stationary State
SAXS	Small angle X-ray scattering
SEM	Scanning electron microscopy
Tg	Glass transition temperature
Tm	Melting temperature
TPEs	Thermoplastic elastomers
UPy	2-ureido-4[1H]-pyrimidinone
WAXS	Wide angle X-ray scattering

x

CHAPTER I

Novel Organic Photoactuators Using Photochromic Units: Context and Objectives

I. Introduction

Undoubtedly, the generation of new smart materials will be the main pillar in the development of new technologies. In particular, smart materials which manifest a deformation under the stimulus of an external force (external stimulus - mechanical energy) such as heat [1], magnetic field [2], electric field [3], humidity variation [4], and light [5], [6] are of particular interest for the development of new technologies in the fields of biomedicine [7], soft robotics [8], molecular machines [9], military (camouflage) and even in the fashion industry. Within this context, photo-responsive materials, or organic photo-actuating materials (convert light energy into mechanical energy) have a great advantage compared to other material stimuli since a light stimulus can be modified in direction, magnitude, intensity, wavelength, and polarization [10]. It also gives the possibility to control an organic photo actuator material without the need to use wires.

Clearly, because photomechanical materials are a vast subject, some clarifications about terminology are necessary and the Figure 1 will be helpful to understand the general context of this manuscript. Photomechanical materials can be classified according to their actuation mechanisms:

- Photoelectric processes which occur mostly for inorganic solids [11–13]
- Photothermal processes for dye containing system [10] and recently enhanced in nanocomposites with nanoparticles and carbons nanotubes (CNT) [14].
- Photochemical systems involving an organic photoswitch embedded into an elastomeric/polymeric environment. This last class of photochemical materials get the advantage to be reversible thanks to photochromic actives units acting as an ON/OFF molecular switch (see below). [15], [16]
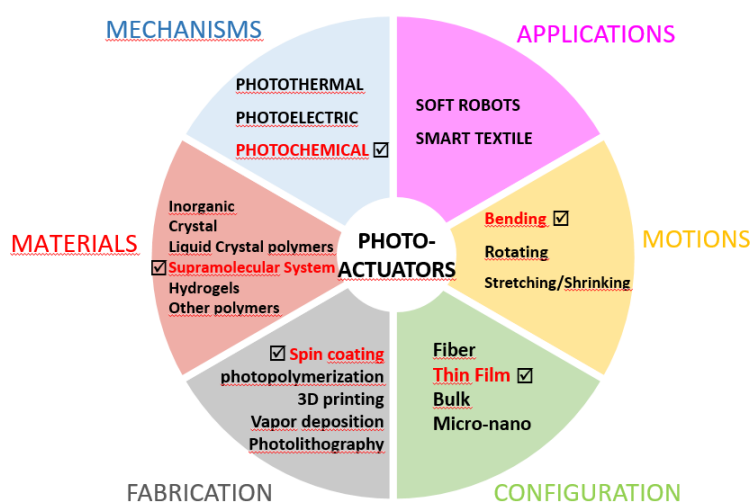
Figure 1. The basic concepts around photoactuators science. The symbol ✓ indicated the fields related with the present manuscript.

The scope of the present manuscript is to elaborate novel organic photoactuators based solely on pure photochemical processes excluding participation of any photothermal or photoelectric effect.

According to the configuration, photoresponsive materials can be classified into (thin) films, fibers, bulk, fluids, and micro-nanostructured actuators, and can generate rotating actuation, shrinking/stretching or bending/flattening under light illumination [16]. We will be interested by the latter case. The different type of materials used for photoactuators will be enumerate in the bibliographical section below.

Introduction of a photoactive units inside a thermoplastic is the key to our work, reason why we will introduce in the following both concept of photochromism and thermoplastic elastomer before the bibliographic section.

I.A. Basic concepts of Photochromism

I.A.1. Generality

Photochromism is the reversible photoinduced process between an isomer A and a second isomer B, both having different absorption spectra [17]. In consequence, a color change takes place during the phototransformation between states A and B, as shown in Figure 2a with the typical absorption spectra and photochromic solution pictures. Starting from thermodynamically stable form A (uncolored), irradiation at the wavelength λ_A (typically maximum of absorbance) induces the photochromic reaction $A \rightarrow B$ into the new colored form B (blue in this example). Then, irradiating the isomer B with the wavelength λ_B induced the back-reaction $B \rightarrow A$. Actually, this back reaction can take place thermally (Type T) and/or photo-chemically (Type P).
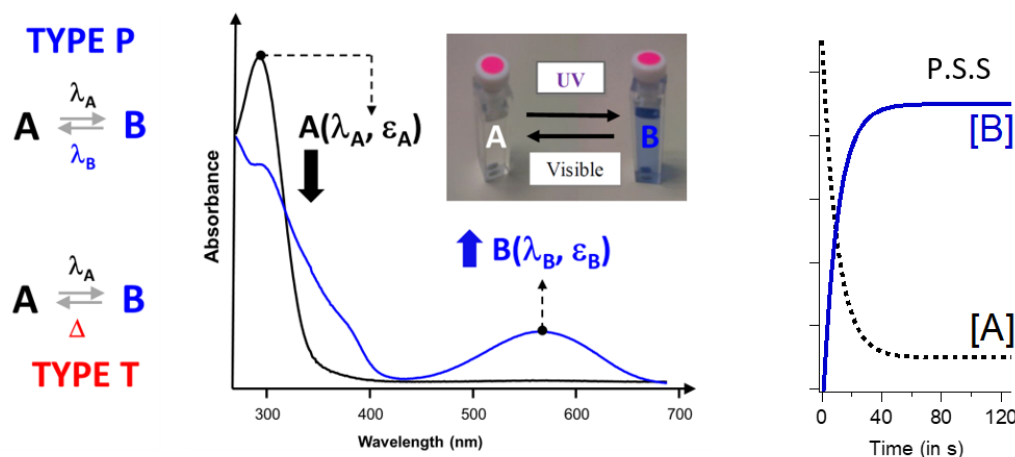
Figure 2. a) Scheme of definitions of photochromism where there is a isomers T-type and P-type and photochromic reactions and absorption. b) Maximum absorbance point, Photo-Stationary State (PSS).

3

Quantum yields. To characterize a photochromic units, apart the absorption parameters (extinction coefficient ε, position of maximum absorbance λ) for both A and B isomers, the quantum yields must be defined

$$\phi_{A \to B} = \frac{\#\ molecules\ B\ photoinduced}{\#\ photons\ absorbed\ by\ A} \tag{1}$$

$$\phi_{B \to A} = \frac{\#\ molecules\ A\ photoinduced}{\#\ photons\ absorbed\ by\ B} \tag{2}$$

Fatigue. In photochromic materials, fatigue refers to the loss of reversibility by processes such as photodegradation, photobleaching, photooxidation, and other side reactions. All photochromic suffer fatigue to some extent, and its rate is strongly dependent on the activating light and the conditions of the sample. A targeted performance for photochromic molecules is therefore a good fatigue resistance.

Photo-Stationary State. For UV excitation, both processes A→B and B→A can be induced with different efficiency. Because converted molecules within both processes will reach an equilibrium denoted Photo-Stationary State (PSS), it is important to irradiate a period long enough to well characterized the PSS asymptotic behavior (see figure 2b). Note that for Visible irradiation, only the conformer B absorbs the light.

I.A.2. Dithienylethene vs Azobenzene

A photochromic family [18] is related with the photoinduced chemical reaction involved. with few examples give below:

- intramolecular hydrogen transfer (quinolone-acetone)
- dissociation processes (spironaphtoxazine)
- pericyclic reactions (fulgide, diarylethene).
- cis-trans isomerization (azobenzene)

The interested reader can find an exhaustive list on dedicated reviews.

Azobenzenes. As we will see below, the photochromic molecule most used in the development of photoactuators are azobenzene and its derivatives (AZOs), because one of the great advantages of AZOs is the large dimensional change induced by light between isomers trans (9Å) and cis (5.5 Å) through N=N bond isomerization (Figure 3), the basic photochromic reaction for AZOs.
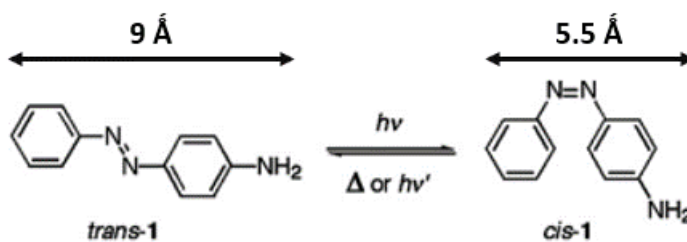
Figure 3. Photochromism of 4-aminoazobenzene.

Light irradiation transforms the thermally unstable trans-isomer into the cis-isomer, whereas the opposite reaction is thermally spontaneous (T-type molecules), Note however that the back reaction can be enhanced by light as well.

Dithienylethenes Diarylethene (DAEs) and more specifically Dithienylethenes[1] (DTEs) have gained great popularity in photoactuator research for its bistability (P-Type photochromes) in contrast to AZOs [19], Good quantum yields, high fatigue resistance, and a fast photochromic response [20–22]. A perfluorocyclopentene bridge is typically substituted for the C=C to block cis-trans isomerization [23], [24]. In 1988 Irie et al. reported diarylethene's photochromism for the first time [25], based on pericyclic reaction [20]. The open form isomer (**OF**) is the most stable isomer. According to the electro-cyclization reaction of a 1,3,5-hexatriene unit, which involves 6 atoms and 3 double bonds (π pairs), the photochromic reaction – also denoted photo-cyclization– consists of the ring-closing of OF to result in a close form (**CF**). Then, the back reaction, i.e. the ring opening induced by the light

---

[1] When aryl nuclei are thiophenes

is denoted photoreversion. In general, for most of the DTEs, the photocyclization is induced by an UV light while the photoreversion is induced by ta visible-range radiation.
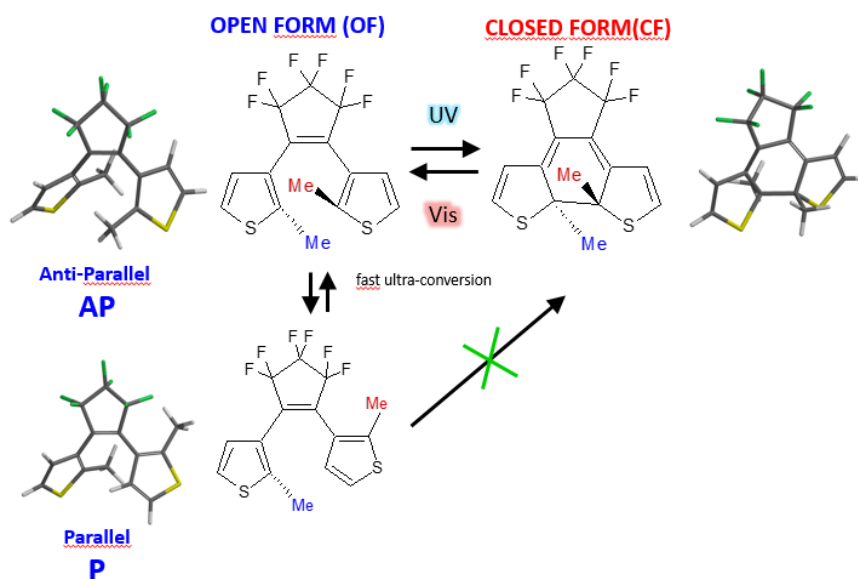
Figure 4. Photocyclization (UV) /photoreversion (Vis) between Open Form and Closed Form. Between OF conformers, Antiparallel (AP) is photoactive, Parallel (P) conformer is not.

The OF has two stable conformations, as shown in Figure 4.

- **Anti-parallel conformer** (AP) having a C2 symmetry axis where both aryl groups on either side of the central double bond plane. Because of good position of the reactive carbons, this conformer is photoactive

- **Parallel conformer** (P) having a plane of symmetry with the aryl groups in mirror symmetry. The two reactive carbons being too far, this conformer is not photochromic.

The portions of the photoreactive AP and photoinactive P conformers are nearly equal in solution [20]. However, the AP proportions can be elevated in solid state when the DTEs are confined [26]. In contrast, whether in solution or in the solid state, the parallel conformation remains unreactive. Additionally, single crystals can undergo a photochromic reaction with an effective photocyclization quantum yield

6

nearly unit when the DTEs molecules are in their pure AP conformation and the distance between the reactive carbons is less than 4.2 Å.

I.B. Basic Concepts of Polymers

I.B.1. Molecular configuration and microstructures

There are several molecular configurations that can be observed for polymers. The basic configurations are as follows (Figure 5).

- **Linear Polymers** consist of long chain-like structures where repeating units are joined together end to end (ex: polyethylene). The long linear chains are flexible, where van der Waals and hydrogen bonding may occur between polymer chains while in proximity – leading to chain entanglement.
- **Branched Polymers** feature short side branched chains that are connected to the longer polymeric chains. The packing efficiency of the polymer with side branching is reduced, lowering the polymer density.
- **Crosslinked Polymers** present linear chains with crosslinks, i.e. covalent bonding of smaller molecules acting as bridges between them. The crosslinking process often takes place through a non-reversible chemical reaction process (curing). Crosslink formation characterizes thermoset polymers.
- **Networked polymers** feature monomer units with three active covalent bonds and have the ability to form interconnected three-dimensional network configurations. Networked polymers include highly crosslinked polymers.

Polymers can exhibit two basic morphologies (structures), or a combination of the two, when "frozen" in their solid state. These basic morphologies are Crystalline, (Periodic 3-D repeating array of molecules folded up into densely packed regions), Amorphous (Randomly coiled chains without structure and no repeating array) or Semi-Crystalline (combination of both).

7
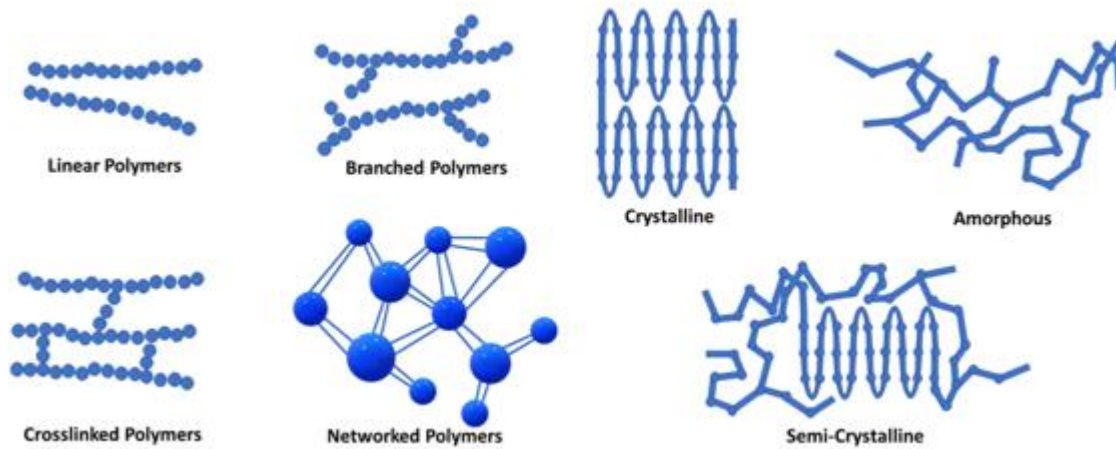
Figure 5. Molecular configuration and microstructures of polymers.

Taking into account configuration and microstructure, polymers can be denominated into three categories based on the strength of intermolecular forces present in polymers (Figure 6):
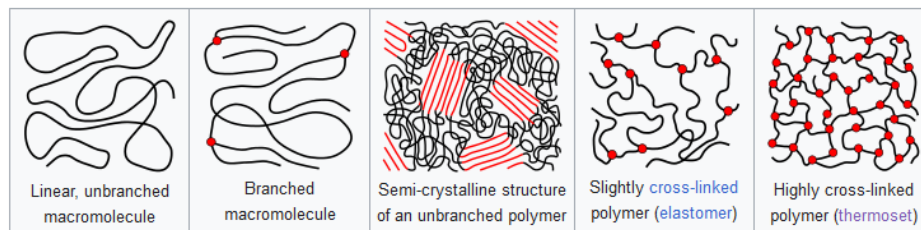
Figure 6. Various kinds of polymers.

- **Thermoplastics:** The relatively weak intermolecular forces cause the material to soften when exposed to heat and then returns when cooled to its original condition. Thermoplastics are the bulk of linear and slightly branched polymers.

- **Thermosets:** Thermosets are usually three-dimensional networked polymers in which polymer chains have a high degree of cross-linking. The cross linking limits the chains ' movement and contributes to a solid material that makes thermosets strong and robust (Heating cannot reshape the thermosets).

8

- **Elastomers:** Elastomers are rubbery polymers that can be extended easily to their unstretched length many times and that quickly return to their original dimensions when the pressure is released. Elastomers are cross-linked but have a low density of cross-link. An elastomer must have a glass transition temperature[2] T_g below room temperature (glassy otherwise) and a low crystallinity. By consequence, an elastomer is a polymer with viscoelasticity (i.e. both viscosity and elasticity) and with weak intermolecular forces, generally low Young's modulus[3] (E) and high failure strain compared with other materials. At ambient temperatures, such rubbers are thus relatively compliant (E ≈ 3 MPa) and deformable.

I.B.2. Thermoplastic Elastomer

Thermoplastic elastomers (TPE), are a class of copolymers (or a physical mix of polymers) that consist of materials with both thermoplastic and elastomeric properties. While most elastomers are thermosets, thermoplastics are in contrast relatively easy to use in manufacturing, for example, by injection molding. Thermoplastic elastomers show advantages typical of both rubbery materials and plastic materials. The benefit of using thermoplastic elastomers is the ability to stretch to moderate elongations and return to its near original shape creating a longer life and better physical range than other materials. The principal difference between thermoset elastomers and thermoplastic elastomers is the type of cross-linking bond in their structures. In fact, crosslinking is a critical structural factor which imparts high elastic properties.

---

[2] The glass transition temperature (T_g) is a phenomenon of amorphous polymers. At this temperature, polymers undergo a transition from glassy to rubbery state. Tg is an important feature of polymer behavior. It marks a region of dramatic changes in the physical and mechanical properties: i) **below T_g**: due to lack of mobility, the polymers are hard and brittle like glass; ii) **Above T_g**: Due to some mobility, the polymers are soft and flexible like rubber.

[3] **Young's modulus** is a mechanical property that measures the tensile or compressive stiffness of a solid material when the force is applied lengthwise. It quantifies the relationship between tensile/compressive stress σ (force per unit area) and axial strain ε (proportional deformation) in the linear elastic region of a material and is determined using the formula:

$$E = \frac{\sigma}{\varepsilon}$$

Young's moduli are typically so large that they are expressed not in pascals but in gigapascals (GPa).

The most common principle of photo-actuation of chemically cross-linked elastomers and/or TPEs is based on the presence of soft segments responsible for shape changes under illumination, and hard segments responsible for returning the material to its initial stage before illumination [27], [28]. We will pay attention to this aspect later in the document.

I.C. Survey of organic photo-actuators

As already said, the exhaustive list of possible photo-actuators is far beyond the scope of this manuscript, and we invite the interested reader to refer to recent book or review [15]. Throughout this section, we will focus mainly on DTEs and AZOs compounds.

I.C.1. Dynamic single crystals

I.C.1.1. Macroscopic observation

DTEs. Single crystals made from photoresponsive materials have shown photomechanical responses [18], [29], [30], those crystal being classify as "dynamic crystals". Several chemical systems have been investigated and recent reviews give an exhaustive list of such dynamics crystals with variety of motions [31–34]. In the following, we will focus our attention on DTEs and AZOs based systems with a special emphasize on the bending/flattening effect.

More than fifteen years ago, Irie et al. has first brought evidence for the reversible shrinkage of 7% of the volume of a losange shape crystal formed by derivatives of DTEs [35]. This reversible shrinkage was due to the photocyclization-photoreversion reaction of the DTEs upon irradiation with UV /visible light (Figure 7a). This photomechanical effect (PME) was rationalized in term of crystallographic unit cell parameters changing with light.

Since then, bending/flattening photoactuation have been observed for co-crystallization of two DTE (See Figure 7b) [36]. A rodlike crystal was curling

toward the UV light direction and going backward under visible irradiation with a very high speed displacement (56 µm.s^{-1}) . Repeatabilty of the photoactuating process was excellent (more than 100 cycles) and small crystals were used to bring about gearwheel rotation as illustration of µ-micrometrique machines. X-ray analysis before and after irradiation (identifying key photosensitive cell parameters) have shown that less that 10% conversion of the OF molecules (rather at the surface of the crystal than inside the bulk) is enough to get the PME.

In the same vain, Morimoto etal. has reported PME for a cocrystalization of a DTE with a non photochromic unit (perfluoronaphtalene) (Figure 7c) with a high speed displacement (59 µm.s^{-1}) for UV and much slow for the visible (5 µm.s^{-1}). They demonster the ability for this molecular canteliver to lift metal balls. Indeed, the maximum stress generated by UV irradiation was estimated to be 44 MPa, which is 100 times larger than that of muscles ($\sim$0.3 MPa) [37].

AZOs. Few years after DTEs crystals, Kohima etal. have reported trans-4-aminoazobenene crystals dispalying a bending motion ($\sim$5 µm.s^{-1}) under UV light with a slower themal relaxation when the light is turn OFF (Type T photochromic molecule). We note that AZOs are slower to compare to DTEs crystals. However, It has been found that the back motion is speed up with a use of visible light. Note that for the two examples of the Figure 7d , the directions of bending /flatettening upon alternate UV/vis irradiaton follow the same trend.
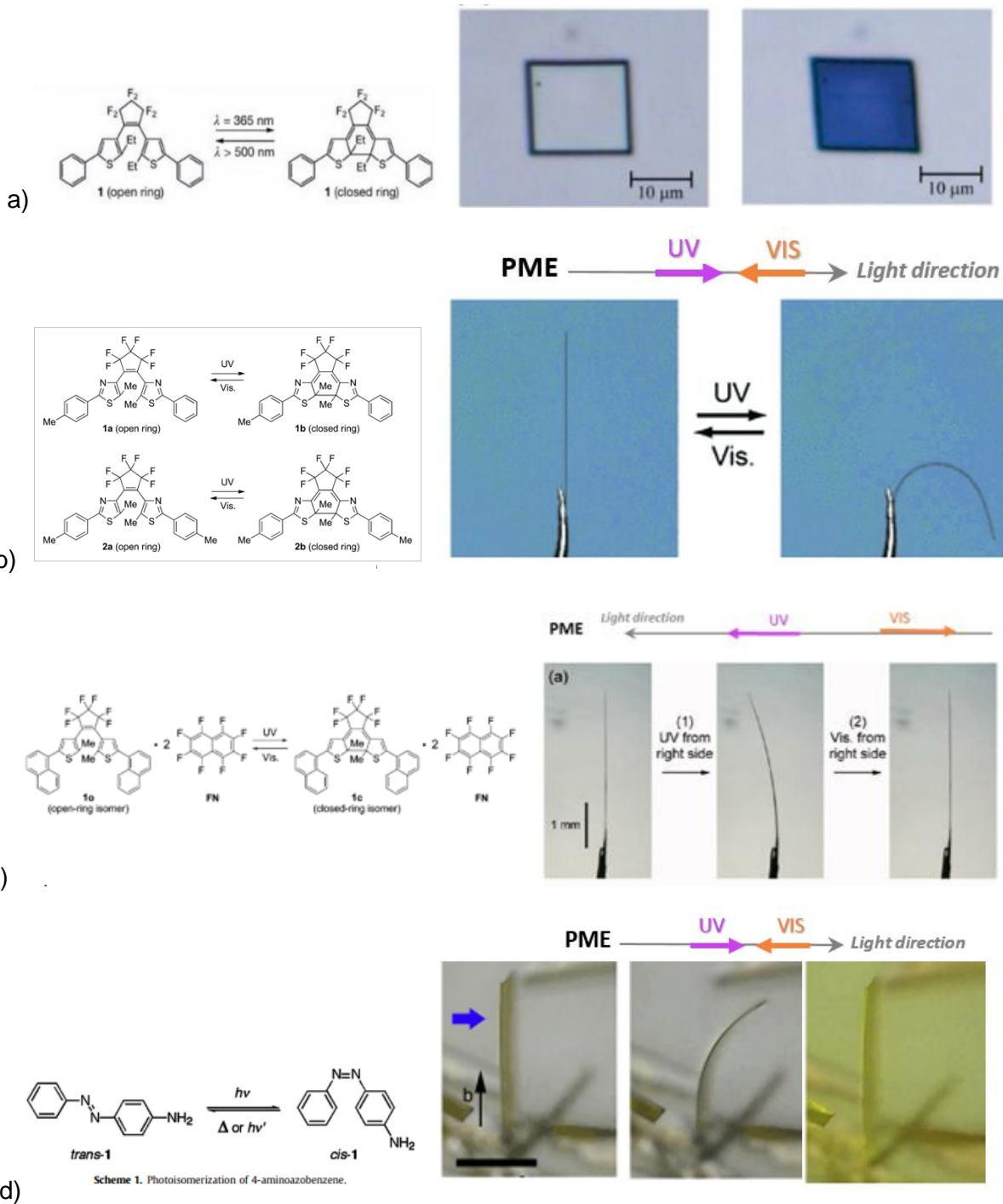
Figure 7. a) Diarylethene molecules undergo a reversible ring-opening and ring-closing isomerization, driving a square single crystal to show reversible deformation under UV and visible light irradiation [38]. b) Reversible curling to a hairpin shape upon irradiation with UV light (crystal length: 3.0 mm). The crystal kept the crystalline state even after the curling and returned to the original straight shape upon irradiation with visible light. [36] c) reversible bending for cocrystal DTE/perfluoronahtalene under UV/Visible irradiations, and d) similar PME for 4-aminoazobenzene monocrystal [34].

I.C.1.2. PME rationalization (Theoretical models)

Beyond the phenomenological observation, the fundamental question was the multiscale relationship between microscopic photochemical reaction and macroscopic deformation. In 2017, Kobatake and collaborators have corroborated the bending behavior of various DTE crystals (molecules 1 and 2 presented in Figure 8a) with crystallographic results. First, the PME is related with the photoisomerization from OF to CF upon UV irradiation causes either contraction or expansion along the long crystallographic axis (Figure 8c), which results in bending of the crystal. Note that when UV light is OFF, the crystals curvature is stable. Then, the bent crystals can return to their initial straight shape upon irradiation with visible light. The opposite bending directions for the two molecules are rationalized in term of kind of molecular packing: unlike molecule 2, molecule 1 presents herringbone packing[4] and presence or lack of this **structural feature** at microscopic level will lead the macroscopic bending forward or backward to light direction. Furthermore, it has been shown than the initial bending velocity is directly proportional to the irradiation Power (Figure 8d) and the crystal thickness.

Theoretical models. Kobatake have successfully described the dependence of the photomechanical response of DTEs crystals using the bimetallic Timoshenko's equation (3), [31], [39]:

$$\frac{1}{R} = \frac{\alpha_2 - \alpha_1}{h_2} \left(\frac{6mn(1+m)}{1 + 4mn + 6m^2n + 4m^3n + m^4n^2} \right) \tag{3}$$

Where $m = h_1/h_2$ and $n = E_1/E_2$ are the Moduli Young ratio, R is the curvature radius, h_1 and h_2 are the layer thickness and, α_1 and α_2 are the actuation strains. The actuation stress is the coefficient of expansion or contraction of the first layer under UV radiation. In the non-photoreactive layer, the actuation strain α_1 a is always zero because the layer cannot expand or contract, Figure 9.

---

[4] Herrigbone packing:

When the sample bends away from ultraviolet light, the value of α_2 is the coefficient of expansion. In opposition, α_2 is the coefficient of contraction when the crystal is bent towards ultraviolet light. Furthermore, the assumption is made that the Young's modulus E_1 is the same as E_2 because only a small percentage of diarylethene molecules in the crystal are converted from the ring-opened to the ring-closed isomer in the initial stage of bending. As a result, the Timoshenko equation becomes:

$$\frac{1}{R} = \frac{\alpha_2}{h_2} \left(\frac{6m(1+m)}{1 + 4m + 6m^2 + 4m^3 + m^4} \right) \tag{4}$$

In this model, h_2 plays an important role in dictating the extent of the bending reaction: when h_2 is very small relative to the thickness of the crystal, the crystal cannot bend significantly. However, the crystal can be greatly bent when h_2 is approximately half the thickness of the crystal.

The structural features will influence the sign of the curvature and the amplitude of the PME: the higher α_2, the stronger the bending. In contrast, the velocity of the bending depends solely on the gradient of the photoconverted form through the variable $m = h_1/h_2$.
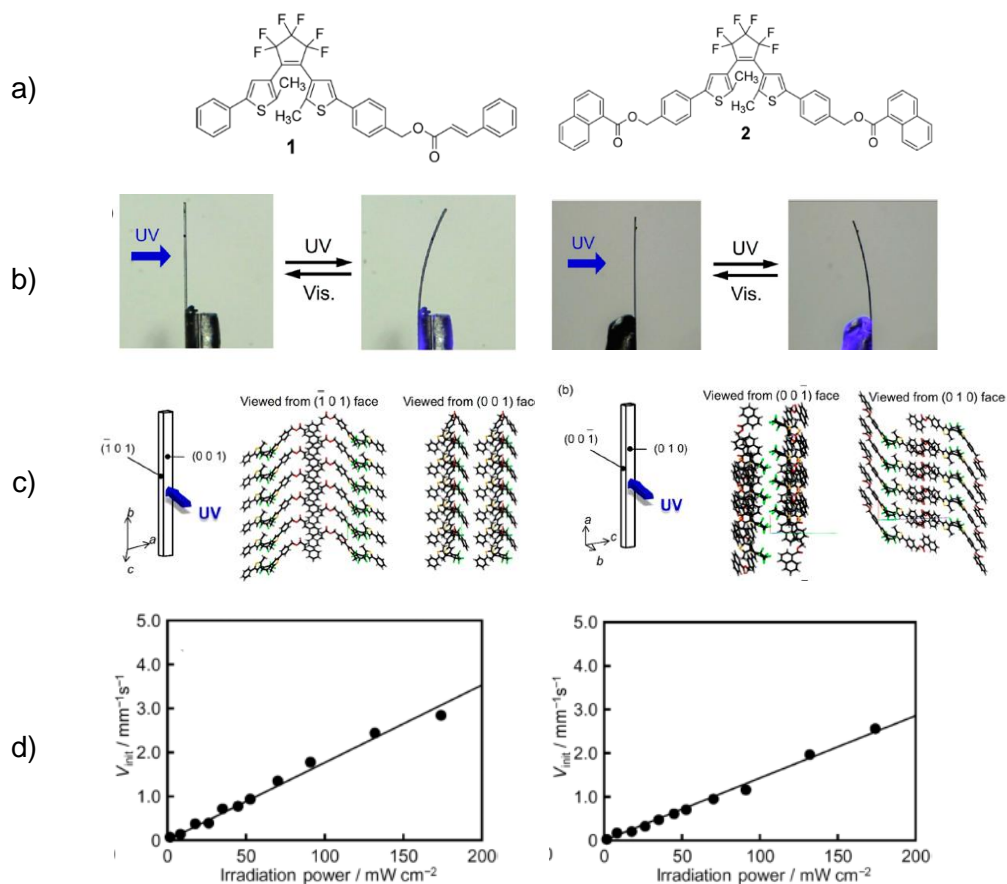
Figure 8. Results from the paper of Hirano et al. Two DTE molecules 1 and 2 (a), the respective pictures of monocrystal bending (b) the respective molecular packing representation for the illuminated crystallography planes(c) the respective initial velocity bending function of light power [40].
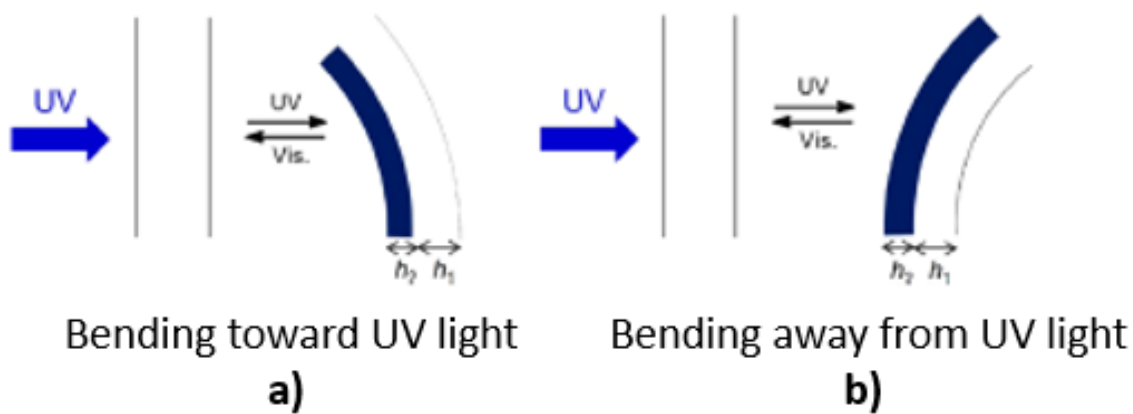
Figure 9. schema of the Timoshenko bimetal model in case of a) bending toward UV light and b) bending away from UV light.

I.C.2. Preliminary approaches for polymeric photoactuators

During the 1960s, initial research was conducted on photomechanical effects in polymers. These initial studies focused on incorporating photochromic molecules into polymeric or crystalline materials. The most common method of sensitizing polymeric materials to light involves functionalizing them with azobenzene [14]. Considering bulk polymeric systems, the very first example of photomechanical effect was reported for a nylon fiber dyed with azobenzene and displaying 0.1% magnitude shrinking upon irradiation [41].

Then, azobenzene-functionalized polyimide films were displaying 0.5% deformation [42]. Little improvements were achieved with polymers containing photochromic moieties in cross-links or main chains, the magnitude of the photoresponse remaining smaller than 1% [43]. However, the PME were very moderate, and improvements were necessary.

I.C.3. The Liquid Crystal Elastomer (LCE)

To gain in efficiency, a simple idea was to align and orientate the photoresponsive units inside the polymeric matrix. Taking benefit of the alignment and orientation of Liquid Crystalline[5] (LC) systems, it become possible to amplify small changes at the molecular level to yield large macroscopic deformation. Then, combining structural advantages of LC with large geometrical changes under photoisomerization of AZOs was an idea extensively investigated throughout the literature. Some recent reviews give an exhaustive list, here we present only some representative examples.

---

[5] Liquid crystal (LC) is a state of matter whose properties are between those of conventional liquids and those of solid crystals. For example, a liquid crystal may flow like a liquid, but its molecules may be oriented in a crystal-like way.

I.C.3.1. Hegemonic use of AZOs-LCE

More than twenty years ago, thanks to the development of the cross-linked liquid-crystalline elastomers (LCEs) [44] and their mesogens alignment requirement (Figure 10) (electric field, magnetic field, external stretching, appropriate glass cells coatings…etc) [37], improvements of the photomechanical effects were achieved. Indeed, since 2001, professor Finkelmann was a precursor to afford new functionality to well-known thermomechanical LCEs [45] by enriching mesogen units with azobenzene moieties [46].
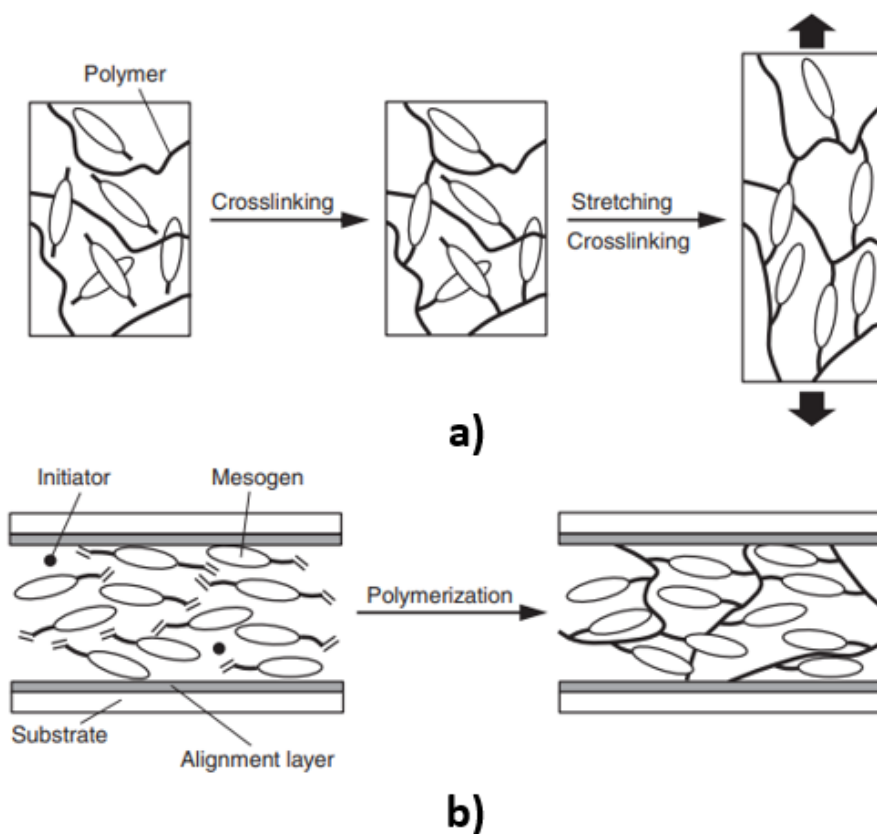
Figure 10. Preparation methods of cross-linked LCE (up) a) two-step cross-linking b) *In situ* polymerization.

Monodomain films with homogeneously aligned mesogens were prepared by a two-step cross-linking method follow by photo-polymerization, the overall process being illustrated in Figure 11a (Note that the preparation of LCE-AZOs systems is

not straightforward). The PME for Finkelmann systems was displaying a drastic improvement compared to the past with a 20% contraction along the alignment direction under UV irradiation (Figure 11a) After the UV was turn off, the sample returned to the initial shape through eiher thermal cis-trans isomerization or visible light irradiation. The molecular rationalization of the PME taking into account the mesogen alignment (disordering) upon UV or Visible light is illustrated in Figure 11c.

Further improvement was obtained by Ikeda's group by the synthesis of polydomain LCE for which both thermal polymerization LC monomer and crosslinker are based on azobenzene derivatives. Consequently, due to high concentration of Azo units, light penetration is restricted to the surface which induce a bending or flattening behavior of the thin film under UV or Visible irradiation respectively [47–49]. To go further, for polydomains materials this group has demonstrated a possible control of the deflection of the films taking advantage of the linearized polarized light (Figure 11b) inducing the photo alignment of the mesogen leaded by the polarization vector.[47] To bring some additional resistivity to the final photoactuator, they have investigated composite systems combining Azo based CLCPs with flexible plastic sheet (polyethylene). By this way, they were able to elaborate a light driven motors (1 LCE-AZO composite strip and two pulleys) that is to date one of the most impressive examples of plastic machine working not with electrical wires but UV and Visible light instead. (Figure 11d) [50].

More recently, Ikeda and co-workers have investigated photomobile films with glassy nature (elaboration process with $T > T_g$) made from a thermoplastic polyurethane (PU) LCE containing AZOs moieties, the system being stabilized by the formation of physical cross-links through hydrogen bonding interactions. The films showed reversible bending-flattening movements which could be repeated for 100 cycles. The PME effect, illustrated backward to the UV light and toward to visible light, Figure 12c [51]. Note that displacement speed for UV $\sim\sim 15\,\mu ms^{-1}$ (lower tan for DTEs crystals) is clearly higher than for Visible $\sim 2\,\mu ms^{-1}$ and such performances are achieved for high power LED intensity.
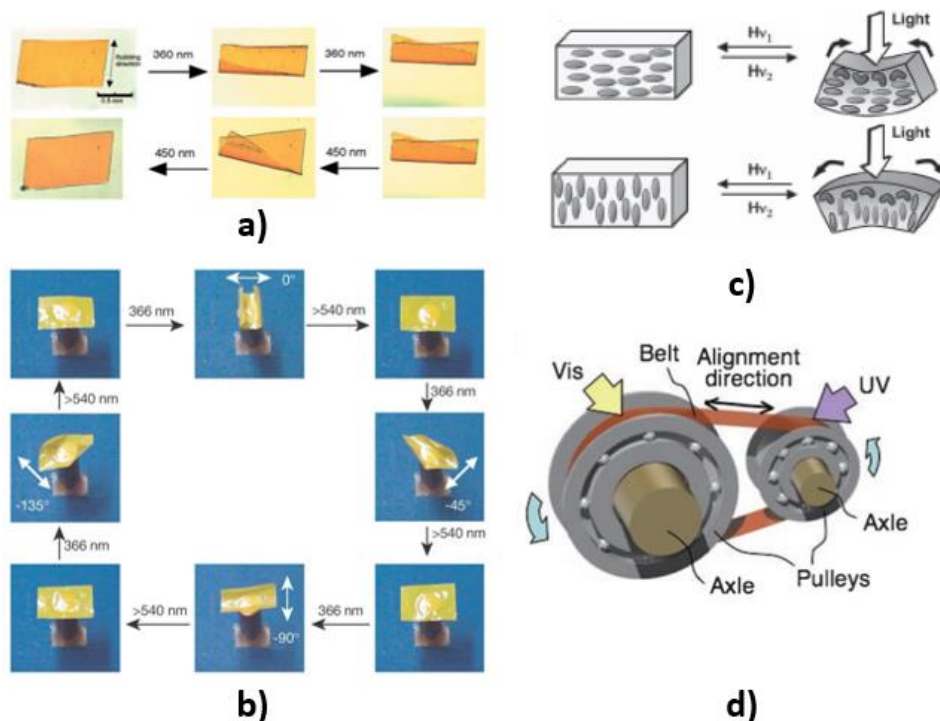
Figure 11. a) Bending of a monodomain film [52]. (b) Direction-selective bending of a polydomain film by linearly polarized light [10]. (c) Photomechanical effect in LCEs: the homogenous alignment of LCs produces bending towards the actinic light, whereas the homeotropic alignment of LCs causes bending away from the light source [21]. d) Schematic illustration of a light-driven plastic motor system used in this study, showing the relationship between light irradiation positions and a rotation direction [50].
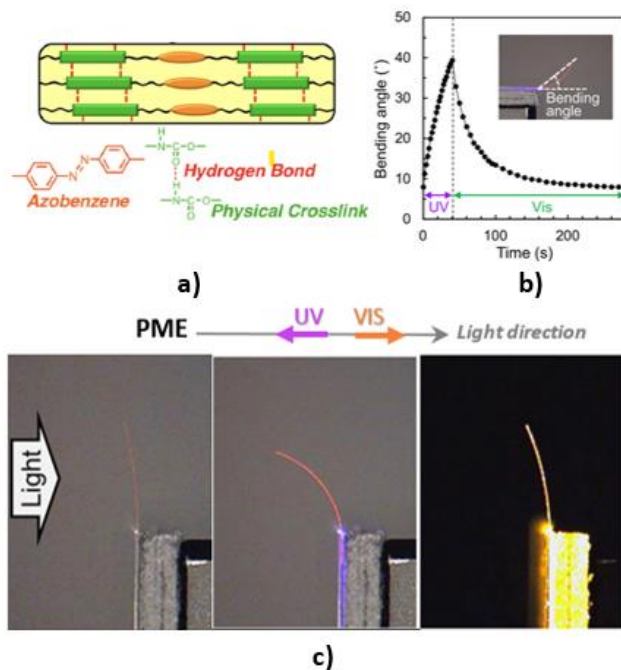
Figure 12. a) illustration of PU-AZOs LCE system; b) bending-flattening tracking profile; c) Pictures of films irradiated with UV (365 nm, 10 mW cm2) and visible light (540 nm, 40 mW cm2); Film dimensions: 5 mm x 2 mm x 16 μm. [51].

I.C.3.2. Toward LCE- DTEs system?

As previously mentioned, the main drawbacks of AZOs are the presence of back thermal reversion and slow time response, combining real bistable photochromic molecules as DTEs is an excellent alternative through the incorporation of DTEs in LCN networks. Very few recent examples are found in the literature. Lahikainen et al. reported a light-driven actuator based on a liquid crystal polymer network containing diarylethene (DAE) photoswitches as crosslinks, Figure 13a. Note that DTE in this study have been used to tune a photothermal effect (both UV and Visible light are irradiated same time) and finally the actuator bent negligibly despite very high LED power [53].

Very recently, diarylethene-functionalized liquid-crystalline elastomers containing thiol-anhydride bonds by Hebner et al [54]. This photoactuator demonstrated to be optically reversible over five cycles of alternating UV/Visible light exposure with minimal photochrome fatigue. The incorporation of thiolanhydride dynamic bonds allowed for retention of actuated states while thermal stability (Figure 13b).
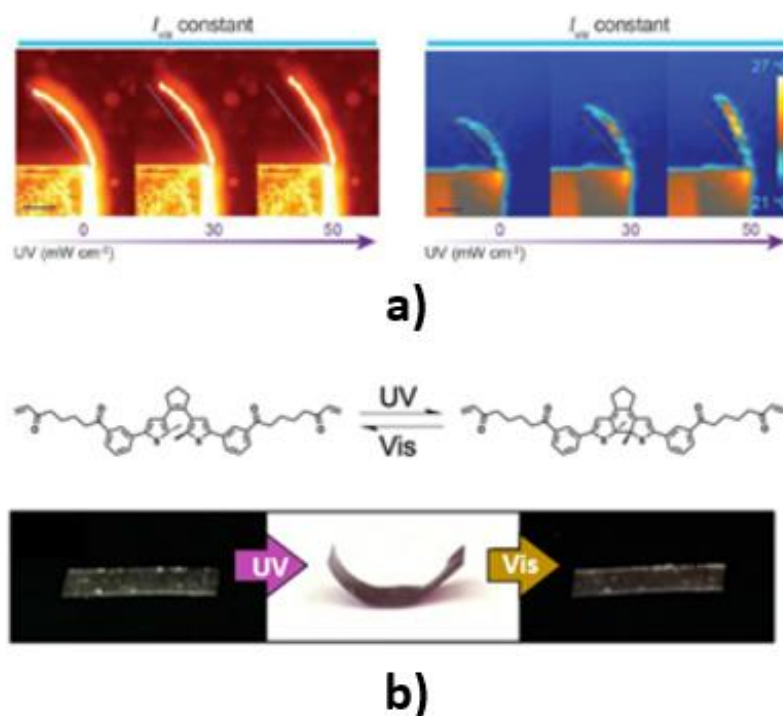
Figure 13. a) Optical and thermal images of the strip under 285 mW·cm-2 visible light illumination using UV exposure of different intensities. [53] b) Chemical structures for ring-opened and ring-closed forms of DAE and photographs of film before UV exposure, after 30s UV exposure, and after 10 min visible light exposure [54].

I.C.4. Supramolecular polymeric photoactuator

The area of supramolecular polymers combines supramolecular chemistry and polymer materials. Supramolecular polymers define polymers where small molecular units designed monomers, are assembled via highly directional and reversible non-covalent bondings [55]. When the interactions between the neighboring monomeric units are strong enough, long molecular chains can be formed leading to polymeric properties in solution and solid state. Unlike conventional covalent bonded polymers, supramolecular polymers exhibit a variety of non-covalent interactions that define their properties including host-guest recognition, donor-acceptor interactions, metal-ligand coordination, hydrogen bonding and $\pi - \pi$ interactions. Furthermore, the supramolecular polymers exhibit dynamic properties and their responsiveness depend on their sensitivity to external stimuli such as temperature or environmental chemical composition.
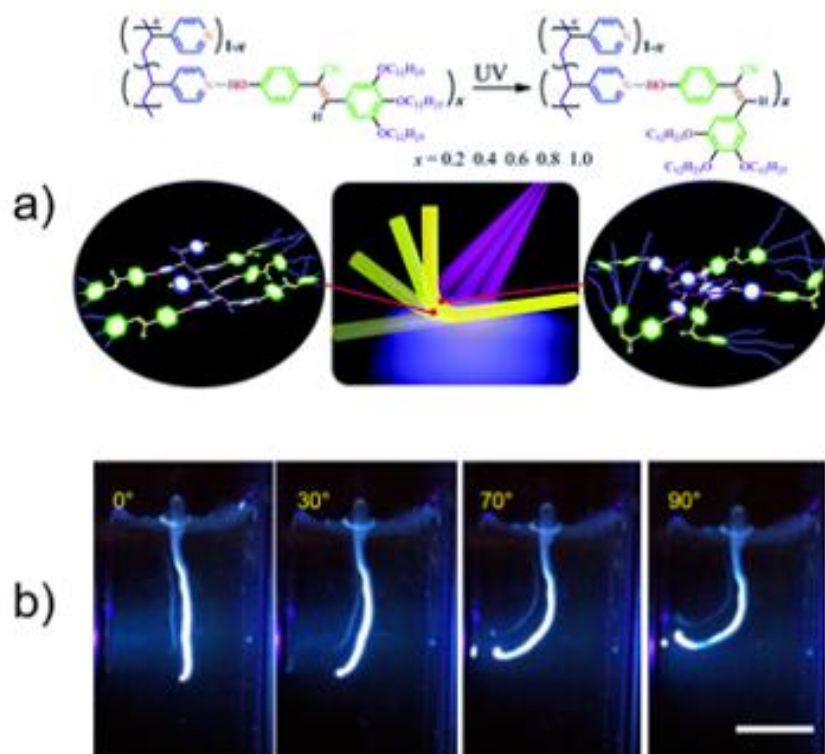
Figure 14. a) Model of photoinduced bending mechanism to packing of P4VP(Z-TCS)x and schematic drawing of the photoresponsive bending [56]. b) Photoactuation and thermal reversible process of the molecular motor-based string in aqueous solution. (Irradiation from the left). The string bends towards the UV light from 0° to 90° within 60 s [57].

The creation of novel supramolecular systems introduces a new step in the creation of photoresponsive materials. An example of this development is the new hydrogen-bonded supramolecular polymer P4VP(Z-TCS)x, which are composed of poly(4-vinyl pyridine) as the main chain and an α-cyanostilbene derivative (Z-TCS) as side groups, Figure 14a. These polymers show excellent photoinduced deformation ability under UV irradiation, and their fibers can be used for information encryption and other intelligent manufacturing materials [56].

In parallel, new fibers based on supramolecular networks are being developed, by the group of Prof. Ferringa whom manufactured an artificial molecular muscle that relies on the hierarchical self-assembly of a photoresponsive amphiphilic molecular motor, which forms nanofibers and aligned bundles that make up centimeter-long strings. Irradiation induces rotary motion of the molecular motors, leading to contraction of the fibers towards the light source, Figure 14b [57].

In the next section, we will focus on a special family of supramolecular

I.C.5. Supramolecular species based on UPy units

A revolutionary approach about supramolecular polymer chemistry was reported by Meijer and coworkers in 1997. [55]. They have successfully synthesized a 2-ureido-4[1H]-pyrimidinone units noted UPy. This unit is a hydrogen-bonding motif that enables to introduce thermos-reversible linkages and molecular recognition site.

In solution, interactions between UPy-units leads to their dimerization via quadruple hydrogen bonds and the formation of linear supramolecular polymer (Figure 15). In chloroform, the dimerization constant is about $6x10^7 \ M^{-1}$ at room temperature [58, p. 2]. For polymers, the quadruple hydrogen-bonded units can be attached either as side groups of the polymer backbone or as telechelic units (reactive end-groups). These telechelic compounds basically lead to the formation of supramolecular polymers with more improved dynamic properties.
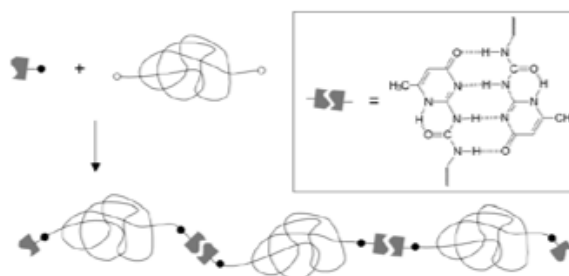
Figure 15. Schematic drawing of functionalization of telechelic polymers with quadruple hydrogen-bonded ureidopyriminone [58].

Besides the well-known examples of UPy polymers application like self-healing material [48], more and more example of photoresponsive system using UPy-UPy bonding were reported in literature recently [59]. To the best of our knowledge, no photoactuators have been reported yet. This is the reason why, in our groups, we have initiated to synthesized and investigated both thermoplastic elastomers based on UPy and DTE based on UPy with the idea to combine ideal viscoelasticity properties and reversible and bistable switching to elaborate original photoactuator.

I.C.5.1. Thermoplastic Elastomer (TPE) functionalized with UPy

Poly(ethylene-co-butylene) copolymer noted PEB is a random copolymer belonging to the polyolefin family. This copolymer that displays a degree of crystallinity strongly dependent on the ratio of ethylene (hard block) to butylene moieties (soft block). To sum up, above a 50% butylene content, the copolymer remains amorphous while below this value PEB is semi-crystalline [60].

The functionalization of PEB (starting from a PEB-diol) involving UPy-end groups were reported by Meijer et al. [46] as illustrated in (Figure). Investigations on UPy functionalized PEB have mainly focused on amorphous PEB [47]
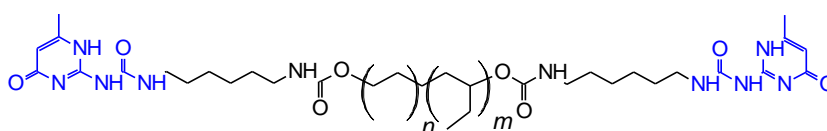
Figure 16. Poly(ethylene/butylene (PEB) functionalized with units UPy.

Preliminary Results. Recently, in our laboratories, we have undertaken a study for the structure of a semi-crystalline thermoplastic elastomer PEB-UPy under different temperature Using Differential Scan Calorimetry (DSC) technics and Wide- and Small- Angle X-ray Scattering technics (WAXS and SAXS), Figure 17.
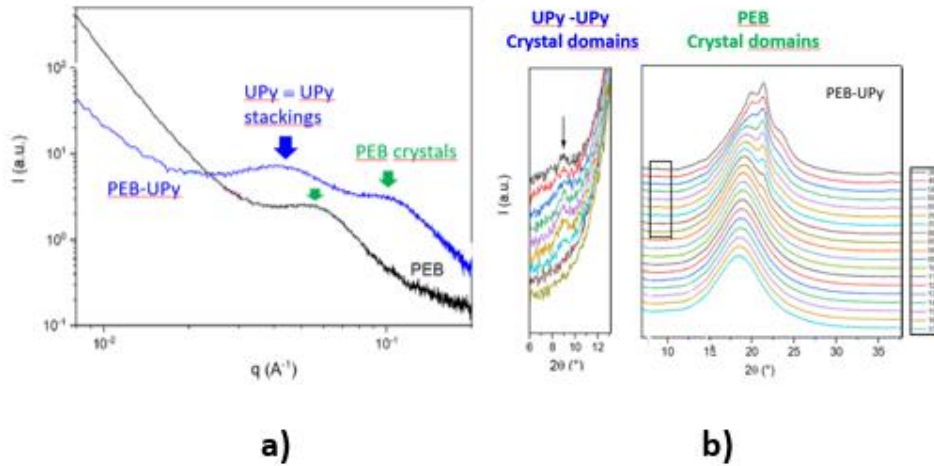
Figure 17. a) SAXS scattering profiles of PEB, PEB-UPy at T = 30 ◦C. b) PEB-UPy the inset is a zoom of the peak at 2θ = 8.7◦ attributed to the reflection of crystalline UPy domains [47].

The presence of crystalline domains of in-plane arrangement between neighboring UPy dimers (Figure 18). is detected by WAXS up to 80°C. The SAXS data reflect the presence of UPy aggregates stable on the whole temperature range. The correlation of these UPy-based aggregates is effective until the PEB crystal melting temperature (T_m). Beyond T_m, the increase of the macromolecular mobility reduces the number of domains in interaction and, in consequence, implies a decorrelation of the aggregates
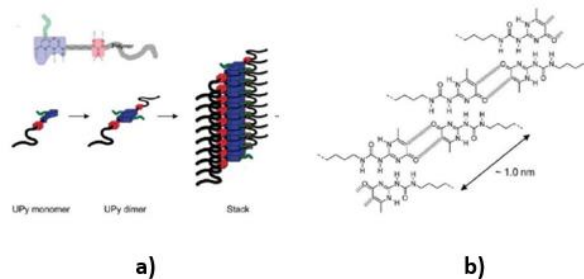
Figure 18. a) stacking scheme of UPy units. b) planar distance between UPy units.

I.C.5.2. Photochromic DTE functionalized with UPy

Supramolecular properties. Professor Takeshita et al. was the first to synthesize a photochromic molecule of DTEs derivative functionalized from both sides by UPy quadruple hydrogen groups noted DTE-UPy [45], [61]. In solution, neighbor UPy end groups tend to self-aggregate due to formation of four hydrogen bonding and then to form long supramolecular polymeric chains. The OF in chloroform is colorless and preserves its clear color for several days. When the solution for a concentration up to 200µM is irradiated with UV light, the blue photogenerated CF started to precipitate in few minutes. This observation not only proves the formation of the supramolecular assembly but also suggests higher aggregation of the monomers in their CF compared to their OF (Figure 19).

The supramolecular principle of such molecule is subtle. The open form (OF) of DTE-UPy molecules being flexible (thermal equilibrium between anti-parallel (AP) and parallel (P) conformers), they are not suitable for intermolecular linking through the UPy recognition patterns. To confirm such statements, the supramolecular assembly mechanisms were studied using Dynamic Light Scattering (DLS) technic [23], [45]. Indeed, for these OF species in chloroform, any object with a size lower than 10 nm (DLS signal sensitivity) was detectable giving evidence about the lack of large supramolecular system for OF object. After UV irradiation, the solution initially colorless becomes blue due to photocyclization process leading to a rigid closed form (CF).

Thanks to this rigidity, the interaction of UPy groups allows the formation of quadruple hydrogen bonding and then the assembly of DTE-UPy molecules creates a supramolecular assembly with final size up to of 600 nm. The overall kinetics takes more than several hours at ambient temperature.
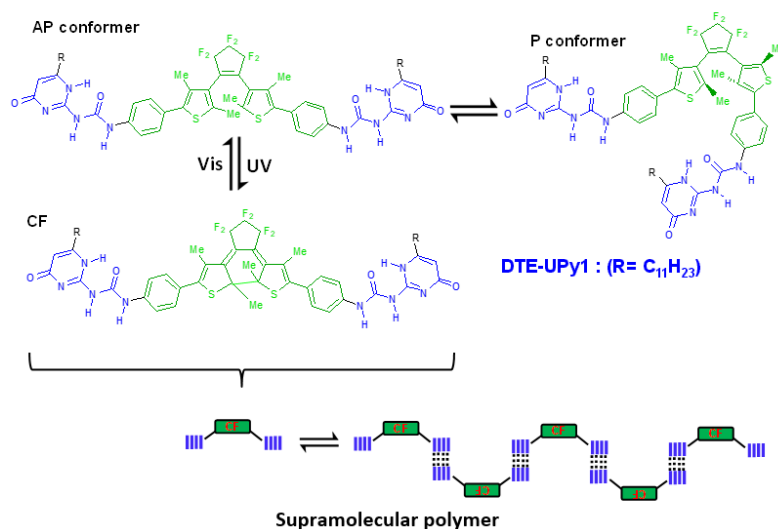
Figure 19. DTE-UPy in OF with antiparallel (AP) and parallel (P) conformers and in CF with the supramolecular self-assembly.

Calculations. Note that recently, Lebras et al. have published a thoughtful study for DTE-UPy molecules based on Molecular Dynamics and DFT calculations [62]. The simulations have shown that, for the OF oligomers, the progression of the supramolecular assembly is hindered due to: (i) the possible formation of a very stable cyclic dimer for the open-form parallel isomer, (ii) the relative flexibility of the open-form oligomers compared to their closed-form counterparts, and (iii) the possible existence of p-stacked dimers that constitute bottlenecks blocking the progression of the supramolecular self-assembly.
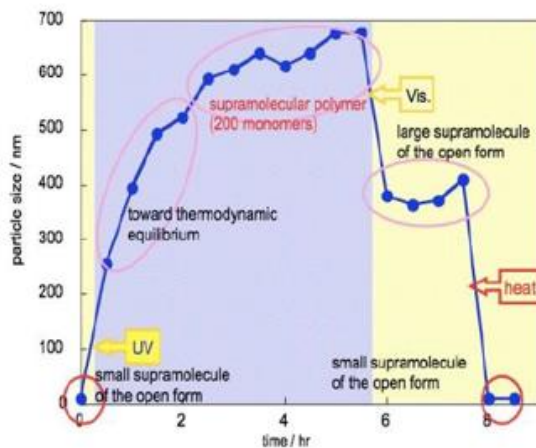
Figure 20. DLS particle size change of the photoswitch aggregation upon irradiation with UV and visible light [45].

Photochemical properties. Few years ago, we have investigated the influence of quadruple Hydrogen bonding on the photochemistry of OF-AP and CF conformers and photophysics of OF-P conformers using femtosecond absorption spectroscopy. Photochromic parameters have been determined and photochemical pathways have been rationalized with clear distinction between the antiparallel and parallel species. A new photocyclisation pathway via triplet manifold (25%) has been evidenced. The typical characteristic times are:

- Photocyclization directly from the Franck-Condon Region ∼200 fs
- Photocyclization from Triplet States ∼ tens of μs
- Photoreversion (classical pathway) 120 fs and 5 ps.

Concerning the influence of UPy units on the photochromic core, if any effect can not be noticed on photoreversion (the rigid molecule is not influence by the molecular forces at the surrounding), small oligomers affect the photocyclisation process and subsequent intersystem crossing reaction.
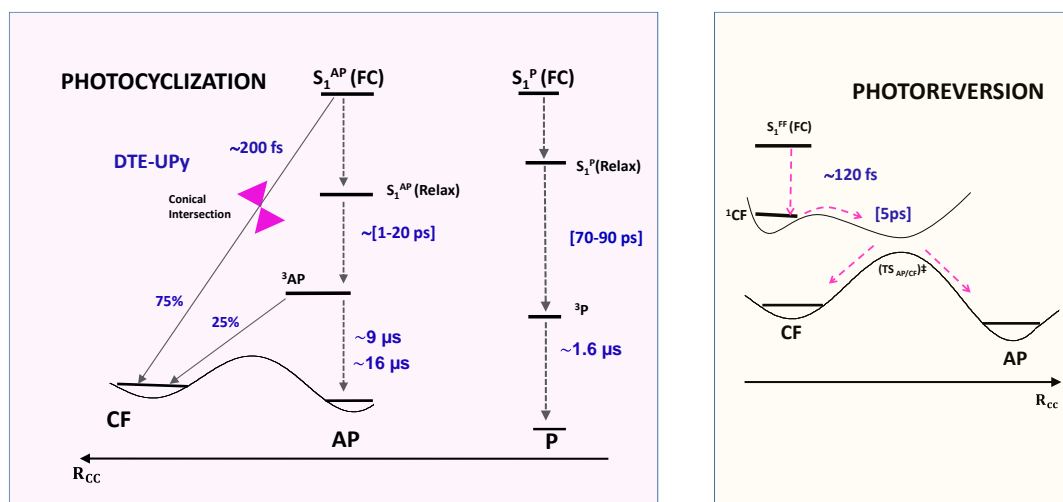
Figure 21. Proposed photochemical mechanism and characteristic times for the photocyclization (left) and the photoreversion processes (right) for DTE-UPy1, "FC" refers to Franck-Condon states.

I.D. THESIS OBJECTIVE

In summary, within the framework of the organic photochromic photoactuators (Photothermal systems excluded), under the impulsion of Finkelman and Ikeda groups, the most widely used photoactive molecule in the functionalization of LC systems has been azobenzene: due to the drastic changes at molecular level (cis-trans isomerization) resulting in important macroscopic deformation. However, cross-linked AZOs-LCE photo-actuators have three major drawbacks:

i)   the process to elaborate the photoactuator is complicated

ii)   the response of the AZOs to light stimulus is relatively slow

iii)   the cis isomer relaxes spontaneously to trans isomer through thermal relaxation

In fact, we have seen that one of the best efficient photoactuators are actually DTE monocrystals, but several limitations immediately arise such as: i) the inability to fabricate photo-actuators beyond a few mm; ii) a limited shape selection capability due to the morphology of the crystalline system and iii) a high brittleness. An alternative to face these limitations is to **combine bistable DTEs photoswitchs with a flexible thermoplastic elastomer** which could be a good candidate for the development of real-world photoactuators.

Taking those requirements into account, our group and collaborators have elaborated a telechelic polymeric system combining a DTE derivative (**component A**) [45] and a thermoplastic elastomer poly(ethylene-1,2-butylene) [46], [47] (**component B**, Figure 22a, both functionalized with a ureidopyriminone (UPy) molecule [46], [48]. The main objective of the functionalization was to connect the A and B subunits to each other by means of a quadruple hydrogen bond, Figure 22. By combining the photochromic units A (DTE-UPy) and the elastomeric units B (PEB-UPy) in solvent and making a thin film, our objective (Figure 22c) is to process a reversible photoactuator with a bending motion toward or backward the light direction upon irradiation of UV or Visible light respectively (the reverse case being an option as well). As DTE crystals reviewed above, the PME of our new

system must be leaded by the photocyclization or photoreversion of the photochromic units. Consequently, the PME will be accompanied by a color change.
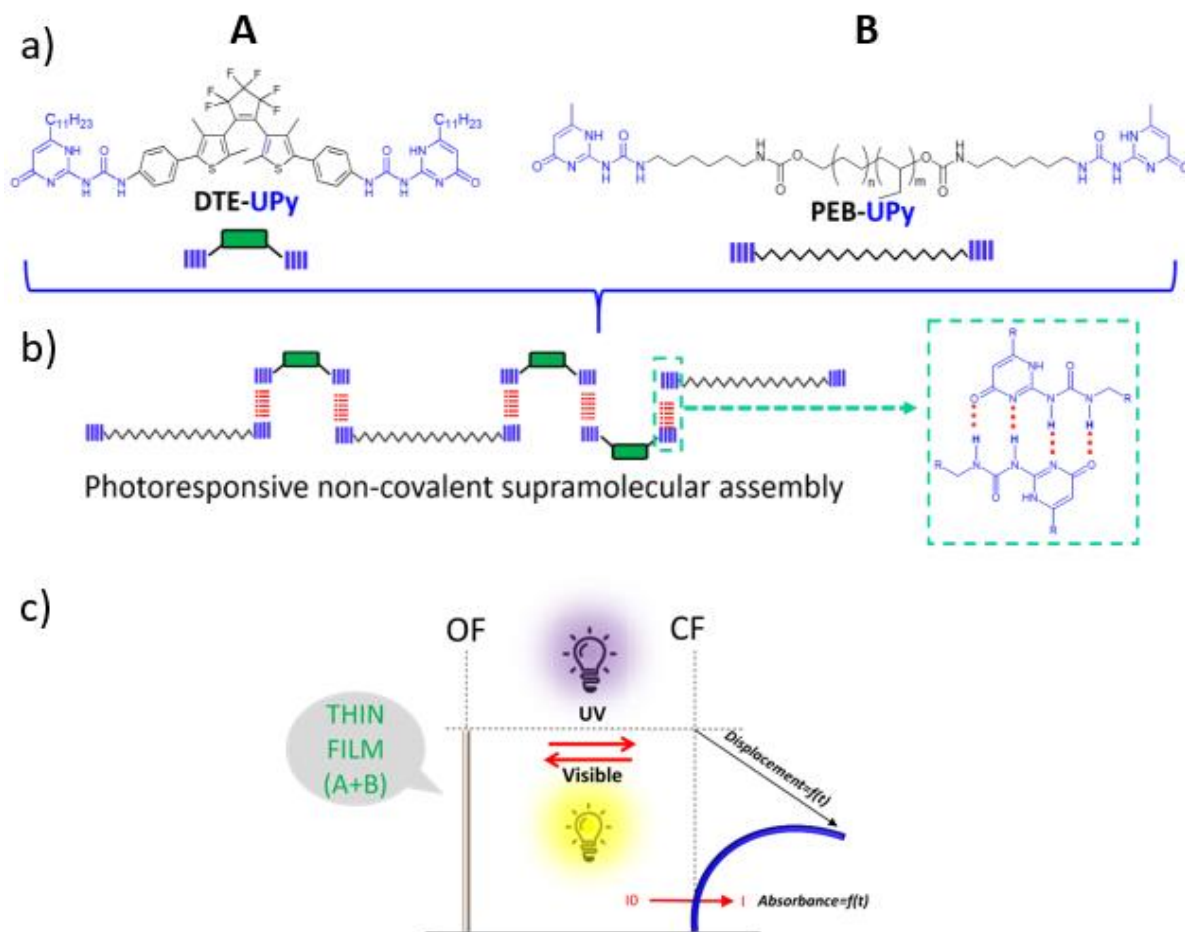
Figure 22. a) DTE-UPy (component "A"), PEB-UPy (component "B"). b) Supramolecular bonding due to quadruple hydrogen bonding. c) Illustration of the photoactuator principle based on A photochromism. Illustration of the displacement and absorbance tracking profile are given as well. c) Process a reversible photoactuator with a bending motion toward or backward the light direction upon irradiation of UV or Visible light.

Within this context, the main objective of this thesis is to follow up on the research previously carried out by our group within the framework of the ANR TACTIL project, exploring new processes in the fabrication of a photoactuator (thin film) based on a DTE-UPy/PEB-UPy supramolecular chemistry. Likewise, this research aims to rationalize the processes involved in the bending of thin films irradiated with UV-Visible light, in addition to finding the ideal parameters by analyzing their

deformation to maximize the photomechanical effect of the photoactuator and increase its performance. Therefore, this study will focus on the changes produced in the internal structure of the material as well as in its morphology and photochemistry when it is subjected to alternating cycles of UV and Visible light irradiation.

The strategy to perform a global study on thin films began with the study of the optimal parameters for the fabrication of the thin films (DTE-UPy/PEB-UPy) noticed also thin film (A+B) in the following. Then, development of two novel setups are required to get in parallel the displacement and the absorbance of the thin film in the real-time (data processing as well). The results of the photomechanical effect were later related to structural, photochemical and morphological analyses by using WAXS, SAXS, AFM, SEM, UV-Vis spectrometry and absorption analysis techniques.

This thesis is divided into six chapters, the first one focuses on the fundamental basis for the development of DTE-based photo actuators. The other chapters focus on the fabrication and analysis of DTE-UPy/PEB-UPy thin films.

More particularly, the present chapter has given a basic and fundamental overview of photochromic phenomena, supramolecular systems (based on UPy functionalization) and DTE-based photoactuators, from single crystals to recent advances in elastomeric liquid crystal (LCE)-DTE systems.

Chapter II describes the methods, analysis, and materials, including the protocols for the elaboration of thin films using the Spin Coating (SC) technique. It also describes the development and fabrication of two setup developed for the photomechanical study, i.e. Real-time displacement tracking profile and absorbance tracking profile. Finally, brief descriptions of the characterization techniques used are presented.

Chapter III is dedicated to the photochromic study using UV-Vis and absorption spectrometry of DTE-UPy and DTE-UPy/PEB-UPy solutions and solid thin films. The absorbance tracking profile results will be thoughtfully commented.

Chapter IV focus on the displacement tracking profile results from preliminary results to good operative parameters conditions. With the optimum system, results are analyzed and corroborated with Absorbance tracking profile results. Finally, chemical, and structural parameters discussion is initiated by comparison with analogs system (not optimized UPy network, amorphous vs crystalline PEB).

Chapter V deals with the surface, structural and morphological characterization by SEM, AFM, WAXS, and SAXS techniques of DTE-UPy/PEB-UPy systems. With this chapter, we will be able to get a better multiscale understanding from microscopic changes under illumination-when the photoswitch is active- to the macroscopic photomechanical change.

Finally, **Chapter VI** provides a general conclusion on the studies carried out, as well as perspectives within the framework of the development of the ANR TACTIL project.

CHAPTER II

Materials, Films Fabrication and Characterization Methods

This chapter presents methods and processes employed for the fabrication of thin polymeric films based on a supramolecular self-assembled elastomer which is a mixture of the photochromic molecule A and thermoplastic elastomer (poly(ethylene-butylene)) B both functionalized with UPy units. Then, structural, and morphological, and thermal analyses employed for the rationalization of the photomechanical effects are presented. At the end of this chapter, the two new setup relying on the absorbance and displacement tracking profile are presented in detail.

II.A. Presentation of individual chemical components

Although the synthesis and functionalization of the photoactive units and the thermoplastic elastomer were not performed in this thesis project, a brief summary of the synthesis and functionalization process will be given in order to broaden the framework of the study and to increase the reader's understanding of the development and fabrication of the supramolecular self-assembled polymer.

II.A.1. The photochromic- DTE-UPy (A)

The synthesis of DTE-UPy molecule is not straightforward and a 12 step protocols with 43% yield was published by Takeshita et al. fifteen years ago [45], [61]. Recently, Gilles Alcaraz (University of Rennes) has elaborated a new protocol for which the final step is summarized below (Figure 23):
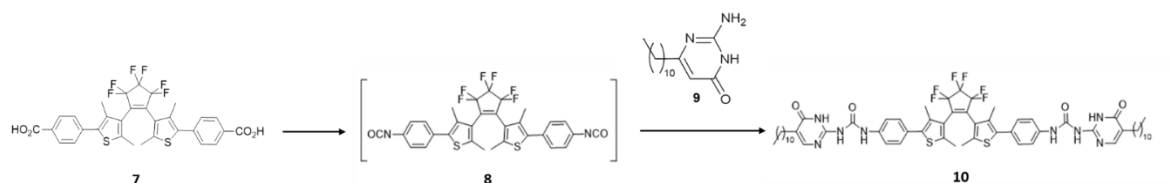
Figure 23. Functionalization of DTE with Ureidopyriminone UPy units.

His novel approach was a divergent functionalization using dibromine DTE precursor to get molecule 7 and a different choice for the precursor of 9. With this new strategy, the quantum yield was improved to 83% allowing for a large quantity to be deliver (5g).

II.A.2. The thermoplastic Elastomer, PEB-UPy (B) and analogs

The Synthesis protocol of PEB-UPy has been adapted and optimized from several protocols described in the literature and more particularly from the synthesis reported by Meijer et al. [18] and then adopted by Louati et al. [63].
In these supramolecular polymers, the main principle is that PEB monomers are bi-functional molecules. They are expected to connect two strongly dimerizing UPy-groups with an intermediate linker.

As mentioned in Figure 24, the synthesis is based on two steps. The first step involves coupling of fourfold excess of the methylisocytosine (2) to hexamethylenediisocyanate (1), which are commercially available. From the reaction of mixture, the obtained precipitate represents an ureidopyriminone (UPy) with an isocyanate function attached into a linker chain (3) that can easily react on

34

hydroxy telechelic polymers. For this propose, a telechelic polymer PEB(OH)2 commercially available with a molecular weight of 2500 g/mol is applied. PEB(OH)2 is a hydrogenated random copolymer of 1,2- and 1,4-polymerized of 1,4-butadiene units. The two hydroxyl end group of PEB(OH)2 (4) are functionalized with the issued (3) involving the formation of urethane group. The UPy-end PEB (5) was accurately determined. To assess the role played by the UPy network, we have also elaborated a hybrid elastomer with incomplete UPy functionaization –product (6) noticed also B50. The rate of 50% functionalization was assessed by NMR.
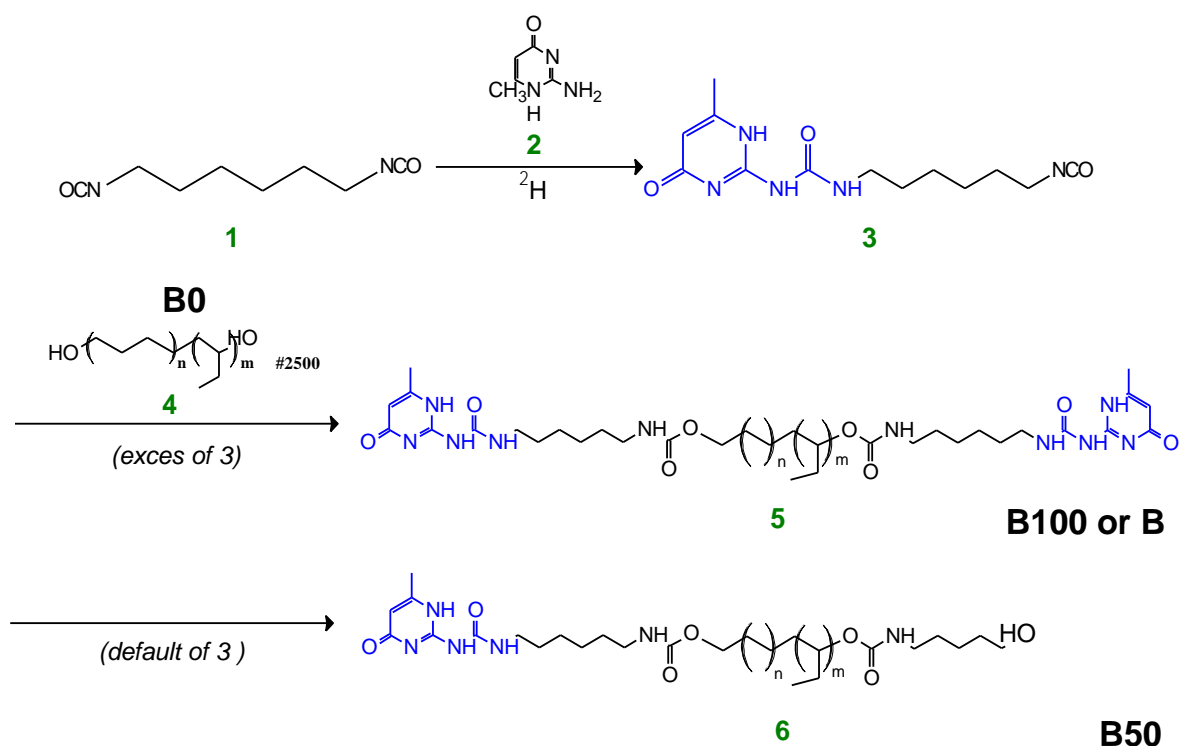
Figure 24. Synthesis of telechelic PEB-UPy elastomer B and the analog B50 using commercial PEB-diol B0 (from Sigma –Aldrich).

II.A.3. Notation used for the different compounds
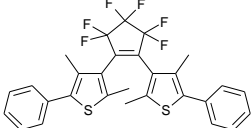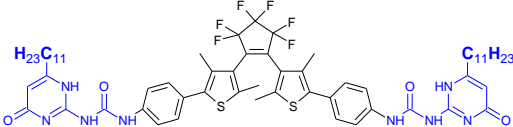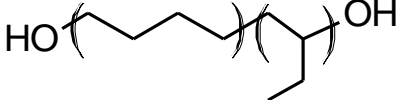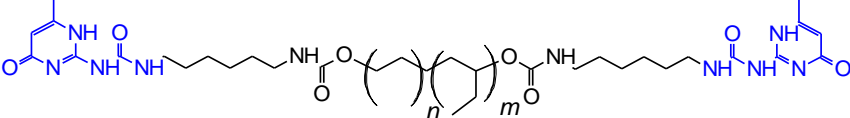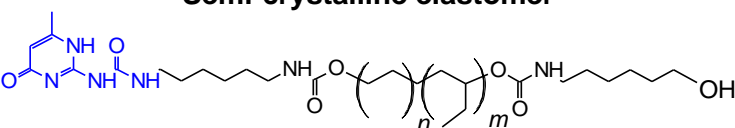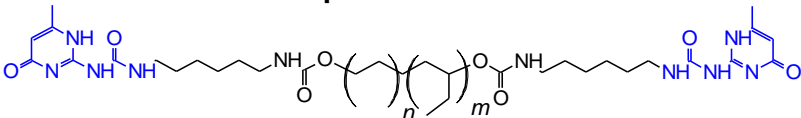
Schema	Nomenclature	Symbol
	DTE	**A0**
	DTE-UPy	**A**
Semi-crystalline elastomer	**PEB-diol**	**B0**
Semi-crystalline elastomer	**PEB-UPy**	**B**
Semi-crystalline elastomer	**PEB-UPy-OH**	**B$_{50}$**
Amorphous elastomer	**PEB$_{amp}$-Upy**	**B$_{amp}$**

Table 1. Schemes, nomenclature, and symbols of the molecules used in this thesis.

II.B. Fabrication of photoactuators PEB-UPy/DTE-UP and analogs

Inspired by previous results obtained in our laboratories [63], different strategies were tests to elaborate photosensitive thin films: melt molding, drop casting, and spin coating. Because the performances in term of photomechanical effect were very small for the two former methods, we have decided to present in this manuscript the most efficient method based on spin-coating approach.

II.B.1. (A+B) Solution preparation.

As evidence, the overall process combining DTE-UPy and PEB-UPy rely on the good connections between the photoactive units and elastomeric units via the quadruple supramolecular hydrogen bonding which implies that the blending in solution must be rigorous. This process for preparing the solution is shown in Figure 25a according to successive steps:

1) The photochromic units DTE-UPy (25 mg, white powder) and elastomeric units PEB-UPy (75 mg, transparent crystals, [B]=3.85 mM) in molar ratio 1:1 (mass ratio 1:3) were dissolved in 0.5 ml of commercial chloroform of spectroscopic grade in a small bottle with PTFE cap.

2) To break the hydrogen bonding networks originating from the solid sates (A- $A \cdots A$ and $B \cdots B$) and enhanced cross connections between the two components ($ABAB \cdots$), The mixture was introduced into an ultrasonic bath at medium intensity for 15 min at a temperature of 60 °C, to increase the dispersion of the DTE-UPy molecules.

3) At the stage, two routes are possible. Most of the films made during this thesis were elaborated from the solution in the OF state (amber color). To do so, the solution was kept in constant agitation for 60 min at a temperature of 80 ºC (temperature higher than the average Melting Temperature [19]). The main advantage of the OF route is the avoiding of DTE-UPy precipitates when the solution is at rest and room temperature [61]. Alternatively, to obtain thin films in CF state (blue color) the solution was irradiated for 60 min with ultraviolet light @ 310 nm. The main advantage for processing from CF state was supposed to be the enhancement of supramolecular association due to the increase of rigidity of DTE-UPy molecules in the CF state. In contrast, an additional difficulty with this route is related with the possible precipitation of the CF for a concentration beyond the 200 µM limit [45], [63]. The importance of choosing one or other route will be discussed in the next chapters.
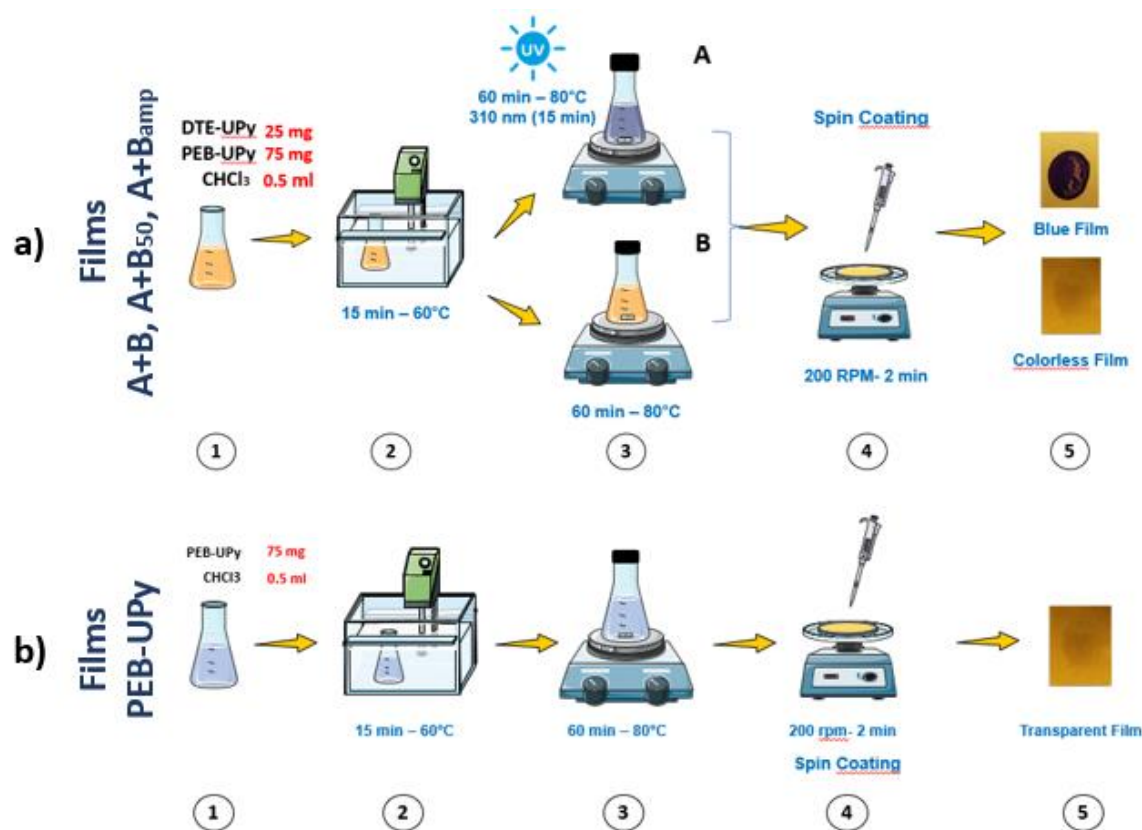
Figure 25. a) Fabrication process of PEB-UPy/PEB-UPy based thin films. 1) Dissolution of DTE-UPy and PEB-UPy molecules in Chloroform. 2) Agitation and heating of the solution for 60 min. 3) Irradiation of the solution for the fabrication of films in "CF" state. 4) Deposition of the solution on the substrate for subsequent film formation by using the Spin Coating technique. 5) Films obtained on silica paper substrate, (blue- "CF", colorless- "OF"). b) Similar process for the elastomer alone.

II.B.2. Thin films (A+B) by spin coating.

The thin film elaborated from the solutions described above (OF or CF) were elaborated with a standard spin coater (APT GmbH, model SPIN150) using a typical volume deposition between 50 and 100 µL. More than one hundred tests were performed with different substrates silica paper, PPFT, Quartz, Glass substrates (12mm x 10 mm) and different spinning conditions (1, 2 or 3 steps varying the spinning velocities). We only present here the most efficient protocol to obtain the thin films.

As illustrated in the Figure 26a, a thin films were made by dispensing 100 μL droplets onto silica paper substrates using the 2-step spin coating method, the initial step being to hold the droplet in a quiescent state for one minute and then accelerate it to 200 RPM during 200 seconds. The final thin film was a disc of ~2 cm diameter stacked on the silica paper but easily removable with the aid of a scalpel. (Note that the adhesion of the film on the other substrates was so strong that it led us to put them aside).

II.B.3. Thin Films B alone by spin coating

In order to make a more complete study, elastomer-only films, Film "B" (PEB-UPy) were fabricated by the process mentioned in the previous section, respecting a similar concentration of 3.85 mM, Figure 25b. 1) 75 mg of PEB-UPy was mixed in 0.5 ml of chloroform, 2) then the solution was kept in an ultrasonic bath at medium intensity for 15 min at 60 °C, 3) thereafter, the solution was kept in constant agitation at 80 °C for 60 min, after this time the solution was allowed to cool to room temperature. 4) thin films were made by dispensing 100 μL droplets onto silica paper substrates using the 2-step spin coting method, the initial step being to keep the droplet in a resting state for one minute and then accelerated to 200 RPM for 200 seconds, Figure 26.
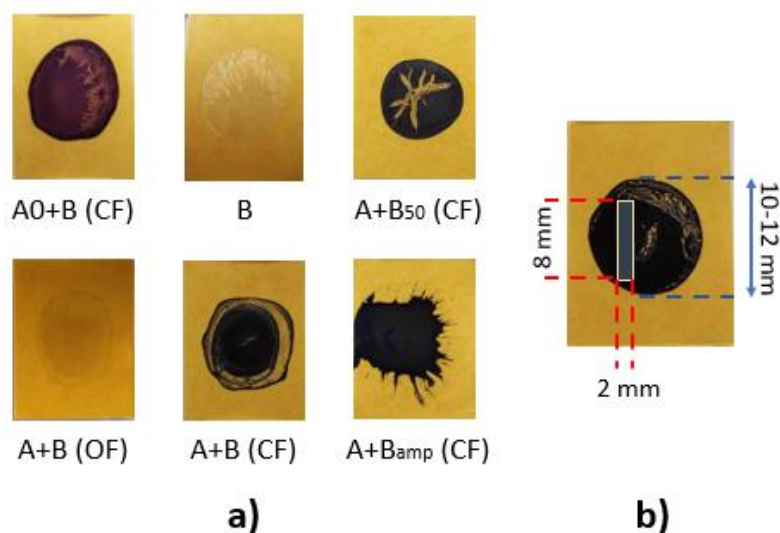
Figure 26. a) Photographs of films fabricated on silica paper substrates with solutions (A0+B) (CF), B, (A+B$_{50}$) (CF), (A+B) (OF), (A+B) (CF), and (A+B$_{amp}$) (CF). Graphical representation of the size of the fabricated films and the cut size of the films.

II.C. Characterization of morphological properties.

II.C.1. Thickness measurements by optical microscopy

The thickness measurement of the films was carried out using an industrial microscope with a Hayear 1138 video camera and a 150X objective lens. Specifically, the thickness of each film was measured by sampling the thickness of the cross section of each film and then averaging it to obtain the thickness of each film. Figure 27 shows a scheme of how the films were placed and fixed by means of glass sample holders to be analyzed with the industrial microscope. All measurements were taken using the software provided by the manufacturer of the industrial microscope.
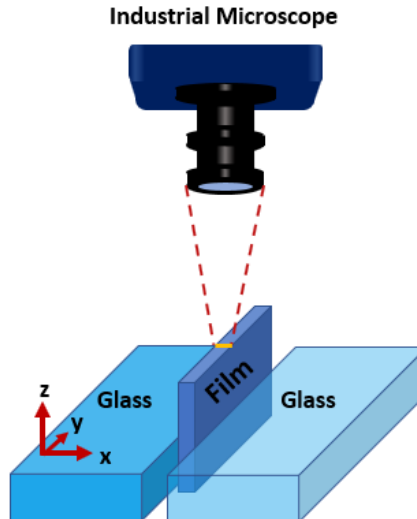
Figure 27. Configuration used to measure film thicknesses.

II.C.2. Surface morphology by Atomic Force Microscopy (AFM)

Atomic force microscopy AFM is a technique that generates an image of the topography of a surface in high resolution by measuring the interaction between a micrometer tip and the surface to be analyzed (in contact or not) by scanning the entire surface [68,69]. Commonly, a laser is directed towards a cantilever which display a piezo-crystal or silicon tip of a few microns at its end. Upon interaction with a surface the cantilever is displaced which causes the laser reflection toward

the photodetector divided into quadrants to move [70]. Each displacement of the laser registers each of the interactions of the tip with the surface, thus contracting a profile of the height difference, Figure 28a. By making a linear sweep over the entire material, the high-resolution topography is then obtained.

The set up used to perform the AFM analysis was an atomic force microscope NTEGRA mod. NT-MDT, used in semi-contact mode with a silicon cantilever with gold coating NTEGRA, mod. NSG30 and an oscillation frequency of 278.34 Hz. The images were taken on the films without any surface preparation, atmospheric pressure, and room temperature. The scanned regions were 2 μm x 2 μm with a resolution of 1024 x 1024 lines. The analysis was performed with Gwyddion software, (open source). As shown on Figure 28b in-situ illumination was achieved with two LED (see below) fixed with an 60° angle at distance of 10 cm. We ensure that the two spot cover the entire thin film.
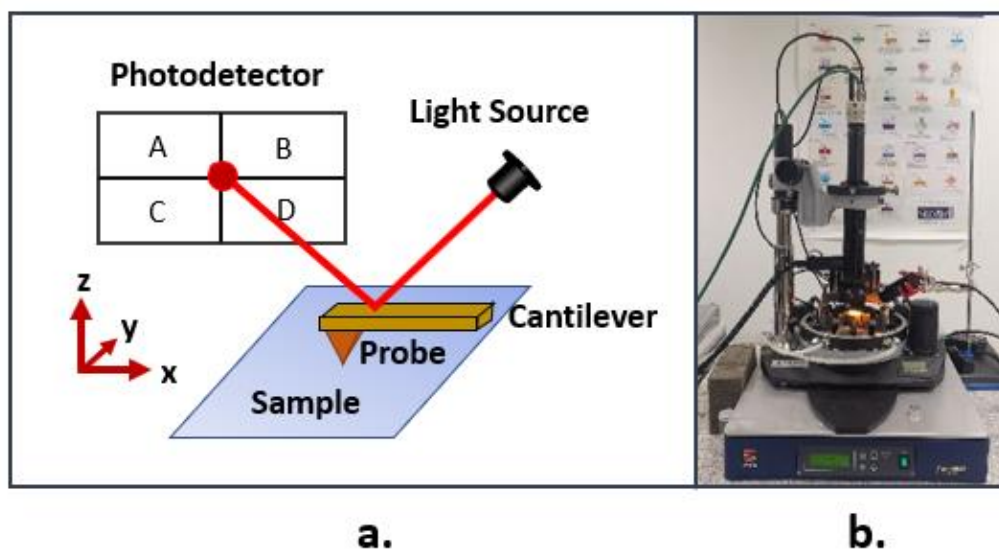
Figure 28. a) The basic configuration of an AFM atomic force microscope. b) Equipment used to perform AFM morphology analysis, NTEGRA. Mod. NT-MDT.

II.C.3. Surface morphology by Scanning Electron Microscopy

The Scanning Electron Microscope (SEM) technique is used to produce a morphological image (topography, texture, and composition) of the material to be

studied. The microscope uses a focused beam of high energy electrons which impacts on the surface of the material generating electron radiation (secondary electrons and backscattered electrons) these electrons provide information according to their type. Secondary electrons give information about the surface of the material, as well as its topography and texture. On the other hand, backscattered electrons provide information on the chemical composition and depending on the material to be studied it is possible to obtain an analysis of elements contained in the sample with a localized contrast [64].

For the morphology analysis, a Hitachi S4700 SEM was used, with an accelerating voltage of 2 kV and a target distance of 10 mm. The films were arranged on carbon substrates with a preprocess of carbon deposition on its surface. This was done to avoid loading effects. Because of the carbon deposition, no in situ illumination was feasible and SEM images of the OF and CF samples were acquired separately (with an illumination before carbon deposition).

II.D. Characterization of structural properties.

II.D.1. Internal structure reveals by X-ray Scattering

WAXS (Wide Angle X-Ray Scattering) is a technique used to characterize the atomic structure of a polymer material. The radiation-matter interactions are the basis of this method. The transmission mode is used for the diffraction. A monochromatic X-ray beam is used to illuminate the sample under investigation. Both the crystalline planes in the Bragg position at a 2θ angle and the amorphous phase of the sample diffuse a portion of the beam. Considering incident X-ray beams, the half angle of deviation θ can be associated to the inter-reticular distance of the planes hkl (d_{hkl}).

$$n\lambda = 2d_{hkl}\sin(\theta) \tag{1}$$

where n the diffraction order and λ the wavelength of X-ray beam.

The schematic of X-ray is given in Figure 29.

.
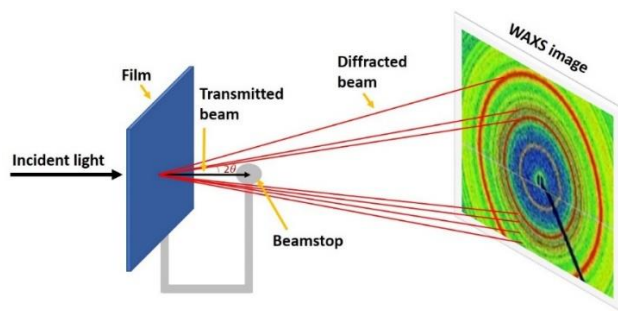
Figure 29. Schematic illustration of WAXS principle.

X-ray scattering techniques have been of great importance in the investigation and characterization of materials in both crystalline and soft matter. Depending on the scale of investigation, it is possible to cover a wide range of systems such as polymers, polymer mixtures and solutions, microemulsions, colloidal or micellar dispersions, etc. On the other hand, depending on the X-ray technique used (Wide X-scattering, Small and Ultra-Small angle) it is possible to obtain information for different length scales 1 nm-10 nm, 10 nm- 100 nm, respectively. Figure 30 shows the spectrum obtained for different scattering angles.
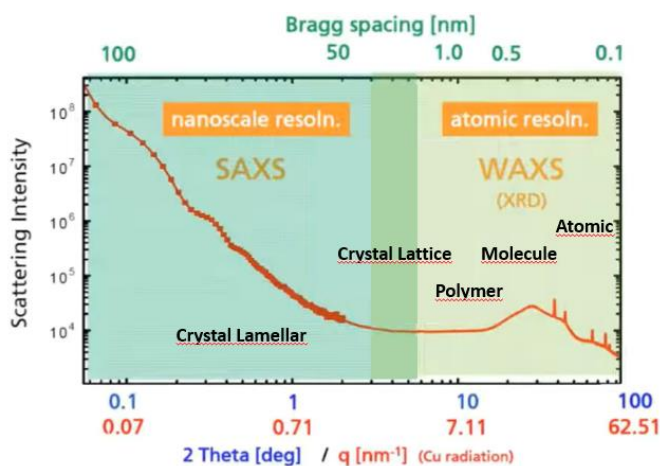
Figure 30. Difference in length scales analyzed and information that can be obtained with respect to the X-ray scattering analysis performed.

Wide Angle X-ray Scattering (WAXS) is an analysis that consists of recording large angles of the diffraction fraction (~10<2θ<100) to examine a wide range of scattering variables for length scales from 1 nm to a few nanometers corresponding to chemical bond lengths or the size of unit cells in crystalline polymers [72].

On the other hand, Small Angle X-ray Scattering (SAXS), records small angles of the diffraction fraction (0.1<2θ<~10), with which it is possible to analyze length scales larger than 10 nm, corresponding to unit cell size in polymers, complex crystalline structures, porosity, shape, and size of structures immersed in polymeric matrices or emulsions, etc.

The main difference between SAXS and WAXS analysis is the distance of the detector from the sample, Figure 20. For WAXS the detector must be placed a few meters away from the sample, while for SAXS the detector is a few centimeters away from the sample. Both WAXS/SAXS rely on a highly collimated beam and a detector capable of registering scattering/diffraction in two dimensions at a 2θ angle to the direct beam.

II.D.1.1. Atomic resolution with WAXS

Diffraction pattern depends on the structural organization within the sample. In the case of an isotropic amorphous material, only a broad and diffuse halo is observed as shown in Figure 15a. Whereas an isotropic semi-crystalline polymer leads to intense rings additionally to its amorphous halo as shown in the Figure 31.

From the peaks related with crystalline domains, the calculated distance d_{hkl} allows the determination of the crystalline unit cell parameters (Bragg law) and thus to identify the crystal phases of the material.
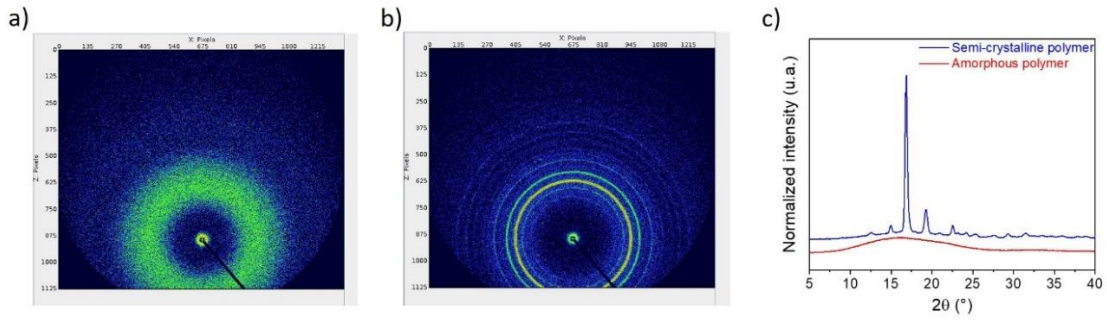
Figure 31. Examples of WAXS patterns: a) amorphous and b) semi-crystalline polymers and c) the corresponding integrated profiles.

II.D.1.2. Nanoscale resolution with SAXS

Small angle X-ray scattering (SAXS) probes the structure at nanometric scale. To overcome the air diffusion phenomena, a vacuum section is placed between the sample and the detector. The integrated SAXS image leads to a diffractogram (Iq^2) as a function of the diffusion vector q, independent to wavelength of incident light. The scattering vector q is defined as following:

$$q = \frac{4\pi \sin(\theta)}{\lambda} \tag{2}$$

In semi-crystalline polymer, X-ray diffusion leads the access to the long period (L_p) because of the difference in electron density between amorphous (L_a) and crystalline (L_c) phases. This periodicity is defined as a repetition distance occurred between La and L_c blocks (Figure 32b). In some case, a distance different from L_p and defined as a correlation distance d_c (Figure 32c) can be observed. In order to calculate L_p or d_c, Iq² is represented as a function of scattering vector q (Figure 11a).

$$L_p = \frac{2\pi}{q_{max}} \tag{3}$$

$$d_c = \frac{2\pi}{q_{max}} \tag{4}$$

where q_{max} represent the q-value at the maximum of diffusion.

45
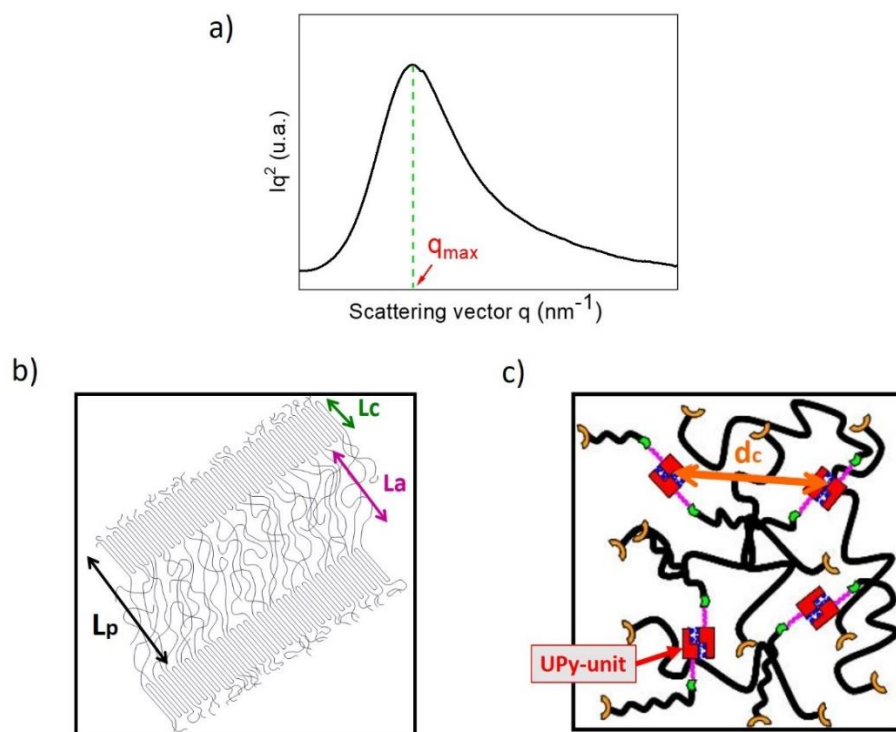
Figure 32. a) SAXS profile of Lorentz representation $Iq^2 = f(q)$. Schematic representation of b) long period L_p and c) correlation distance d_c (in orange).

II.E. Characterization of luminescent and photochromic properties.

II.E.1. Stationary spectroscopies.

The stationary absorption spectra of the solution and the PEB-UPy/DTE-UPy films were carried out using a double beam VARIAN spectrometer (CARY100 bio-visible), with a spectral range of 200 to 800 nm. For spectra in solution, concentrations of 1 to 10µM were used, with chloroform as reference. For thin film spectra, air was used as reference. All measurements were made at atmospheric pressure and room temperature. As we will present later, the thin films (A+B) present some unexpected photoluminescence properties. To obtain quantitative information, emission spectra in solution were record using a HORIBA fluorometer (FluoroLOG).

II.E.2. Real-time absorbance measurement.

One of the main objectives of this manuscript is to relate the photochromic kinetic (the rate of the color change) with the photoactuation processes (the rate of the position change). To do so, a home-made set up has been elaborated to get more versality to study solution as well as thin films.

II.E.2.1. Irradiation System.

The solutions as well as the thin films were irradiated in situ using an illumination system consisting of 2 MIGHTEX LED lamps with wavelengths of 310 nm (LCS 0310-03-23), and 590 nm (LCS 0590-03-22), respectively. The lamps were controlled by a Driver with manual-analogical control MIGHTEX (SLA-1000-2) as display on
Figure 33a.
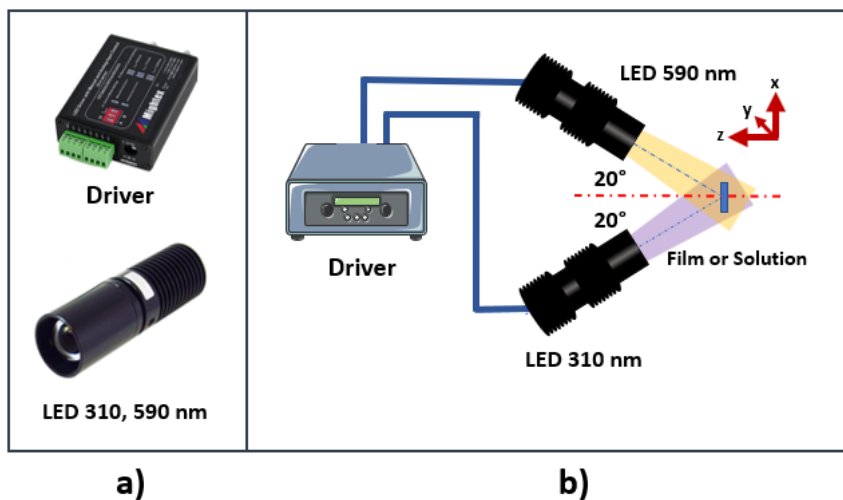
Figure 33. a) Photographs of driver and LED lamps used to irradiate the films. b) Diagram of the irradiation system configuration.
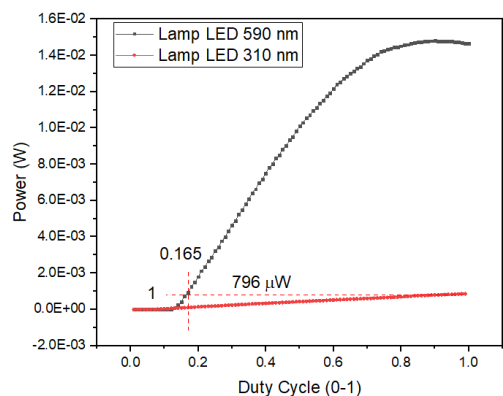
Figure 34. Power calibration with respect to the voltage supplied from the Arduino UNO to the driver (Duty Cycle).

Calibration was perform starting with measuring the power supplied by each lamp and then finding the point to obtain identical power, Figure 34. Indeed, the choice has been made to work with a similar power from UV and Visible LED. Subsequently, the necessary voltage that must be given by the Arduino UNO to the Driver (see connection in Figure 37a) was analyzed to obtain the desired power. It was found that the power of the lamps was equal to 796 µW, while the voltage supplied to the Driver (Voltage supplied=5V x Duty Cycle) from the Arduino UNO was 5 V and 0.825 V for the 310 nm and 590 nm lamps respectively.

II.E.2.2. Absorbance tracking profile in real-time

In order to assess the color (absorbance) change of our samples – solutions or thin films- under continuous illumination, we have taken benefit of the special properties of the photochromic DTEs illustrate on Figure 35b. Indeed, unlike the UV region, the visible region is indicative only on the CF absorbance. Therefore, with a laser chosen @ an appropriate wavelength falling in the CF absorbance band – 635 nm in our case, one can easily determine the absorbance of the CF species according to the basic equation:

$$A(CF) = log\frac{I_0}{I} \qquad (5)$$

48
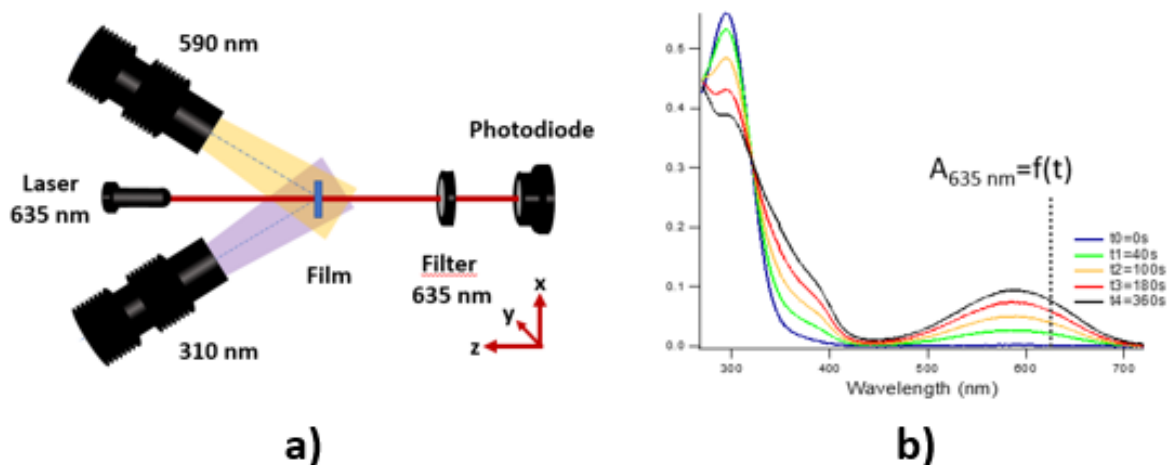
Figure 35. a) Configuration scheme for the absorbance measurement system for PEB-UPy/DTE-UPy films. b) Absorption spectrum for different irradiation times with UV light.

The absorbance tracking profile (real time) for the PEB-UPy/DTE-UPy films were performed in situ using an OPHIR power meter (StarBright, 7Z01580), see Figure 36, using a photodiode (PD300R-UV) with a spectral range from 200 to 1100 nm and a power measurement range from 20 pW to 3 mW. A THORLABS laser (PL202) with a wavelength of 635 nm was used as excitation medium, to which a filter lens of optical density (OD=2) was added to decrease the laser intensity and avoid a photoreversion process. To avoid contributions in the absorbance measurement due to the visible LED, a 635 nm laser line filter (THORLABS, FL635-10) was added front of the photodiode. Figure 35a shows the configuration that was used to measure the absorbance of the films or solutions. Quantitatively, for a reference in solution (A0 in Chloroform), we have ensured that the absorbance measured @ 635 nm given was the same compared with measurement from CARY100 (Figure 35).
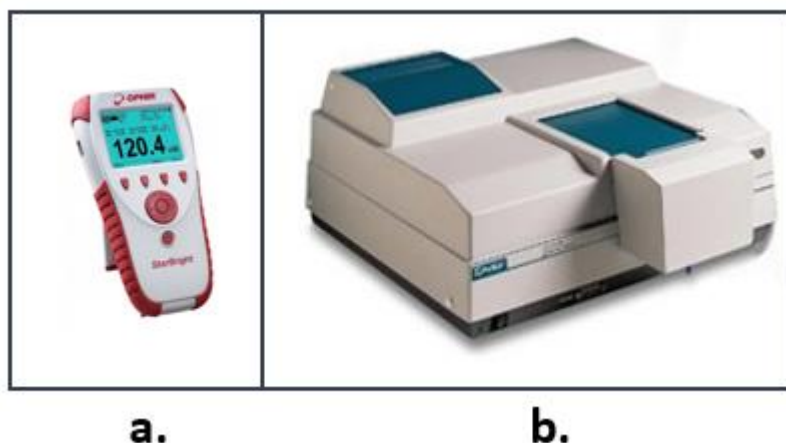
Figure 36. a) Power-meter used to measure absorbance in real time. b) Spectrometer for measuring stationary UV-Vis absorption spectra.

II.F. Displacement tracking profile in real-time.

The main objective of this thesis is the quantification and rationalization of the displacement of the thin film (A+B) under UV or Visible irradiation. An automatic system combining an industrial microscope with the irradiation system presented above was developed in order to record the displacement of thin film in real time. A dedicated software has been developed, which was able to manage and store images coming from allowing to manage: i) the irradiations periods between UV and Visible (with a possible lag time in between); ii) the power of illumination; iii) the repetition cycles. The entire system was housed in a custom-built black box to avoid the parasite light.

In the following, we described step-by-step the "photodisplacement setup" and the related video tracking software and the final data treatment to obtain the displacement.

II.F.1. Displacement Measurement Set up

A rectangular strip (2 x 10 mm) with a typical thickness of 10-50 µm cut from spin coating thin films (either (A+B), (A0+B), (A+B0) or B alone) is clamped at least for 24H with a metallic tweezer in vertical position; the microscope objective is fixed @

90° with respect to the normal direction of the thin film as illustrated in Figure 37b. The two LEDS were kept with a separation distance of 7 cm from the film surface and a mutual angle of 20° (10° each from the normal direction).
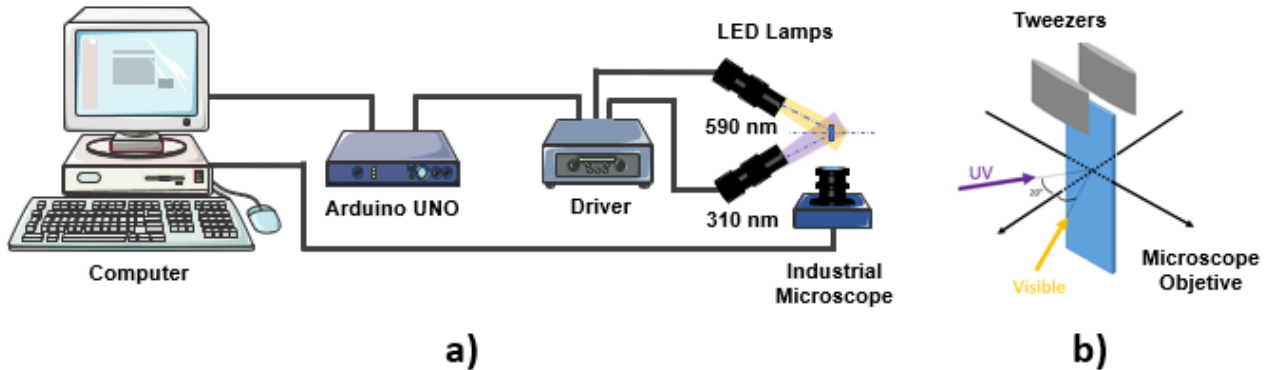
Figure 37. a) Connection diagram of the displacement measuring system. b) Clamping diagram in the displacement analysis.

An Arduino-UNO was used to connect the computer and driver which is the element to manage the power of the LED lamps (through the voltage supplied by the driver) and to register the rate of image acquisition through homemade software, Figure 37a.

II.F.2. Homemade Video Tracking software (LabVIEW)

The main screen of the software developed with LabVIEW for imaging, analysis, and irradiance control is displayed on Figure 38. The windows on the upper right-hand side allow real-time observation of the images captured by the industrial microscope, while the black background graphs show the displacement and angle analysis performed by the program. In the lower part there are windows for the introduction of storage paths, as well as paths for the storage of the analysis records. Likewise, the program allows performing a zoom calibration with respect to the lens of the industrial microscope for the purpose obtain the actual displacement measurement in units of micrometers or millimeters.
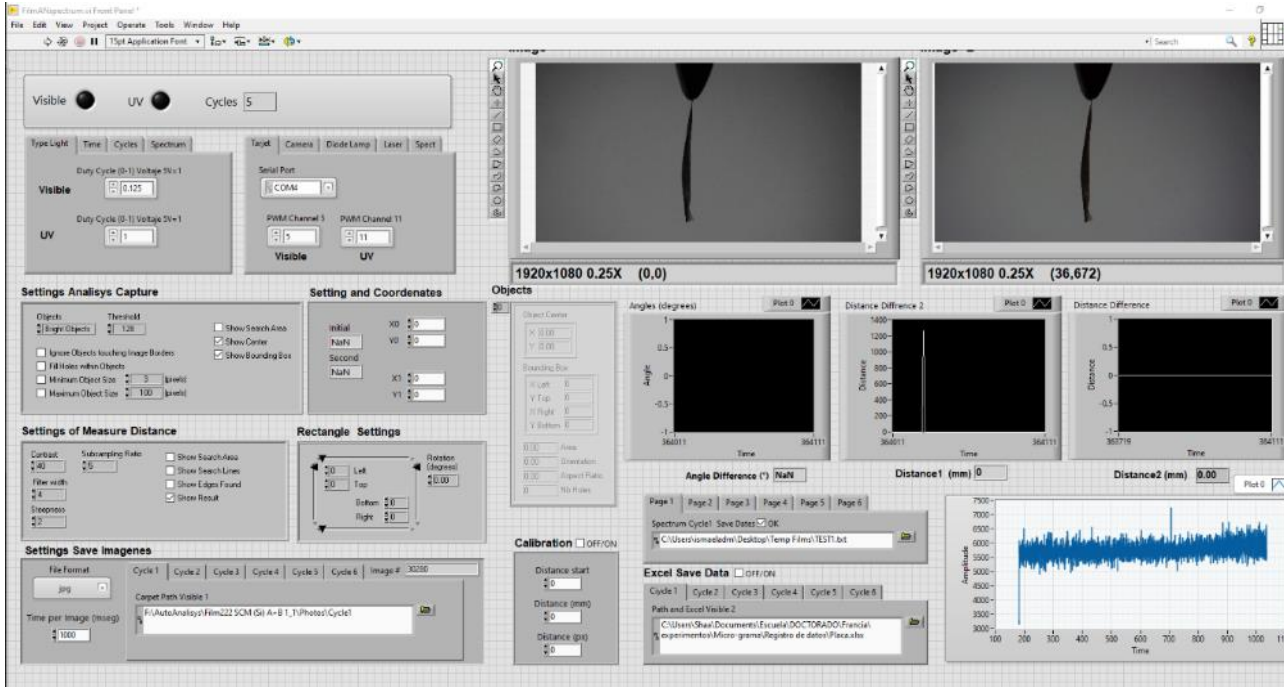
Figure 38. Display of the displacement measurement program developed for image storage, processing, and analysis, as well as manipulation of power and irradiation time of the films.

II.F.3. Post-processing analysis.

Figure 39 shows the scheme that defines the way in which the displacement of the film was calculated. The point $P_0\ (X_0, Y_0)$ (pixel coordinates) is the initial point arbitrarily taken in the first frame, then the displacement was measured by following the point P_0 in each of the subsequent frames P_{n+1} and calculating the distance traveled from each of these points with respect to the initial point

$$d_{P_0} = D_{P_n - P_0} - D_{P_1 - P_0}$$
$$= \left((\omega) * \sqrt{(X_n - X_0)^2 + (Y_n - Y_0)^2} \right) - \left((\omega) * \sqrt{(X_1 - X_0)^2 + (Y_1 - Y_0)^2} \right) \quad (6)$$

Where $\omega = 89\ mm/pixel$ is calibration factor associated with lens microscope that factor converts pixel distance to mm.

52
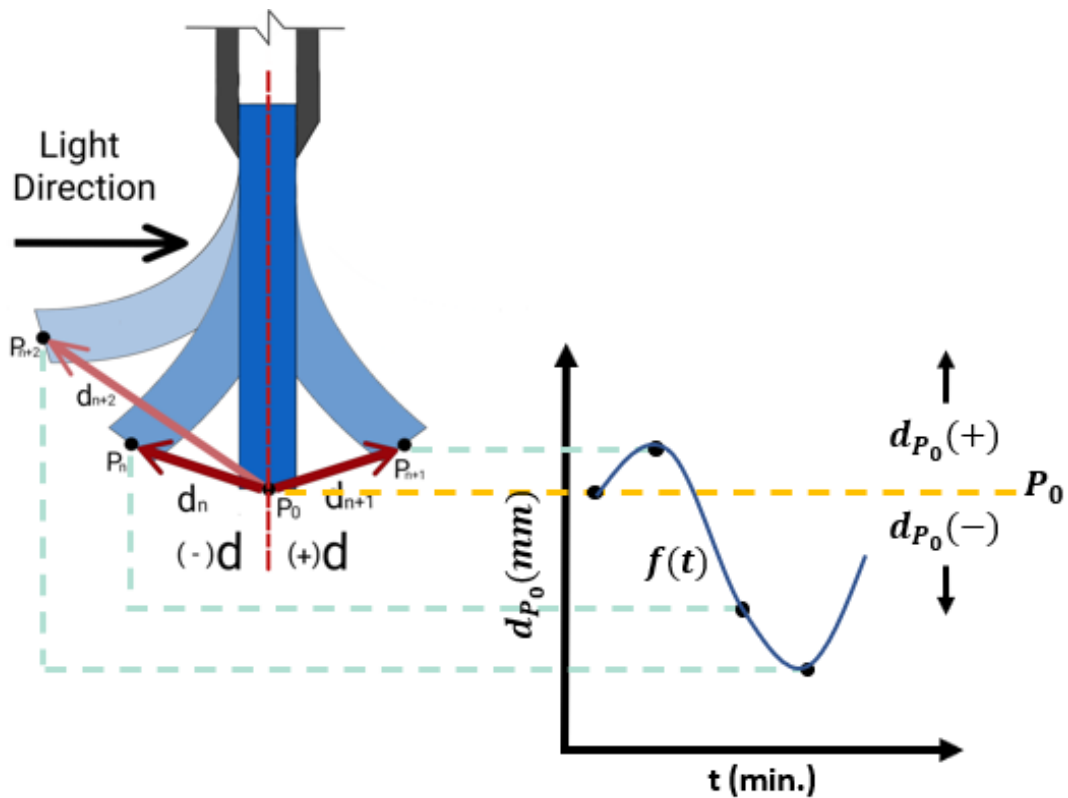
Figure 39. a) Schematic of the displacement distance calculation performed by the films.

Although the software developed in LabVIEW is capable of performing this analysis, it was chosen to do it by using the ADOBE AFTER EFFECTS program, with which more accurate measurements were obtained. The results consist of a curve $d_{P_0} = f(t)$. When the film moves to the right (toward light direction), the signal is rising and when the film moves to the left (backward the light direction), the signal is decreasing. A negative signal means that the thin film position has moved on the left well beyond the starting point.

II.F.4. Precautions to avoid artefact measurements.

Due to the clips between the two tweezer branches, mechanical relaxation has been detected. The Figure 40 displays the displacement d_{P0} function of time of irradiation, just after the clips. One observes a drastic displacement
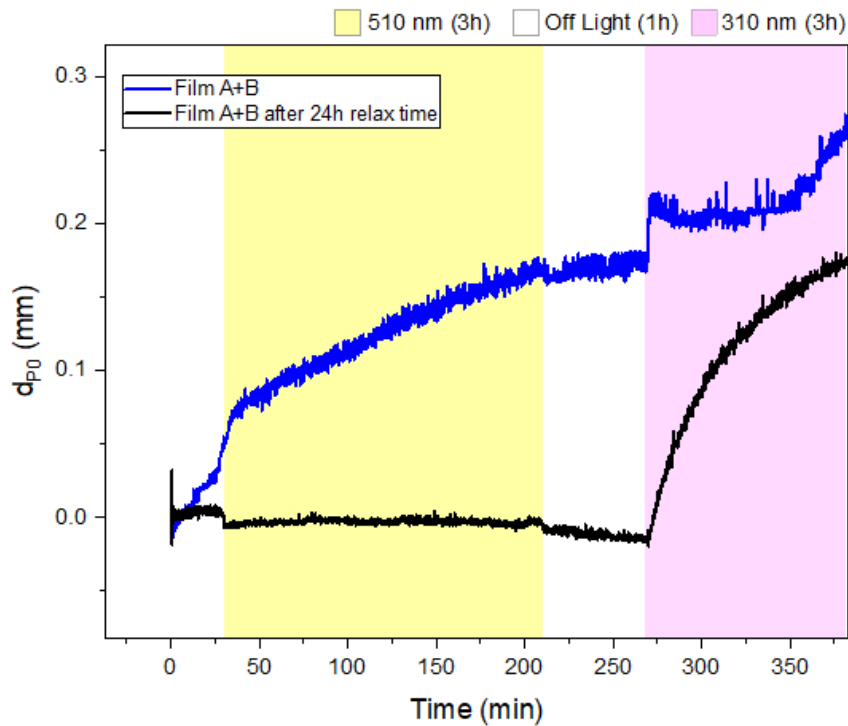
Figure 40. Initial displacement due to mechanical relaxation.

The mechanical relaxation that the films undergo when handled during mounting is shown in Figure 40. This behavior will be avoided by leaving the films mounted in the clamps without any manipulation (relax time) for a period of 24 hours prior to any displacement analysis.

II.F.5. Temperature measurement

To verify possible contribution of thermal effects due to light absorption, a thermal study was carried out, which consisted of monitoring the "In situ" temperature of thin film under various illumination cycles (displacement study, see irradiation system section). The monitoring was obtained by recording a film with a Quianli thermal camera with a measurement range of -20 °C to 120 °C, with an accuracy of ±5%. The camera was placed in two different positions as a way have a better compression of the heat conduction and to verify the thermal effects, Figure 41. The videos were analyzed using the software provided by the thermal camera manufacturer.

54
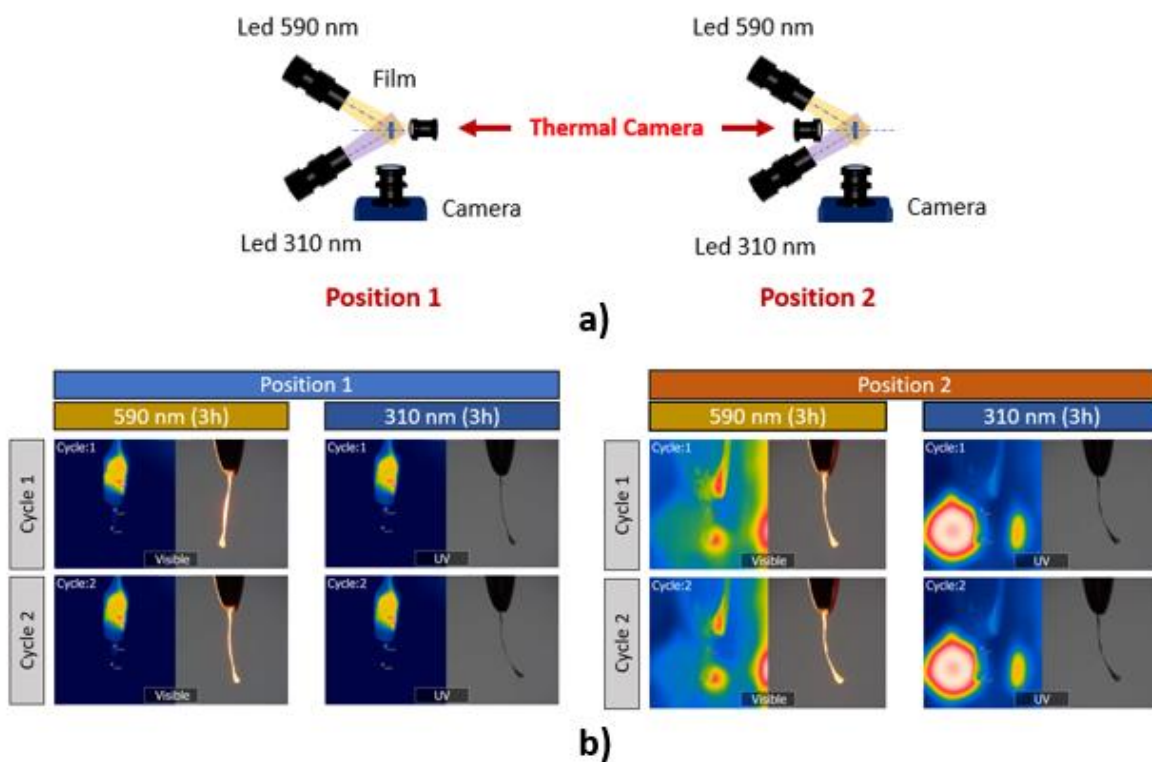
Figure 41. a) Scheme of the positioning of the thermal camera in relation to the illumination system. b) thermal photographs taken for two positions at the end of illumination for two cycles of alternating UV/Vis irradiation.

For the two positions, and the two successive cycles, the temperatures have been found to vary between 23°C to 27°C – far from the T_g (-50 °C) of the B elastomers [63], [65] which proves that:

> *The photomechanical effects present throughout this manuscript are clearly not related to photothermal processes.*

CHAPITRE III

Photochromic and Luminescent Properties of Thin Films (DTE-UPy, PEB-UPY)

As evidence, before focusing on the photomechanical effect of DTE-UPy/PEB-UPy thin films, i.e. thin films (A+B), the first prerequisite is to assess the photochromic properties of the overall system. In the past, unlike the elastomeric case (A+B), the photochromic properties of A molecule dissolved in chloroform (A alone) have been published [23], [24].

The first objective of this chapter is therefore to determine the photochromism properties of the thin films (A+B) and compare them with the solution case. Then, one needs to figure out if the presence of the elastomeric units B –via the hydrogen bonding networks- affect the photoswitching processes or not. The main objective of this chapter is to present and rationalize the absorbance tracking profile results, first step to reach the objectives presented in the first chapter: a reversible photochromic thin film free of photodegradation is targeted.

Finally, following preliminary results in our group [63], we will pay attention to possible competitive luminescent mechanism for the photochromic thin films.

III.A. Supra-molecular species in solution

First, to have a better understanding of the supramolecular system in the elastomeric case, it is safe to have a clear picture of the species present in solution. A first inspection of the NMR spectra of A in d-chloroform presented in Figure 42 give a very important information. The NH proton-a located @ 13 ppm together with the NH protons (b,e) centered near 12.2 ppm are characteristic of the UPy dimer which suggest that the OF molecules interact each other's as cyclic oligomer (lack of free UPy units). Such cyclic species have been reported previously for other UPy- substituted diarylethene [2].
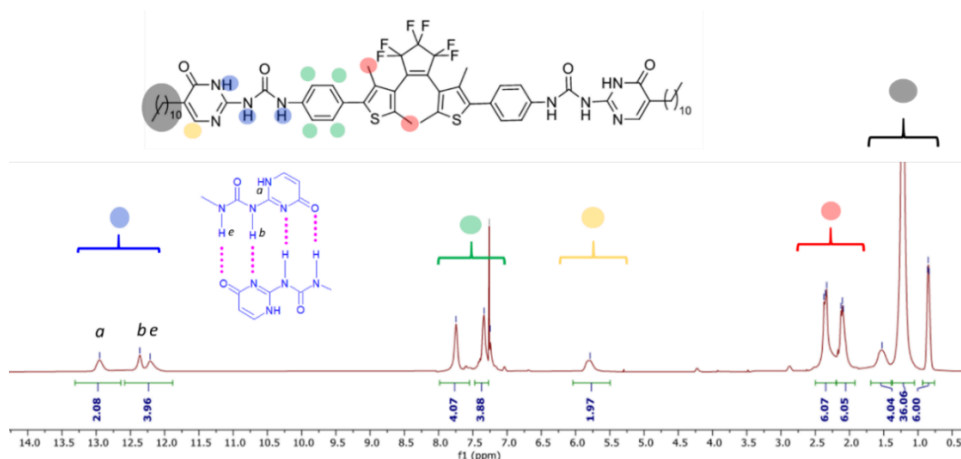
Figure 42. H-NMR spectrum of DTE-UPy (OF solution) in d-chloroform.

From Molecular Dynamics calculations [3], those cyclic species have been identified and presented in Figure 43:

- AP conformers dimers Figure 43a, with free UPy does not exist (according to NMR results above).

- P conformers Figure 43b may self-associated due to ideal UPy mutual orientation. We have reported in the past that addition of elastomer B probably dissociate such dimers.

58

- Instead, AP conformers are found inside cyclic quadrimer species engaging 3 antiparallel (AP) conformers and one parallel (P) conformer. Note that the existence of such stable cycle structures justifies the rise of temperature during the thin film protocol to allow appropriate A and B blending.

Then, *what is the influence of such cyclic structures on the photochromic performances?* according TDDFT calculations of DTE-UPy molecule, no electronic delocalization (from the photochromic core to the UPy moieties) have been noticed and regular photochromic properties are expected. Anyhow, due to the complicate chemistry of UPy units, it is safe to review the photochromic properties of molecule A in solution first before investigating the elastomeric case.
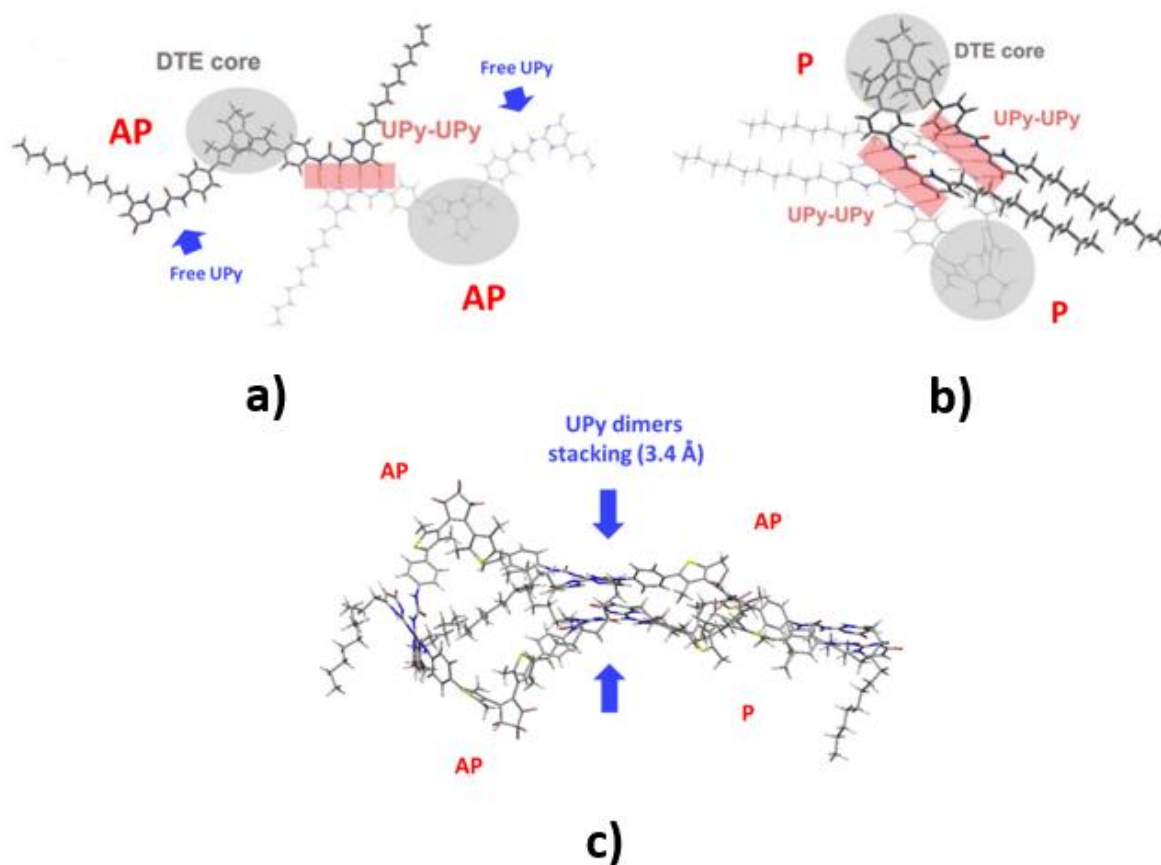
Figure 43. a) Snapshot from Molecular Dynamic calculations for distinct species: AP dimer a) P dimer b) cyclic tetramer (3AP,1 P), [62].

III.B. Photochromism of DTE-UPy in solution

III.B.1.Qualitative characterization

The absorption spectrum of a DTE-UPy in chloroform is show on Figure 44a. First, the colorless OF solution gets a characteristic band in the UV region peaking at 296 nm. After irradiating with 310 nm light, photocyclization is initiated and the solution turns to blue color. The OF absorption bands decreases giving rise to a new band peaking @ 586 nm with an isosbestic point located @ 320 nm. After 2H of irradiation, the photostationary state (PPS) is reached with a conversion efficiency of 70 % close to the 76% DTE value. This suggests that both UPy-UPy hydrogen bonding or the existence of small cyclic dimers does not prevent the photoswitching processes from taking place.
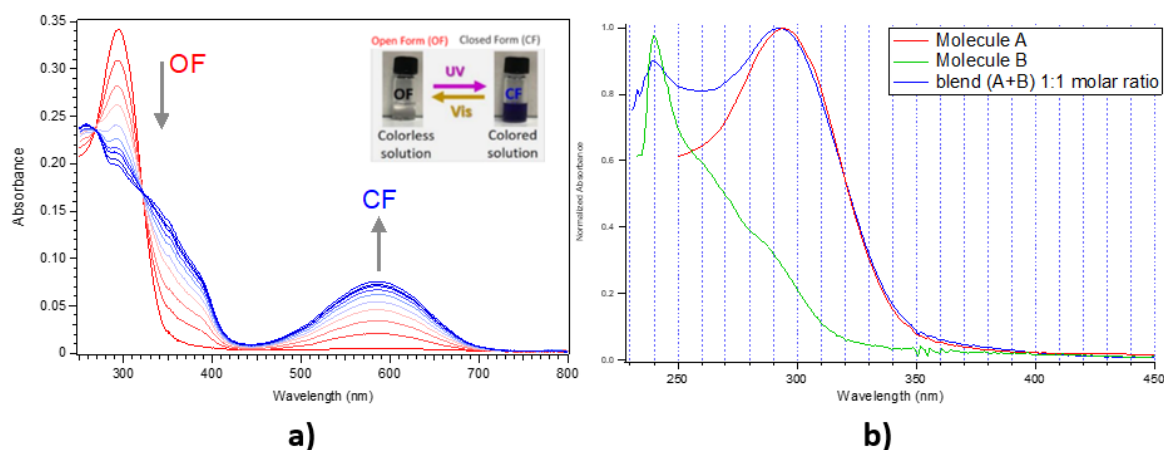
Figure 44. a) Absorption spectra of DTE-UPy solution in chloroform for the OF (red line) and PSS (blue line) with the characteristic band for CF in the visible region after being irradiated with 310 nm at room temperature (picture of the solution before and after irradiation); b) normalized absorption spectra for solution in chloroform of molecules A, B and blending of (A + B) for a molar ratio 1:1.

The spectra of B in chloroform are displayed as well in Figure 44b. It worth to notice that in solution the elastomer gets a maximum of absorption near 240 nm; concerning the typical working wavelength in the UV-310 nm, the DTE gets an absorbance 6 times higher compared with the elastomer. The extinction coefficient has been determined both molecules and the results are displayed in table 2. Note that for comparison we have also included the results for A0 molecule (commercial DTE).

A closer inspection of this table highlights the much higher coefficient extinction for DTE-UPy conformers compare to DTE value, for both OF conformers (factor 2.2) and CF conformers (factor 1.5). This effect is probably due to the UPy self-association ability reported above.

	PHOTOCHROME											ELASTOMER		
	Spectroscopic parameters								Photochromic parameters			Spectroscopic parameters		
	OF			CF					OF		CF			
	λ_{max}	ε (λmax)	ε (310 nm)	λ_{max}	ε (λmax)	ε (310 n)	ε (590 nm)	ε (635 nm)	ϕ_{cycl}	% Conversion (OF→CF)	ϕ_{rev}	λ_{max}	ε (λmax)	ε (310 nm)
A0 (Chloroform)	272	2.8	0.6	570	1.1	1.3	1.1	0.5	0.54	76	0.021			
A (Chloroform)	289	6.2	4.8	586	1.7	3.1	1.7	1.2	0.36	70	0.018			
B (chloroform)												240	1.1	0.4
(A+B) (Thin film)				607					0.0007	-	0.0002			

Table 2. Spectroscopic and photochromic parameters for A0, A, B compounds in solution and (A+B) thin film. All the ε units are (10^4 L mol^{-1} cm^{-1}); the λ units are nm.

III.B.2. Quantum yield determination (in solution)

We have determined the absorbance tracking profile @ 635 nm with the new setup presented in the previous chapter. Note that for solution study the LED are rearranged in opposite direction and @ 90° with respect to the IR laser. The results are displayed on Figure 44 for successive illumination of UV light @ 310 nm (during 1h45) follow by illumination of Visible light @ 590 nm (during 1h45 as well). In order to deduce the quantum yield, the absorbance profiles were fitted with an IGOR Pro procedure[6] that fit the signal taking into account the differential equations for a simple kinetic model [63]. The inputs are the power of the LED, the volume of the solution, the extinction coefficient for OF and CF and the initial guess for the photocyclization/photoreversion rates.

---

[6] collaboration with Dr. Rémi Métivier

The quantum yields are included on table 2. For both DTE and DTE-UPy molecules. For DTE-UPy the photoreversion is 0.018 close to the 0.021 value of DTE. As already stipulated in the past with time resolved spectroscopy data [23], the reversion process is slight affected by the presence of the UPy moieties due to rigid photochromic core. Reversibly, the photocyclization yield at 0.54 for DTE drastically decrease to 0.36 for DTE-UPy. This effect is explained by the actual influence of the UPy moieties that pull apart the reactive carbon atoms during their mutual attraction. Note that the difference with the value published few years ago (ϕ_{cycli}=0.17) [23] stands for the more approximative quantum yield determination (initial slope method).
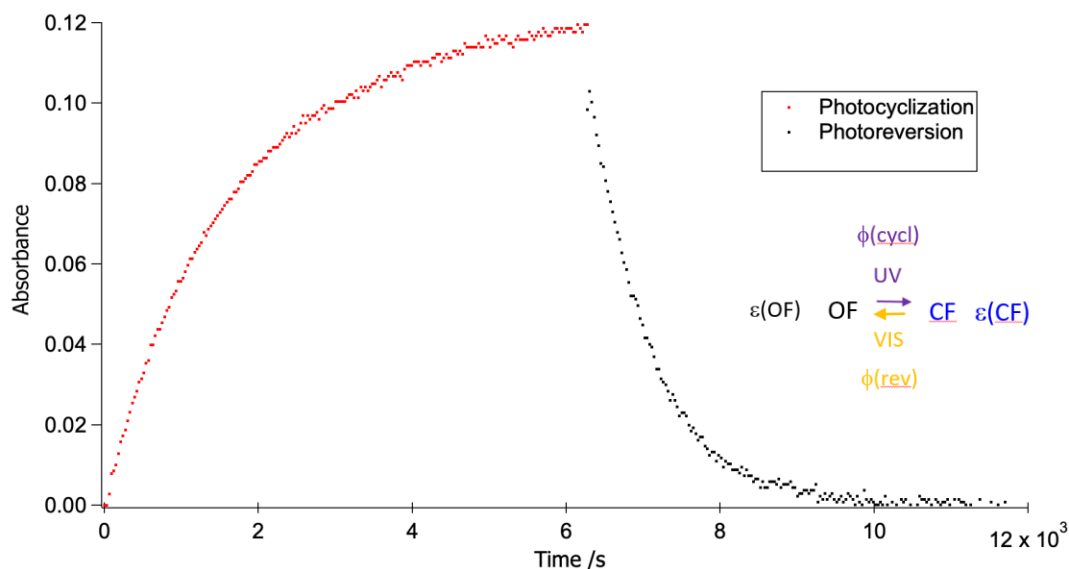
Figure 45. Absorbance tracking profile by measuring the absorbance @ 635 nm under 310 nm irradiation (during 3H) follow by 590 nm irradiation (during 3H).

III.C. Photochromic properties of DTE-UPy/PEB-UPy thin film

III.C.1. Qualitative characterization

Spectra. A thin film (A+B) is shown just after spin coating elaboration in one part and after 1 hour UV illumination in another part. As in solution, films (A+B) change from amber to blue color when irradiated with 310 nm UV light. Successive

absorption spectra were acquired during the illumination process which allow to distinguish the characteristic band is observed in the visible region with a maximum peak at 607 nm (after subtraction of B contribution), Figure 46a. For wavelengths shorter than 350 nm the spectrum is limited by saturation. Comparison of this spectra with the solution case is displayed on Figure 46b. From solution to elastomeric environment, a bathochromic shift of ~20 nm is noticed while the Gaussian width of the quasi-unaffected (less than 100 cm^{-1}). The photochromic unit seem to be operative in their elastomeric environment.
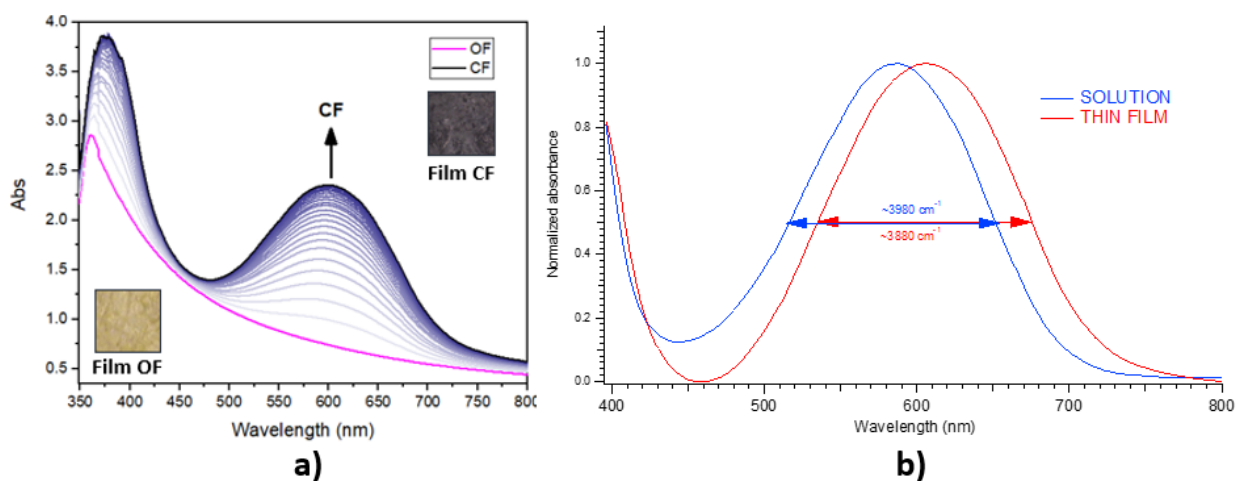
Figure 46. a) Thin film absorption spectrum of DTE-UPy. Sample illuminated with 310 nm UV lamp. b) the absorption spectra in solid and solution.

Kinetics $A = f(t)$. The kinetic of coloration (310 nm excitation) or discoloration (590 nm excitation) of the thin films (A+B) were determined by measuring the 635 nm laser absorbance in the right edge of the CF band (experimental details are given in Chapter II). Figure 47 shows the normalized absorption kinetics described for the photocyclization (black line) and photoreversion (red line) processes for a similar power of illumination (690 µW). At first glance, the discoloration kinetic (photoreversion process) is approximately 2 times faster than the coloration kinetic (cyclization process).
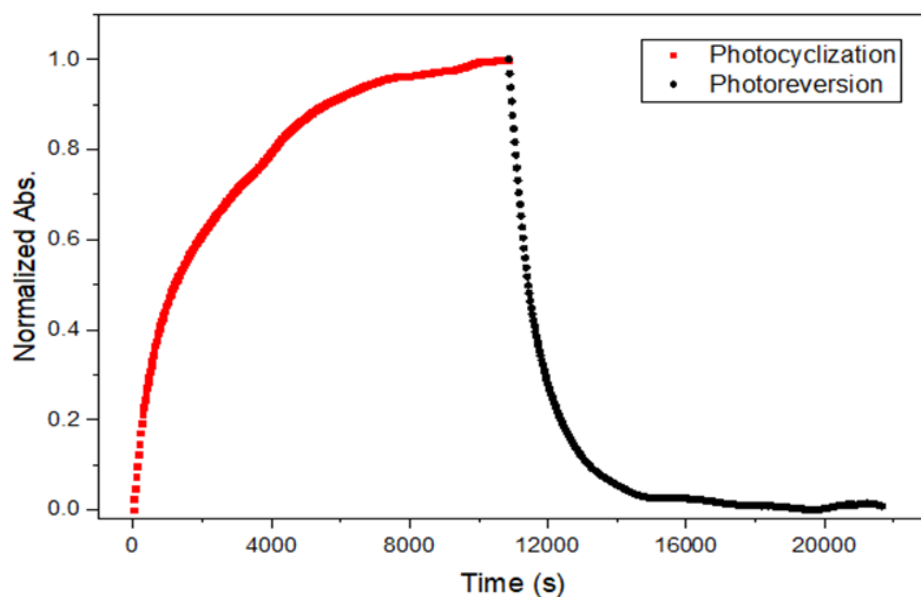
Figure 47. Normalized absorbance @ 635 nm of a DTE-UPy film.

For a similar irradiation power, a quasi-complete photoconversion (97%) is achieved in about 64 min for photoreversion while for the photocyclization process it takes 140 min. At first glance, taking into account results in solution (see above), this result was not expected because the photocyclization yield is 200 times larger than the reversion process. However, this result is rationalized considering that:

- for 310 nm illumination, the contribution of the elastomer is not totally negligible the ratio $\varepsilon_A/\varepsilon_B$ being close to 6.
- The penetration of the light is much more efficient for the visible compared to the UV.

Illumination periods. On the other hand, the kinetics measurements allow to design the illumination cycles. Since 100% of the absorption in the photocyclization process is around 3h, this period of time will be perfect to start the studies of the photomechanical effects. Another time to consider is the period of 1h, during this period return to the zero value. In this same period the absorption in the photocyclization process reaches 78%, which can guarantee the reversibility of the process.

III.C.2. Quantum yield determination

III.C.2.1. Mathematical model

A lot of attempts have been made in the past to give a mathematical description of the kinetics of photochromic systems, both in solution [66–68] and at the solid state [69], [70]. Unlike the solution case for which mathematical model is able to fit properly experimental data [68], [71], the solid case is much trickier to decipher taking into account the anisotropy of the system compared to the homogenous solution under magnetic agitation. In the following, we will present a mathematical treatment for reproducing coloration/discoloration kinetics for photochromic thin film based on the excellent paper of Bertarelli and coworkers. [72].
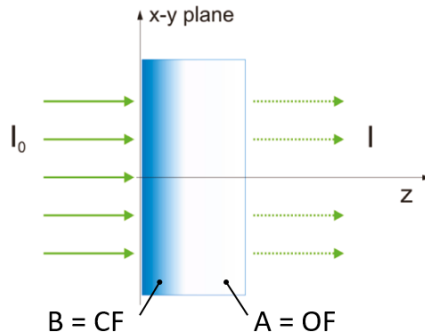
Figure 48. Progression of the Light-Triggered conversion across the film thickness.

The model that describes the uniform illumination of a photochromic film can be conveniently represented as the progression of the conversion profile through the thickness of the film, as sketched in Figure 48 illustrating the gradient between OF and CF. The fraction of molecules in each state varies along the z axis and with time t and can be defined as follows:

$$x_A(z,t) = \frac{N_A(z,t)}{N} \tag{7}$$

$$x_B(z,t) = \frac{N_B(z,t)}{N} \tag{8}$$

$$x_A + x_B = 1 \tag{9}$$

Where N_A and N_B are the number of molecules in OF and CF respectively. It is worthwhile defining $\varepsilon_A(\lambda)$ as the absorption cross section of species A and $\sigma_A(\lambda)$ as the interaction cross section for molecules in state A to absorb a photon to induce the transition to state B. The ratio between the interaction cross section and the absorption cross section gives the well-known quantum yield of the photoreaction, which is the probability of the transition from A to B:

$$\phi_{A \to B}(\lambda) = \frac{\sigma_A(\lambda)}{\varepsilon_A(\lambda)} \tag{10}$$

The quantum yield for backward reaction B to A will be similar defined

$$\phi_{B \to A}(\lambda) = \frac{\sigma_B(\lambda)}{\varepsilon_B(\lambda)} \tag{11}$$

Considering uniform photon flux @ the irradiated surface $(I(0,t) = I_0)$, and considering first-order kinetic rate, the population of A molecules is expressed as:

$$\frac{dx_A(z,t)}{dt} = -I(z,t)\varepsilon_A(\lambda)\phi_{A \to B}(\lambda)x_A(z,t) \tag{12}$$

Then, after integration between the surface (z=0) and position z, the photon flux at position z is expressed as:

$$I(z,t) = I_0 exp\left[-\int_0^z A(z',t)dz'\right] \tag{13}$$

here the total absorbance takes now into account both A and B species:

$$A(z',t) = \varepsilon_A x_A(z',t)C + \varepsilon_B(1 - x_A(z',t))C + \alpha \tag{14}$$

Where C is the concentration of photochromic units and α represent the absorption of the polymer matrix non negligible for UV excitation.

66

The exact analytical solution of mathematical problem is not straightforward, and the explicit derivation can be performed only in two particular cases:

(i) Photoreversion

(ii) Photocyclization exciting an isosbestic point

(iii) Otherwise, numerical methods are required

CASE 1 – PHOTOREVERSION ($\varepsilon_A = 0$; $\alpha = 0$; $\varepsilon_B \neq 0$)

We are dealing with the discoloration process (B→A) under visible excitation for which both the A form and the polymer does not absorb ($\varepsilon_A = 0$; $\alpha = 0$). The photon flux detected by the photodiode –considering the appropriate extinction coefficient ε_B^d - along the film thickness simplified as:

$$I(z,t) = I_0 exp\left[-\int_0^z \varepsilon_B^d x_B(z,t)Cdz'\right] \tag{15}$$

The fraction of the B form can be analytically derived, as follows:

$$x_B(z,t) = \frac{1}{1 + e^{-\varepsilon_B^d Cz}(e^{kt} - 1)} \tag{16}$$

Where the conversion rate contains the targeted value $\phi_{B\rightarrow A}$ for the excitation wavelength considering the appropriate extinction coefficient ε_B^e:

$$k = I_0 \varepsilon_B^e \phi_{B\rightarrow A} \tag{17}$$

From previous equations, and appropriate integration between 0 and the whole thickness D, the time dependent absorbance results in

$$A(t) = ln\left[1 + \left(e^{\varepsilon_B^d CD} - 1\right) \cdot e^{-kt}\right] \tag{18}$$

Note that the normalized CF spectra presented in Figure 46, the ratio between the two-extinction coefficient:

$$\left(\frac{\varepsilon_B^d(635\ nm)}{\varepsilon_B^e(590\ nm)}\right)_{elastomer} = 0.94 \approx 1 \tag{19}$$

CASE 2 – PHOTOCYCLIZATION @ isosbestic point ($\varepsilon_A = \varepsilon_B = \varepsilon$; $\alpha \neq 0$)

Here, we are dealing with the coloration process ($A \circledR B$) under excitation on the isobestic point in the UV part of the spectrum wich allow to simplify the above equations because $\varepsilon_A^e = \varepsilon_A^e = \varepsilon$; the elastomer does absorb as well ($\alpha \neq 0$). In this case, the fraction of the A form is analytically express as:

$$x_A(z,t) = \exp\left(-e^{-(\varepsilon C + \alpha)z} \cdot kt\right) \tag{20}$$

Where the kinetic rate is defined as:

$$k = I_0 \varepsilon \phi_{A \to B} \tag{21}$$

However, for convenience, we have chosen to track the B species rather than the A species. Then, one needs to assess the following integral

$$A_B(t) = \int_0^D \varepsilon_B^d x_B(z,t) C dz' = \int_0^D \varepsilon_B^d C (1 - x_A(z,t)) dz' \tag{22}$$

Introducing the (upper) gamma incomplete function defined as

$$\Gamma(s,x) = \int_x^\infty t^{s-1} e^{-t} dt \tag{23}$$

The analytical solution is easily express as:

$$A_B(t) = \varepsilon_B^d C D \left(1 - \frac{1}{(\varepsilon C + \alpha)D} \left\{\Gamma\left(0, e^{-(\varepsilon C + \alpha)D} kt\right) - \Gamma(0, kt)\right\}\right) \tag{24}$$

III.C.2.2. Experimental Protocol

The initial plan was to follow the experimental protocol proposed by Bertarelli *et al.* with a precise determination of several parameters prior to photo(de)coloration measurements. The step-by-step measurements can be summarized as follow:

i. The concentration C (molecules/m^3) in photochromic units given by

$$C = \frac{w\%\rho N_A}{M} \tag{25}$$

Where *w%* is the weight amount of photochromic units of molar mass M dispersed in the thin film; ρ (g/m^3) is the density of the elastomeric film; N_A the Avogadro number.

ii. The film thickness D determined by common techniques (spectral reflectance, ellipsometry)

iii. The extinction coefficients (m^2/mol) for both the OF and CF assessed in a way similar to that for the solutions, i.e. applying a linear fitting on the absorbance of thin films to different thicknesses:

$$A(\lambda) = e(\lambda)D \implies \varepsilon'(\lambda) = \frac{e(\lambda)}{C} \implies \varepsilon(\lambda) = \varepsilon'(\lambda)N_A \tag{26}$$

iv. Absorbance changes with time under UV or Visible illumination, i.e. $A_{CF}(\lambda) = f(t)$ Monitored @ CF edge (635 nm).

Fitting the kinetic by analytical equations (18) or (24) or alternatively by numerical approach allow to determine the kinetic constant (equations (17 or 21) and using the extinction coefficients and the intensity of light, the final quantum yields are deduced $\phi_{A \to B}$ or $\phi_{B \to A}$.

III.C.2.3. Final results and comments

Unfortunately, we were not able to experience a control on the thickness of our thin film elaborated with spin coating (due to material limitation, we were not able to multiply the tests). An alternative was to use a thermal hydraulic press [63] with rectangular mold cut into aluminum foil of known thickness (10, 13, 17 ,20 µm). The final films were characterized by thicknesses measured with profilometer with a range between 15µm and 22µm with poor uniformity. Because the graphic $A(\lambda) = f(D)$ was not linear, we were not able to determine the extinction coefficient in the solid state. By consequence, we have taken the decision to make the hypothesis

$$\varepsilon(\lambda)_{solid} \approx \varepsilon(\lambda)_{solution} \tag{27}$$
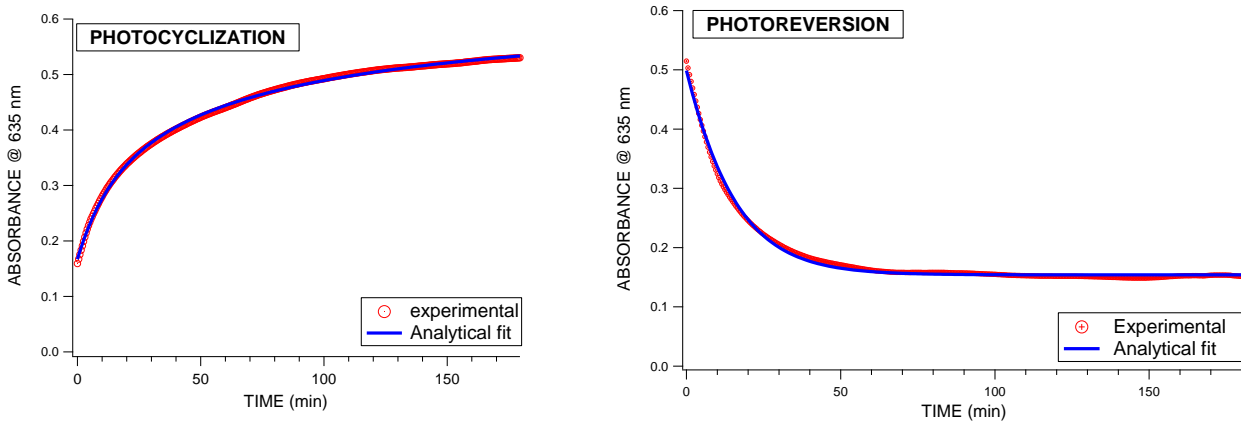
Figure 49. Fitting the experimental kinetic absorbance change with the equation (20) and (24) in the case of photocyclization (left); with equation (18) in the case of photoreversion.

From the fitting curves, we have deduced the kinetic constants k and according to the approximation make above, we have deduced

$$\phi_{cycl} (310 \, nm) = 0.007$$
$$\phi_{rev} (590 \, nm) = 0.002$$

As seen in table 2, compare to the solution case, those values are divided by a factor 6 for reversion and a factor 90 for cyclization case. By considering that our assumptions depicted above are acceptable, the more serious effect to the elastomeric matrix B on the DTE A is quite expected. Indeed, as already prove by our group with time resolved spectroscopy, the photochromic core is much more influenced by the UPy bonds for the flexible OF compared to the more rigid CF [23], [24]. The effect is easily understood in terms of telechelic UPy quadruple hydrogen bonding (either AA or AB) pulling apart two reactive carbons making the photocyclization reaction more difficult to proceed. Reversibly, for the CF this effect is not present due to the rigidity of the central CC bond.

Alternatively, the so low value for ϕ_{cycl} is probably related with the elastomer contribution –the term α- that is omnipresent for more than 10 µm thickness of material (saturation of the absorption spectra for example). In the future, we will need a new precise measurements campaign that include different thicknesses but starting from quasi-nanometric order of magnitude (for example, 0.1µm-10µm) to better stick on the protocol of Bertarelli *et al.*

III.C.3.Characteristic times and reversibility

To test the reversibility of the system, we have operated 6 successive irradiation cycle of 1h duration, for a colorless OF film, starting with visible light (to purge the CF traces present in the film). The results are presented in Figure 50.

Reversibility. For the first irradiation cycle -1h of UV and then Visible light -we recover 98% of initial absorbance. Then, cycle after cycle, this quantity rises to 99.9% for the sixth cycle. Note that, at the end of the entire irradiation process, the film has been dissolved into chloroform and no photodegradation has been notice. Clearly, the supramolecular UPy-UPy surrounding of the photochromic unit does not alter its photoswitching ability.
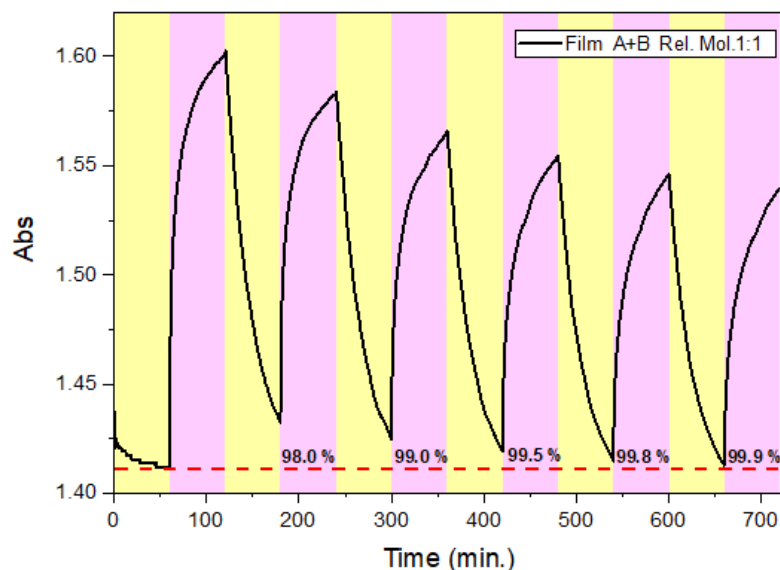
Figure 50. Absorption of a film (A+B) subjected to 6 cycles of alternating UV/Vis irradiation (310 nm, 590 nm at 796 µW).

Kinetic analysis. With the purpose of deducing characteristic time for the photoswitching processes, we were looking for alternatives approaches in parallel to the mathematical models for which numbers of simplifications are required. We have analyzed the kinetic curves $A_{CF} = f(t)$ with a very simple empirical model based on multi-exponential function, the results being presented in table 4. After different test paying attention to the χ^2, it has been found that for the photocyclization process ($OF \circledR CF$), the best fitting function was a bi-exponential model

$$A_{CF}(t)_{UV} = A_1 e^{-\left(\frac{t}{\tau_1}\right)} + A_2 e^{-\left(\frac{t}{\tau_2}\right)} \tag{28}$$

Reversely, for photoreversion (CF→OF) the best fitting function was mono exponential:

$$A_{CF}(t)_{Vis} = A_3 e^{-\left(\frac{t}{\tau_3}\right)} \tag{29}$$

72

Cycle	x_1	$\tau_1(min)$	x_2	$\tau_2(min)$	A_3	$\tau_3(vis)$
1	0.44	1.2	0.56	17.9		
2	0.43	1.3	0.57	18.5	0.195	28.8
3	0.4	2.1	0.6	26	0.181	28.3
4	0.35	2.2	0.65	28	0.166	26.9
5	0.32	2.4	0.68	32	0.154	26.1
6	0.31	2.8	0.69	35	0.146	25.9

Table 3. Values of magnitude of characteristic times from fitting the absorbance (Figure 50).
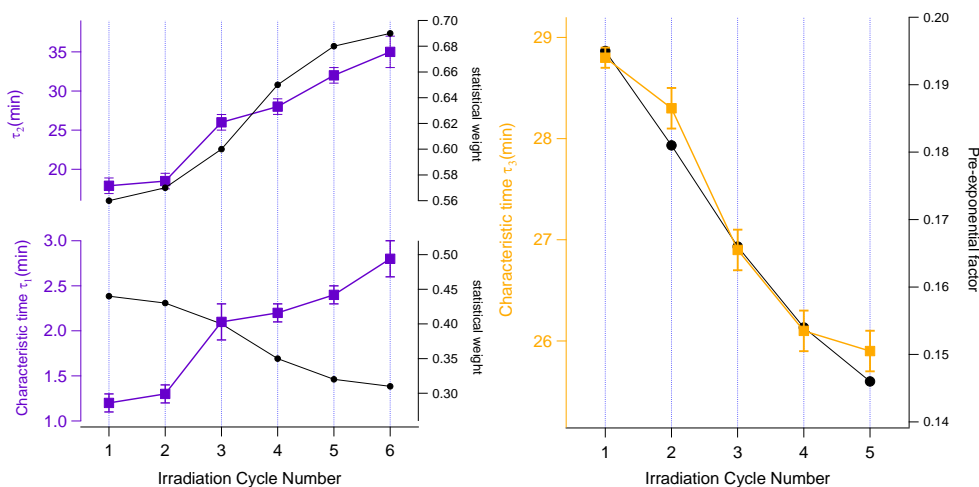
Figure 51 Characteristic times from fitting the absorbance irradiation a) UV and b) visible.

Characteristic time for photoreversion. Besides the mathematical model, we have fitted the discoloration kinetic with the mono exponential function for each cycle. A characteristic time of 28.8 min is find for the first cycle and it decreases – cycle after cycle- down to 25.9 min accounting for a faster process. In parallel, the pre-exponential factor A3 is decreasing as well. Both observations indicate than the quantity of CF to revert is slightly decreasing from one cycle to the next one, which corroborates the decreasing percentage of non-converted form after each cycle. Probably, by choosing a longer irradiation time for the Visible sequence, (for example, 1h30 instead of 1h) may allowed to suppress this effect in order to reach perfect reversibility since the first cycle.

Characteristic time for photocyclization. The two-exponential behavior for the coloration kinetic is trickier to rationalize. Two characteristic times are necessary to

fit the experimental points, one short time τ_1 ranging from 1.2 to 2.8 min and one longer time τ_2 ranging from 17.9 to 35 min. Indeed, cycle after cycle, those two times show a constant increase until reaching a value up to a factor two. However, paying attention to their statistical weight - $x_1=a_1/(a_1+a_2)$ or $x_2=a_2/(a_1+a_2)$ – the short time contribution loose its contribution for almost 15% in benefit to the long-time contribution. Let us try to rationalize such effect.

Two exponential behaviors of photochromic units in solid state have been reported in the literature. Contrasting with the mono-exponential behavior observed in solution, the bi-exponential discoloration kinetics of nanocrystalline spiropyrans have been reported recently by Garcia-Garibay *et al.*, who explained it in terms of molecular packing influence on the photoinduced Z and E merocyanine conformations [73]. Recently, our group have reported for A0 in solid state (either crystalline or amorphous fase) photoswitching kinetics detected by wield field microscopy (see figure 53). First, it is interesting to mention that the photoreversion kinetic was mono exponential as our elastomeric system. Following the analogy crystal vs supramolecular system, the photocyclization kinetic has been found to be described by a biexponential as well including a smaller and bigger characteristic time, i.e. τ_1 and τ_2) respectively. Computing the ratio for those two times is instructive:

	$\dfrac{t2}{t1}$
A0 **CRYSTAL**	15.2
A0 **AMORPHE**	14.7
(*A* + *B*) **#1**	14.9
(*A* + *B*) **#2**	14.2
(*A* + *B*) **#3**	12.4
(*A* + *B*) **#4**	12.7
(*A* + *B*) **#5**	13.3
(*A* + *B*) **#6**	12.5
(*A* + *B*) **SOLUTION**[7]	6.5

Table 4. Ratio of times τ_1 and τ_2.

---

[7] The photocoloration kinetic in solution is not well fitted by a two-exponential function.

First, this result corroborates nicely the macroscopic observation with the microscopic measurements. Then, it may suggest that the local ordering around the photochromic core is altered by the successive irradiation. It will be interesting to verify this hypothesis with the help of X-rays analysis during chapter V.

Another possible explanation can be related with the AP/P content inside to elastomeric matrix taking into account the different cyclic species presented above. A simple kinetic model including AP/P interconversion (constant rates k_1 and k_2) and photocyclization $k_3 = I_0 \varepsilon(AP)\phi_{AP \to CF}$

$$AP \underset{k_2}{\overset{k_1}{\rightleftharpoons}} P$$
$$AP \overset{k_3}{\longrightarrow} CF$$
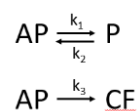
Exact analytical Resolution of the kinetic equations and initial condition $[AP]_0 \neq 0$, $[P]_0 = 0$ and $[CF]_0 = 0$ leads to [74]

$$[CF] = [AP]_0 \left[1 - \frac{k_3(k_2 - \gamma_1)}{\gamma_1(\gamma_2 - \gamma_1)} e^{-\gamma_1 t} - \frac{k_3(k_2 - \gamma_2)}{\gamma_2(\gamma_1 - \gamma_2)} e^{-\gamma_2 t} \right] \tag{30}$$

Where γ_1 and γ_2 are the roots of the quadratic equation:

$$S^2 + (k_1 + k_2 + k_3)S + k_2 k_3 = 0 \tag{31}$$

The interconversion $AP - P$, k_2 constant will affect both kinetic constants and pre-exponential factors which may explain the trends of Figure 50. Indeed, taking into consideration the supramolecular $UPy - UPy$ networks- it can evolve, cycle after cycle to dissolve $P - P$ dimer species for example to create novel DTE elastomer interactions:

P-P + 3 BB → BBAPBBAPBB

Such kind of process will directly affect the constant k_2 (according to Le Chatelier law) and consequently the kinetics constants. All those arguments are speculative and additional experiments are required for future
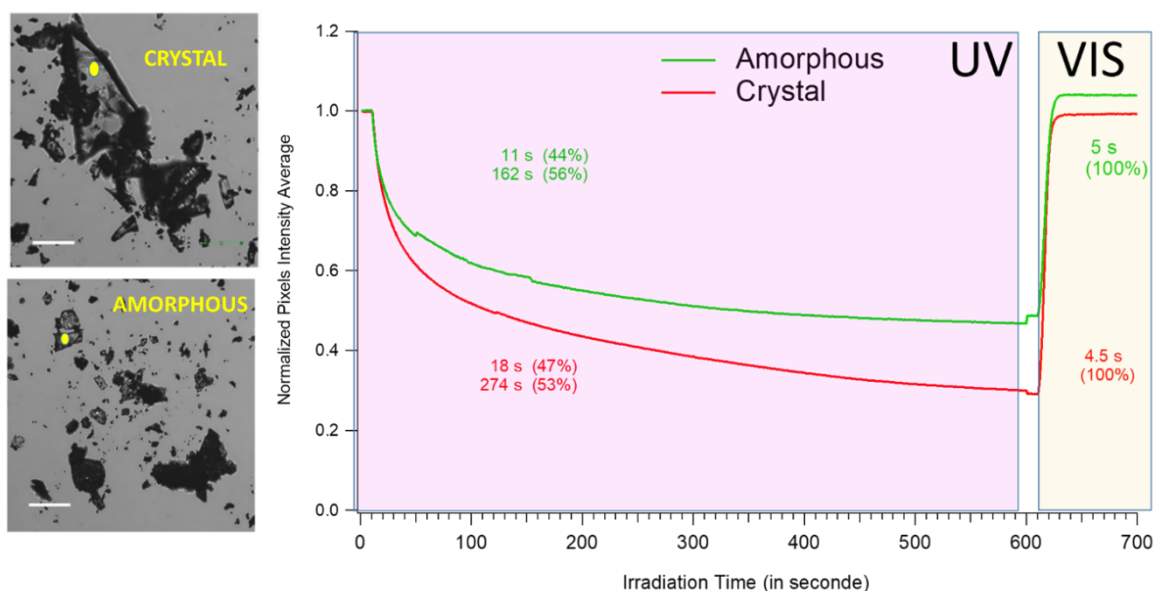
Figure 52. Wide–field microscopy snapshots of A0 in crystalline or amorphous phase in which a batch of pixels are indicated (left); Normalized Intensity function of time for the targeted pixels when A0 illuminated by UV or Visible light (see ref [63]).

III.D. Luminescent properties of the thin film

III.D.1. Observations.

During the video displacement tracking tests, we have noticed a strong White Light Emission (WLE) coming from some of thin film samples irradiated with UV light while such emission is not induced with Visible light. Pictures for two different blue thin film (A+B) and (A0+B) which have experienced several UV/Vis irradiation cycles are presented on Figure 53a. Unlike the (A0+B) thin film, the (A+B) sample displays a strong WLE but for part of the film that has been priory illuminated. Indeed, the yellow arrow Figure 53b (left side) the points the small region of the film trapped between the tweezer tips. In summary, the WLE is observed when:

- DTE-UPy molecules are present in the thin film; Neither B or (A0+B) spin coated thin films present such an emission.
- the thin film is irradiated with UV light; Visible light being inefficient for inducing WLE suggesting a special role for the OF species.
- the thin film is either in blue or colorless form.

- the sample has already experienced irradiation cycles: the intensity of the WLE increased with the number of cycles.

As already said, the photodegradation has been check after 6 cycles of UV-Vis irradiations, which exclude the enrolment of any side products.
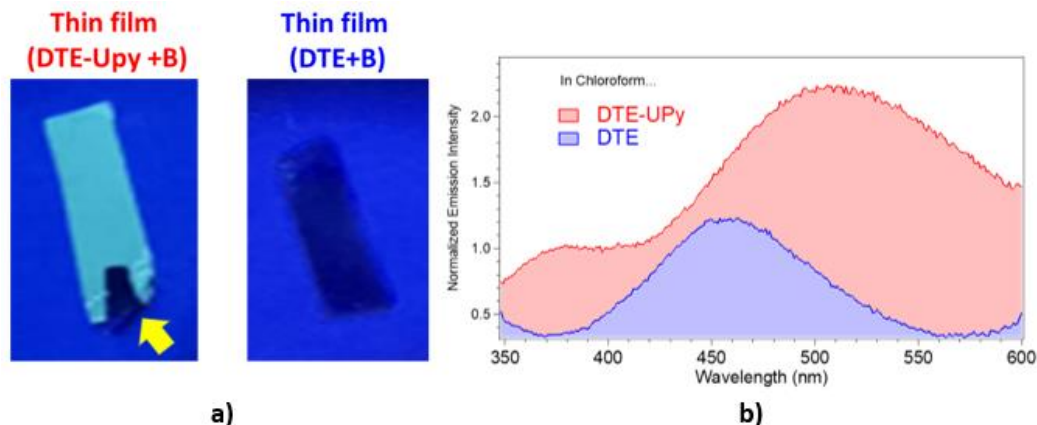
Figure 53. a) Pictures of thin blue films (A+B) and (A0+B) under UV irradiation (LED 310 nm), WLE was observed only for the (A+B) sample. The yellow arrow indicates a not illuminated area due to tweezer tip (up). b) Emission spectrum for A and A0.

III.D.1.1. Interpretations

To identify the nature of such WLE, we have register Emission Spectra in chloroform solution for A and A0 for OF and CF and elastomer B. Indeed, we were not able to register the Emission Spectra for the thin films with a regular Fluoromax spectrofluorometer and homemade optical fiber fluorometer is under construction in our group. Because the emission for elastomer B and CF isomers are lacking or negligible, only the spectra of the OF species for both A0 (DTE) and A (DTE-UPy) are compared for the 310 nm excitation (UV LED wavelength) on Figure 53b.

For A0, the emission spectra is peaking @ 460 nm with a gaussian width of G~2500 cm^{-1}. In contrast, for A molecules the emission spectra is characterized by a dual emission with an intense band peaking @ 510 nm (G~3200 cm^{-1}) and a less intense shoulder peaking @ 375 nm (G~7400 cm^{-1}). Note that this so broad spectra in solution is probably responsible for the WLE in thin film.

What is the hypothesis to rationalize the presence of WLE? A first hypothesis relies on the publication of Meijer group in 2016 reporting for UV induced fluorescence for telechelic UPy –polymers [75]. Based on IR spectroscopy and fluorescence, this UV induced fluorescence (after 16H of irradiation) is interpreted in term of photoenolization of the UPy units through a double UV induced exited sate proton transfer. Indeed, considering the UPy dimer (AADD sequence where A refers to hydrogen bonding acceptor and D refers to hydrogen bonding donors), the longtime UV irradiation induced:

$$AADD \overset{UV}{\rightarrow} DDAA$$
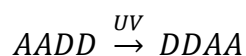
As illustrated in the Figure 54. Note that such an effect would be possible for the DTE-UPy ^{0}UPy-DTE dimer (with the additional $C_{11}H_{23}$ alkyl chains) to justify why such an effect is not observed for PEB-UPy - UPy-PEB analog.
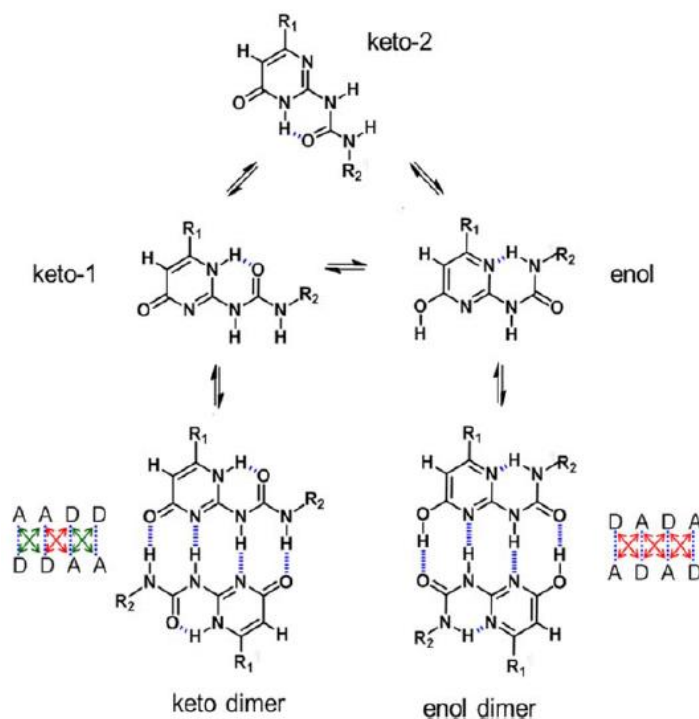
Figure 54. UPy-tautomer and dimerization. Equilibria between monomers and dimers of the three known tautomeric forms UPy. Secondary electrostatic repulsive interactions between two hydrogen bond donor (D) or two hydrogen bond acceptors (A) in a dimer are indicated by the red arrows (based on Beijer et al., 1998) [73,74].

A second hypothesis focused on the photochromic units and the Aggregation Induced Emission process (AIE). Dong et al. have published a pionner study [76] with the synthesis and photophysical study of a series of molecules combining a photochromic core (DTE) functionalized with tetraphenylene – well known chromophore displaying AIE (see Figure 55a) through p-stacking effect [77].

This group have shown that for OF conformers dissolved in pure THF solvent, no emission is observed under 365 nm excitation (for this wavelength, the photochromic yield is low). Then, when increasing the fraction of water up to 90%, a strong AIE takes birth due to stacking of tetraphenylene moieties. Then, irradiating this latter sample with 254 nm light induces the photocyclization and the AIE is quenched by the CF isomers.

In our case, considering PEB-UPy, both UPy units and urea linkers display strong abilities to aggregate with p-stacking process (Figure 55b); the DTE-UPy is known to aggregate as well, the dramatic example being the blue precipitate [61]. In this context, the final key for the future to ascribe the WLE with an AIE process will rely on a good understanding of the mutual DTE-UPy - UPy-PEB stacking mechanisms. To answer why the WLE increases cycle after cycle, dynamics behaviors between the thin film components– A0/A + B0/B, A0/B + A0/B is a possibility to explore.
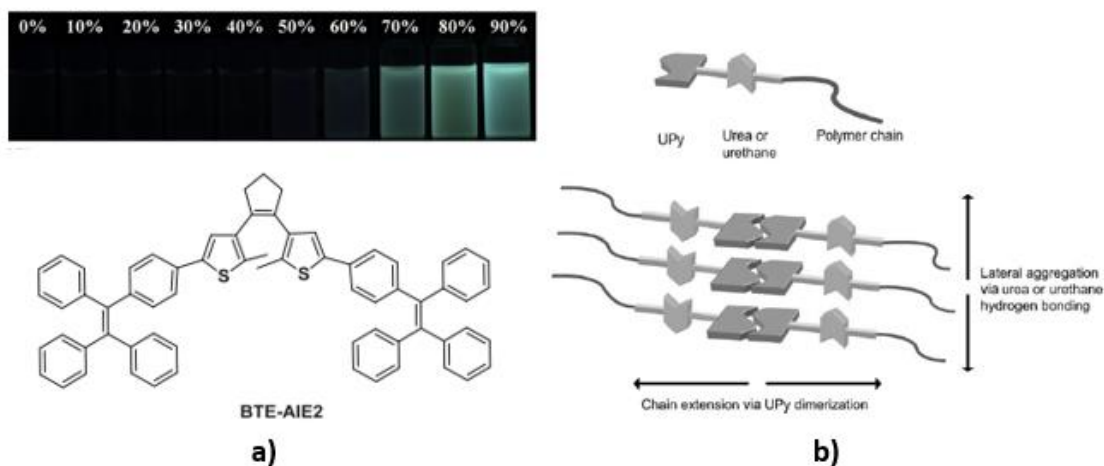
Figure 55. a) AIE process arising for the DTE-tetraphenylene molecule in THF solution with fraction of water [76], b) illustration of UPy dimers stacking [78].

III.E. Conclusions

In this chapter, we have reported the photochromic properties for the system (A+B) in the thin film with appropriate comparison with the solution case. As expected, the adjunction of the UPy unit on both side of the photochromic core does not influence qualitatively the photochromic properties. Compare to the model DTE A0, if an improvement of the extinction coefficients is reported (probably due to cyclic species), the quantum yields are either unaltered (reversion) or lowered due to the UPy units pulling apart the reactive carbon atoms.

Considering the quantum yields in the thin film, we have found very low values compare to solution, a diminution of by several order of magnitude. However, one has to take into account that severe approximation has been made, i.e. ε(film) ~ ε(solution). In the future, we need to precisely determine the extinction coefficients in the elastomeric environment to stick on the exact protocol published by Bertarelli et.al [72].

Anyhow, thanks to the novel absorbance tracking profile setup, we have brought evidence that the photochromic molecule A -surrounded by the elastomers B- is fully operative during 6 cycles of irradiation with no degradation. One the one hand, the kinetic for photoreversion induced by visible is simple described by a simple exponential function. On another hand, the kinetic for photocyclization is described by a two-exponential function with the statistical weight for each characteristic time evolving cycle after cycle. A that point of the manuscript, a fundamental question arises: during the displacement tracking profile, will we see the same trends?

Finally, apart the photochromic properties, we have discovered an intense wight light emission probably related with either i) photoenolization of the UPy units or ii) aggregation induced emission of the DTE inside UPy domains.

CHAPITRE IV

Photomechanical Effect in Thermal

Elastomers with DTEs

During the previous chapter, for the novel supramolecular thin film (A+B) all basic photochromic requirements –found in solution- were full fill for the elastomeric case: i) well defined OF (colorless) and CF (blue) states; ii) reversibility; iii) fatigue resistance (at least for 6 cycles of UV/Vis irradiation of 1h).

In the present chapter, we will address the photomechanical effects (PMEs) of the same thin film (A+B) using the new displacement tracking profile setup presented in chapter 2. First, we will present the preliminary results obtained for the "raw" systems blending a DTE with a thermoplastic elastomer without UPy connections. We will see the importance to find the optimum parameters. Then, we will present the PMEs from a qualitative and kinetical point of view allowing to corroborate (or no) both displacement and absorption tracking profile.

Finally, in order to get first physic-chemical insights to rationalize the PMEs presented, we will undertake the comparison of our optimized system (A+B) with analogs changing the % of UPy units or the microstructure of the elastomer.

IV.A. Preliminary approach: Blending a simple DTE with an Elastomer

Smart supramolecular systems displaying photomechanical effect are difficult to thoughtfully rationalize. A good strategy may consist of first blending a non-functionalized photochromic unit *A0* with the commercial elastomer B0 or with UPy functionalized elastomer B. Thin films are elaborate according to spin coating protocol (*Chapter II.B*) and a strip (2x10 mm) is cut, and the film is placed between two clamps in vertical position 24H before measurements (to release mechanical forces). The thickness is 17 and 15 μm for (A0+B0) and (A0+B) respectively. The video tracking was record for colorless films with the displacement tracking profile setup described in the *Chapter II.*

The displacement tracking profiles for two films, A0+B0 and A0+B are presented in the Figure 56. Both films were exposed to 3 cycles of irradiation alternating between visible light at 590 nm (3 hours) and UV light 310 nm (3 hours), with a time between irradiations and cycles of 1h without any illumination (OFF).

Before going to a more detailed analysis of the two curves, it is necessary to comment that the deformations experienced by the A0+B0 and A0+B films at the macroscopic level throughout the UV/Vis irradiation cycles are produced by the OF/CF gradient generated by the difference in absorption in relation to the thickness of the films.

Raw blending A0+B0. For the thin film A0+B0 (red line) in Figure 56, during the first illumination with visible light "a" no displacement was observed as expected the film being in the OF, it does not absorb the visible light. This displacement remains constant during the first OFF, "1". The film when irradiated with UV light "b" showed a very weak displacement on the left side of few tens μm induced by photocyclization of the DTE molecules to CF state responsible for the change of color as well (the film gradually turns to blue). Then, the film experiences a drastic relaxation leading the film in the opposite direction with a strong amplitude up to 1 mm. An easy way to identify this process as a non-photoinduced process is to pay attention at the displacement when the light is switch OFF. Indeed, during the OFF

"2", there is a continuity in the tracking profile meaning that both portions of the curve – end of "b" and "2" – are one and same process. At first glance, it means that the relaxation of the elastomer B0 is much more consequent compared to the negligible photoinduced effect.
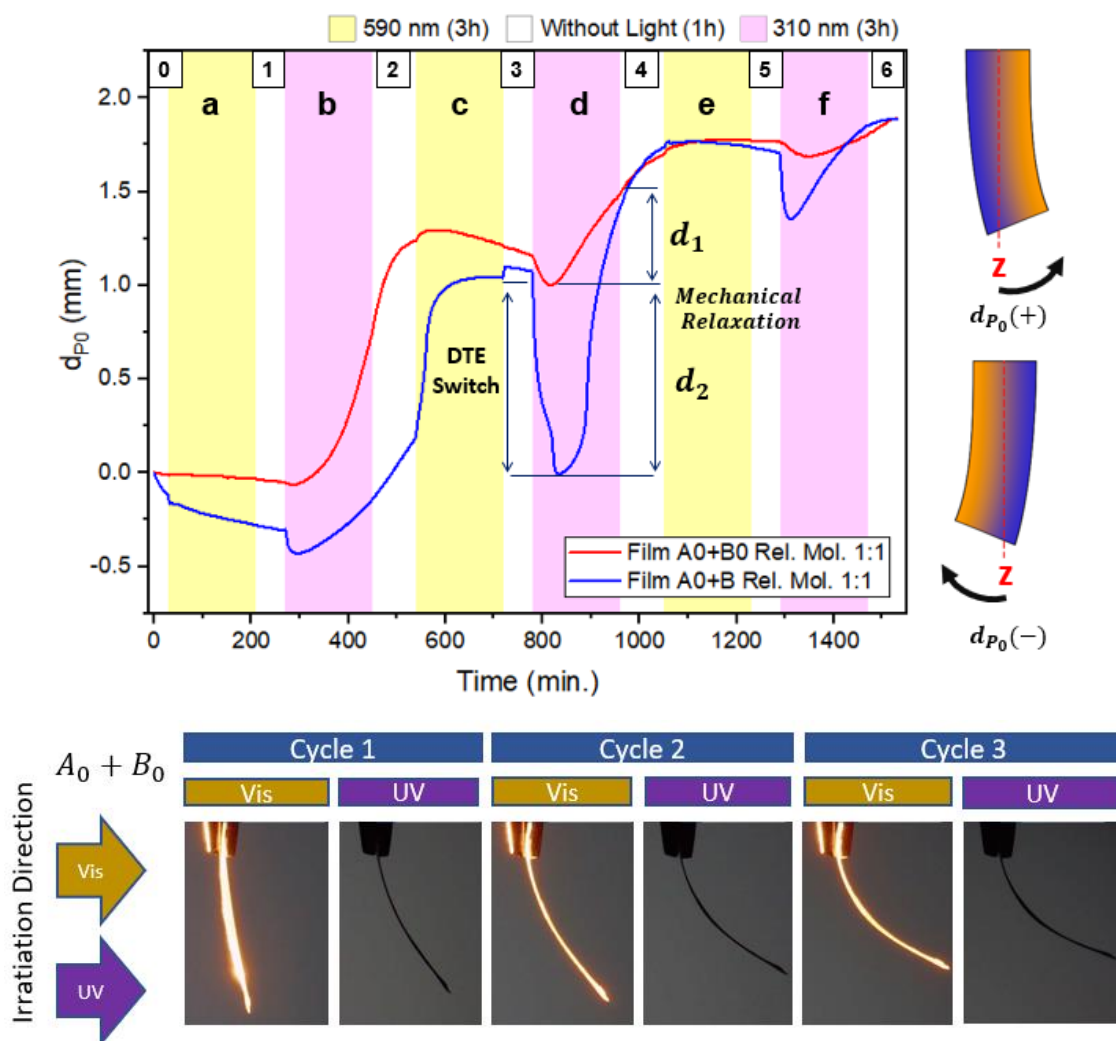
Figure 56. Above, Displacement tracking profile for thin film of (A0+B0) (red line) and thin film of (A0+B) (blue line). Bottom, Snapshot of the 3 cycles of alternating UV/vis illumination for the thin film $(A0 + B0)$.

During the second visible illumination "c", the film moves slightly on the right side 40 µm amplitude) of during few minutes and then, on more time, a strong relaxation (end of "c" +"3") pulls the film in the opposite direction with a magnitude of 70 µm. When the film was irradiated again with UV "d", an actual photoinduced effect moves the film to the left (400 µm) but drastic relaxation in the opposite

direction arise (forming an inverted peak in the displacement profile) with amplitude more than of 1 mm. For the last UV irradiation "f", the film again exhibits the same behavior as in irradiation "d", although to a lesser extent.

In summary, the main results are:

- the photochromic units are active inside the elastomeric matrix.
- the photoreversion process (visible) induces a negligeable PME.
- the photocyclization process (UV) induces a stronger PME.
- the relaxation experience by the elastomeric matrix around A_0 induces a drastic back shift of the thin film.

Introducing supramolecular interaction, A0+B. Regarding the film A0+B (blue line) a constant initial displacement was obtained (OFF "0") due to residual mechanical relaxation due to its handling and placement on the tweezers. Furthermore, there is a slight perturbation in its displacement at the beginning of the visible illumination "a", such perturbation is attributed intensity pixel artefact. For subsequent illumination/OFF cycles from "b" to "f" the behavior of the film is the same compared to the A0+B0 case, i.e. one observe a photomechanical effect only with an increase in the magnitude of the displacement ($d_1 < d_2$), being much more visible at "c", "d" and "f". In addition, relaxations occur in a similar way compared to the previous case, with a larger extent as well.

The UPy-UPy network clearly improve the propagation of the photomechanical effect initiated by the DTE. Additionally, such additional hydrogen bonding linking does not prevent the relaxation from taking place which bring the evidence than the thermoplastic part of the elastomer is responsible for such process.

The dependance on DTE concentration. Another important factor to take into account in the photomechanical effect is the amount of photoactive molecules (A0) present within the supramolecular polymeric network. The displacement tracking profile obtained by two thin films (A0+B) with different molar ratios are presented in

Figure 57. The blue and red line represents displacement tracking for molar ratio A0:B of 1:1 (see above) and 1:3 respectively. Both films show very similar general behavior in their deformation, however, the displacement of the film with 1: 3 molar ratio in the UV/Vis irradiation cycles decreases considerably in magnitude with a lower amount of **A0**. This result shows the direct relationship between the quantity of photoactive molecules present in the supramolecular elastomeric network with respect to the PME. In brief:

The higher the photochromic unit concentration, the stronger the PME.

On the other hand, it can also be observed that the elastomeric relaxations are proportional to the PME amplitude, which seems logical for thermoplastic elastomers.
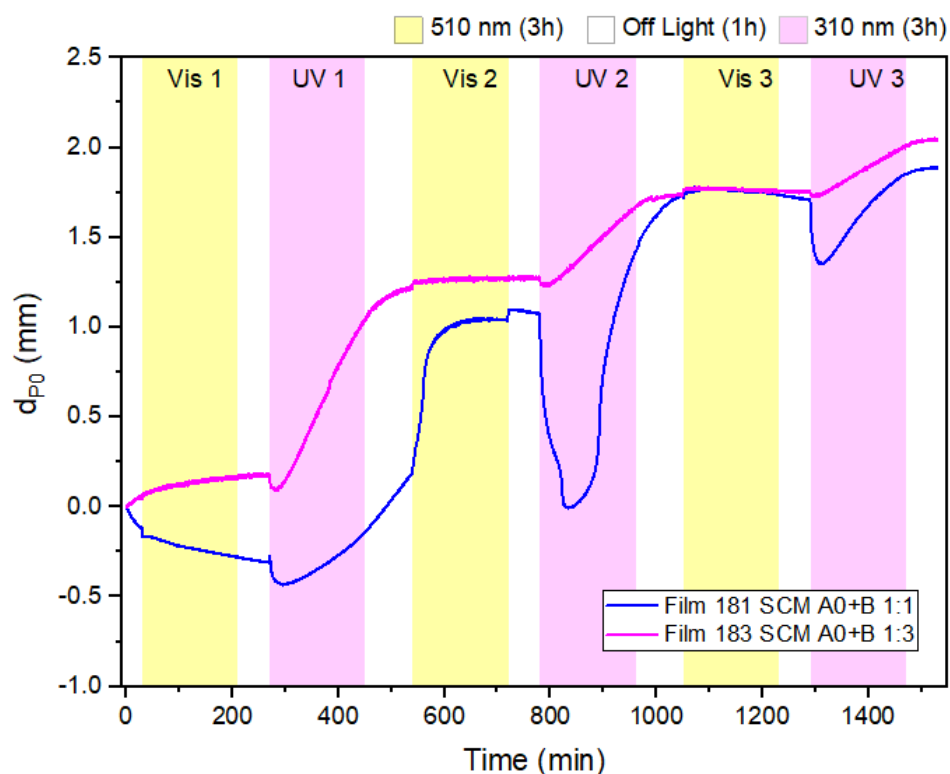
Figure 57. Displacement plot of the observed photomechanical effect of two thin films composed of A0+B with molar ratios 1:1 (blue line) and 1:3 (magenta line).

IV.B. Photomechanical effect in Thin Films (A+B): finding optimum parameters

As observed in the previous section, the formation of a supramolecular elastomeric matrix formed by UPy telechelic elastomer PEB-UPy (B) around the photochromic molecule A0 increases the magnitude of the photomechanical effect compared to its diol analog B0. In this section, the photomechanical effect produced by irradiating a thin film (A+B) made from the mixture of DTE-UPy with PEB-UPy, is analyzed. The objective is to analyze and optimize the novel photoinduced effect by including A in the quadruple hydrogen bonding UPy-UPy supramolecular network. To do so, appropriate comparisons between the video tracking setup $f(t)$ and the absorbance tracking set up $A_{CF} = f(t)$ will be made.

IV.B.1. Relationship between photochromism and PME

The displacement tracking profile obtained for the film (A+B) with a molar ratio 1:1 and 17 µm thickness is shown in Figure 58.This film was exposed to two irradiation cycles which consisted of a 3-hour irradiation with visible light (590 nm, 796 µW) followed by a 3-hour without light and then irradiated with UV (310 nm 796 µW) for 3 hours. The red line in Figure 58 is the 635 nm (CF band) absorbance tracking profile (see previous chapter) for the same thin film keeping the same irradiation sequences. This curve is easily interpreted by an alternance between colorless form changing to blue under UV and returning to the initial absorbance under visible light. As already discuss, the kinetic of coloration (UV) is slower than the kinetic of discoloration (Visible).
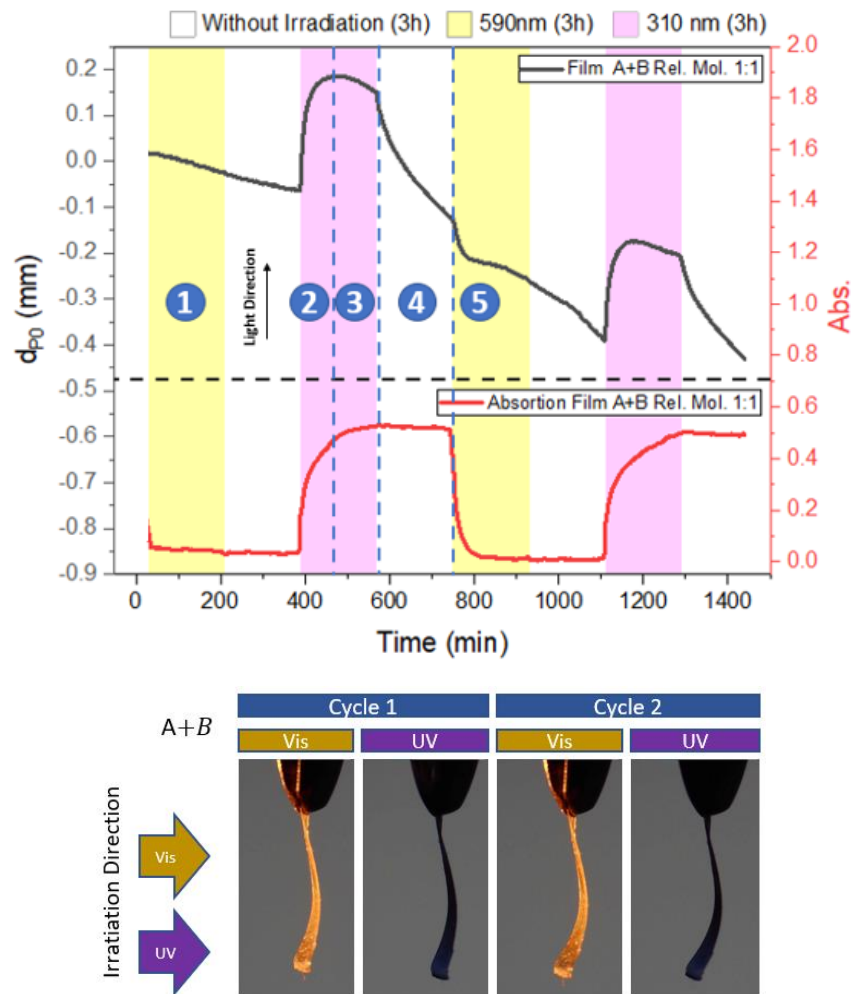
Figure 58. Above, displacement analysis for the photomechanical effect produced by irradiation of film (A+B) at 310 nm and 590 nm and absorption obtained @ 635 nm for film (A+B). Bottom, snapshots of each end of irradiation cycle. (Film thickness=17 μm).
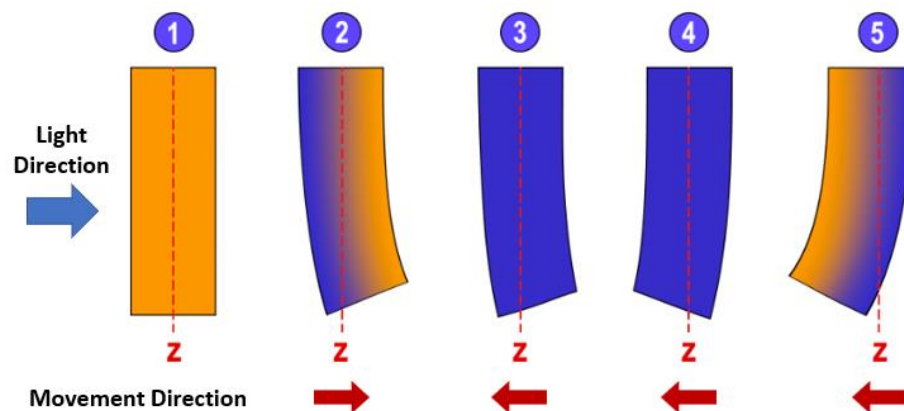
Figure 59. Schematic of the movement experienced by film (A+B) when irradiated with 590 nm and 310 nm. The gradual change in colors represents the change in absorbance relative to Figure 58, red line.

During the first illumination with visible light –phase "1"-, as expected the film in the OF showed no displacement due to the visible light but only a small drift due to mechanical relaxation. Note that this relaxation will probably propagate during the 40h of the experiment. Anyhow, when the film was irradiated with UV –during phase "2", a strong displacement of ~150 μm on the right (light direction) was observed. Then, after approximately 65 minutes of irradiation, the thin film returns slightly on the left (~25 μm amplitude) until the end of the illumination sequence (phase "3"). When the light is switch OFF, phase "4", a much more drastic displacement is noticed still on the left, but part of this displacement is probably due to the initial relaxation. During the visible irradiation period "5", a drastic displacement still in the left occurs reaching an asymptotic position after 60 minutes of irradiation. Then, a relaxation clearly occurs during the end of the phase "5" until the end of the next OFF. The displacement in the subsequent UV irradiation is almost identical to that seen in the previous UV irradiation ("2" and "3"). To rationalize the different PME, inspection of absorbance tracking profile will be instructive. The different "stage" for the thin film (A+B) of Figure 59 is illustrated.

PHASE 2 and 3. when the film is irradiated with UV for the first time, the film turns to blue, and the absorbance increase rapidly. The maximum absorption is reached in approximately 3 hours of irradiation However, although the absorption is continuous and uniform over this period, the film displacement has two different behaviors. As mentioned above, rapid, and non-uniform absorption with respect to film thickness generates an CF/OF gradient which induces the photomechanical stress. This effect is well documented for DTE crystals and application of the bimetallic model of Timoshenko. This process took place during the first 70 minutes of irradiation with UV light ", where the rapid photocyclization of A induced a stress gradient which caused a sudden displacement of the film in the direction of irradiation. The second phase "3" (70-110 minutes of UV irradiation), in which the thin film moves forward to the right, comes from the photocyclization of the remaining A molecules that induce the disappearance of the CF/OF gradient (every molecules are now in CF) inducing a photomechanical stress in the opposite direction. This second effect has a smaller magnitude than the previous one, since the number of molecules to convert is limited, as it can be seen in the kinetic curve.

88

In consequence, this "gradient effect" forward (phase2) /backward (phase 3) does not give the ability to the thin film to return to its initial position.

PHASE 4. For the period of non-illumination "4" of 3h, the film maintains its blue color and its absorbance has remained constant, which bring the evidence that the drift of the film does not depend on the photochromism of A but on mechanical relaxation of the supramolecular network in a process of recovery and reorganization of the polymeric chains. Those types of relaxation have been reported in the literature for several materials doped with photoactive units; it has been shown that the kinetics of shape recovery of materials with photoactive molecules immersed in polymeric networks are not directly related to the reversion of isomerization in periods of darkness (without light irradiation), [79].

PHASE 5. For the second period of irradiation with visible light -phase "5"- as long as the thin film is recovering its starting color, the absorbance (Figure 58, red line) decreased rapidly in approximately 70 minutes until reaching the null absorbance. This demonstrates the complete reversion reaction for the A molecules. Like the UV irradiation case, this change of absorbance induces a CF/OF (blue/colorless) gradient generating the torsion of the film (A+B) in the reverse direction. This is the first step toward a complete reversibility. However, the magnitude of this displacement is more than twice smaller compared to UV irradiation:

- ~250 µm bending on the right for UV excitation, Figure 60a.
- ~100 µm bending on the left for VIS excitation, Figure 60b.

As evidence, for the future, choosing different irradiation power will allow to reach complete back and forth displacement of the thin film, i.e. perfect photoactuator.
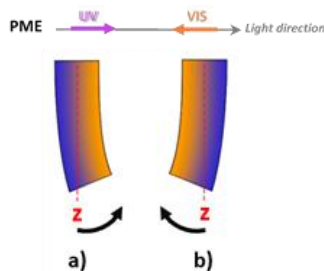
Figure 60. a) Schematic of bending of thin film forward the UV light (a) or backward the visible light (b).

IV.B.2. Focus on relaxation processes

The mechanical relaxation behaviors -that does not depend on light- described above can be classified into two types:

- • **Type 1**: mechanical relaxations observed after photoreversion induced by visible light (phase "5" after 70 min and subsequent OFF in Figure 58).
- • **Type 2**: mechanical relaxations observed after photocyclization induced by UV light (phase "4").

The two types of mechanical relaxations are induced by the reorganization of the chains in the supramolecular elastomeric network. However, the two have different characteristics. Type 1 mechanical relaxation starts before the end of visible light irradiation and its behavior tends to be a straight line with a very low slope similar to the plastic deformation experienced by elastomers. Type 2 mechanical relaxation starts immediately after the end of UV irradiation and its behavior tends to be linear with a steep slope, which could be an indication to an elastic type of deformation.

Further mechanical experiments will be address in the future to investigate the exact nature of those two types of relaxation.

IV.B.3. Choosing appropriate illumination periods

The final goal of our project is to obtain a reversible photoactuator totally controlled by the light, like the DTE crystals [80] presented in chapitre1. However, we have just seen that, either "inverse gradient effect", sudden mechanical relaxation after switching OFF UV light or slower mechanical relaxation after photoreversion, all those processes must be avoided. Choosing an irradiation time of less than 70 min seems to be a good compromise. Furthermore, introducing a dark period between the two UV/Visible sequences is incompatible with the photoactuator requirements. In the following, except for some prospective experiments, the illumination sequences VIS and UV will be 1h each with no dark periods in between.

As observed in section III.B in Figure 47, the absorbance in the photoreversion process reaches 97% (3% absorbance) in a period of approximately 64 minutes. While in the photocyclization process 74% absorbance is achieved in the same period of time. The above gives the possibility of designing an irradiation cycle in which the photocyclization and photoreversion processes are reversible with respect to each other. In particular, by taking an irradiation time of 60 minutes, the absorbance in the photocyclization process (starting from the fabrication of a film in OF) reaches 75%, while the reversion of the isomerization in the photoreversion process in this same period of time reaches 95%, which previously ensures the total reversion of the photocyclization-photoreversion process taking an irradiation of 60 minutes for UV light and visible light.

IV.B.4. Working with CF or OF thin film?

IV.B.4.1. Preliminary approach

In the previous section, the variation of the photomechanical effect was analyzed with respect to the amount of photoactive molecules A, as well as the increase in the magnitude of the effect when a supramolecular network is formed. However, another point to take into account in the analysis of the photomechanical effect is the initial state of the films, i.e., whether the films are made from a solution in OF (transparent or amber) or a solution in CF (blue).

To investigate the influence of the initial state on PME, three films were fabricated with different molar ratios (A:B) 1:1, 1:2 and 1:3 starting with a blue solution (the fabrication of the films is explained in more detail in experimental chapter (see Figure 25a). The 3 films were exposed to 3 cycles of 3-hour UV/Vis irradiation (310 nm, 590 nm at 796 µW), with dark cycles between irradiation periods of 1 hour.

The displacement tracking profiles obtained for the 3 films are shown in Figure 61. It can be seen that the behavior of the 3 blue films varies significantly with respect to the colorless films. Indeed, during the first irradiation with visible light in which the 3 films present two successive drastic effects resulting in an inverted peak" on

the profile: 1) from the beginning of illumination to 75 min (for the black curve), the thin film shift to the left due to the photoreversion of A molecule; 2) a drastic mechanical relaxation will drive the thin film in the opposite direction on ~3 mm distance. To rationalize this intense PMEs, three observations worth to be notice: i) this PME effect is not reported for a film in OF; ii) the amplitude of this PME depends on A concentration (the higher the molar ratio of A, the stronger the effect); iii) this effect is not reversible and observed only once, during the first cycle.

The origin of such effect can be easily understood paying attention to the supramolecular properties of **A alone**. From the pioneer work of Professor Takeshita, he has shown that molecule A can make a large self-assembly only for the CF with its rigid photochromic core. In contrast, the labile OF (with the AP/P equilibrium) is restricted to small monomers [45], [61] or cyclic species as displayed on Table 1. [62]. The evident demonstration of such large self-assembly is the appearance of a blue precipitate few minutes after UV irradiations for concentrations up to 200µM. [17].
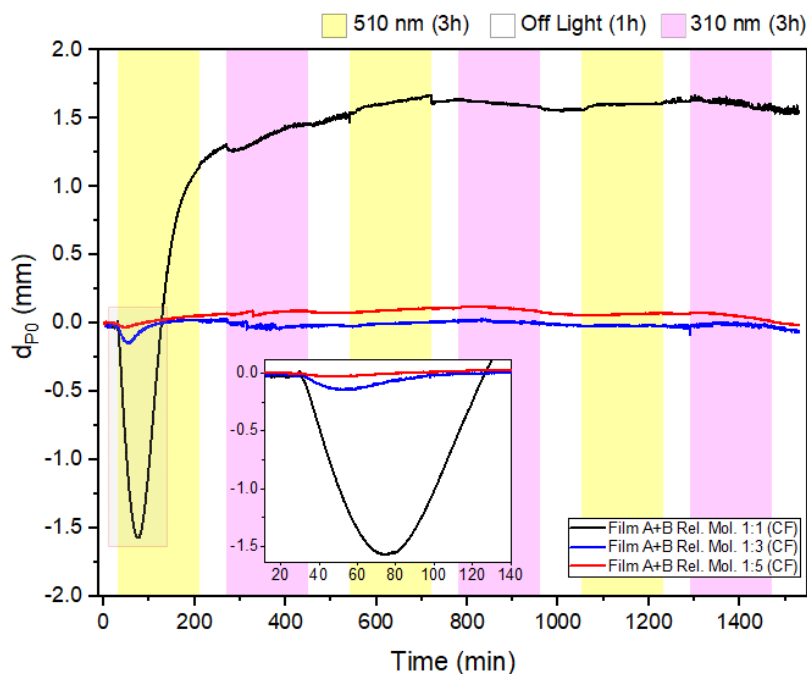
Figure 61. Displacement graph of the photomechanical effect observed in (A+B) thin films with molar ratios 1:1 (black line), 1:3 (blue line), and 1:5 (blue line).

As demonstrated in the past, we got evidence (with the aid of wild-field microscopy allowing in-situ irradiation) [63] that the precipitate of CF shows important photomechanical activity under UV or Visible irradiation (see figure 59). A snapshot of such precipitates illustrates the response of two representative pixels in order to illustrate the difference between photomechanical and photochromic signals. The first was chosen from the edge of the precipitate (red square on sample photograph) and the second in the center of another sample existing in the same photograph, which does not exhibit motions upon UV/visible light irradiations. Note that for this experiment, the intensity power of the visible LED (550nm, 12mW/cm2) was much stronger compared to the results presented in this manuscript. In Figure 62a, it shows that some grains of CF precipitates show some PME activity follow by instantaneous relaxation (thermal effects). Those results corroborate an assignation of this intense "inverted peak" Figure 61 in favor of self-assembly of A alone ($AAAA..$) rather than mutual blending ($ABAB$ ...).
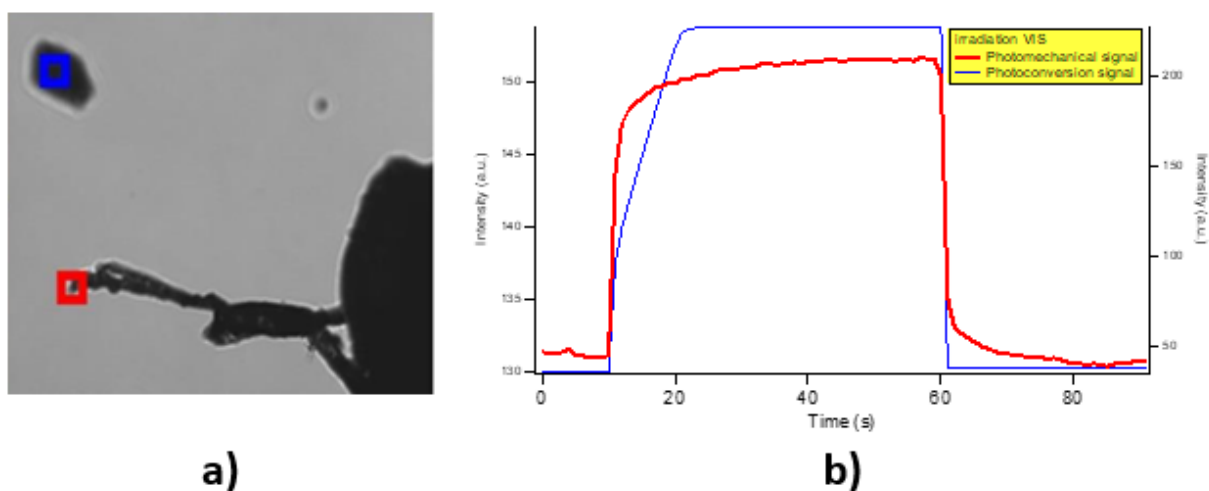
Figure 62. a) Snapshot of the wild-field microscopy image sowing two area of pixel in which the grains are moving (red) or not (blue). b) Intensity tracking profile for the red and blue area.

IV.B.4.2.   Toward optimum system

To confirm that the first peak was due to the molecule A alone, a blue film and a colorless film displacement tracking profile were compared together for an irradiation period of one hour as previously discussed.
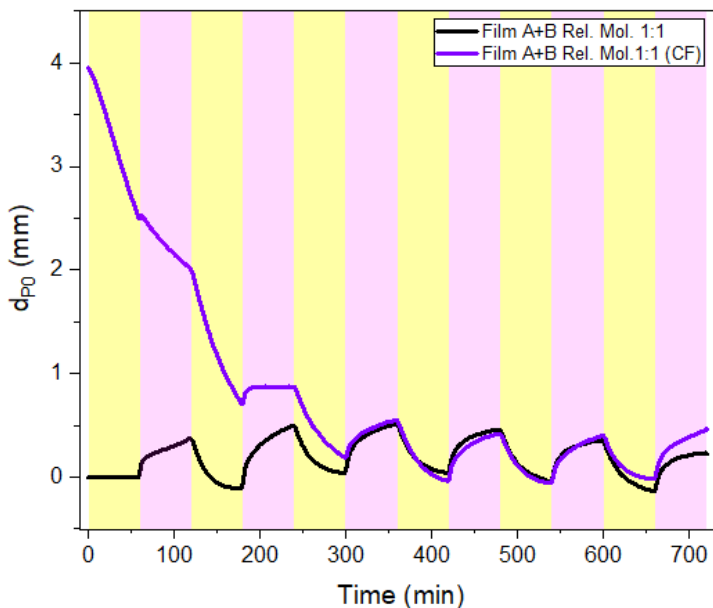
Figure 63. Displacement tracking profile for and film (A+B) from (A+B) solution in CF, which was subjected to 6 cycles of UV/Vis irradiation (310 nm, 590 nm at 796 µW).

Figure 63 shows the tracking profile for the thin film (A+B) in CF (purple curve) and OF (black curve) which was irradiated with 6 alternating UV/Vis cycles of one hour As in Figure 58 a strong shift was observed during the first two cycles of UV/Vis irradiation. However, this shift starts to become periodic from the third cycle onwards and for the final cycles, the two profiles are clearly identical. This result is the strong evidence that the initial effect responsible for the "inverted peak" is disappearing upon successive illumination.

The strong deformations produced in initial cycles, as explained above, are produced by the isomerization of large clusters of A molecules (domains of A), which, when surrounded by the polymeric network and isomerized upon irradiation, induce large mechanical relaxations generated by the movement and diffusion of

the precipitates, as well as the reorganization and sliding of the polymeric chains. On the other hand, as can also be seen in Figure 64, this reorganization decreases and disappears with the passing of the irradiation cycles. In other word, cycle after cycle, those A domains disappear (DTE-UPy-UPy-DTE hydrogen bonding are broken) to be blended with B elastomer (DTE-UPy-UPy-PEB hydrogen bonding are created).

Figure 64. diagram explaining A and B domains reorganization through alternating UV/Vis irradiation

Anyhow, the conclusion points for a photoactuator elaborated with a solution in OF rather than CF. Indeed, the additional PME effect originated from $A \cdots A$ domains are not permanent and disappear with successive irradiation cycles which is not suitable for further technologic applications.

As a conclusion, the thin film (A+B) in the OF is the most suitable system for further investigations (avoiding the parasite PME from A domains alone) compared to its CF analogs. Since now, we will only focus on colorless thin film.

IV.C. Correlation between PME and Photochromism

In the section above, a photomechanical effect study was carried out on a film (A+B), which was exposed to alternating UV/Vis irradiation with an exposure time of 3 hours and dark period in between. In order to avoid either reverse "gradient effect" or elastomeric relaxation, it has been concluded to restrict the 1 hour of illumination period to 1 hour. Both displacement and absorbance tracking profile

will be register with the same experimental conditions: UV/Vis irradiation (310 nm, 590 nm at 796 µW)

In this part, our aim is to rationalize quantitatively the relationship between the change of color and resulting mechanical effect by comparing the displacement and the absorbance tracking profile (the latter being presented in the previous chapter)

IV.C.1. General observations

The normalized displacement (black line) and absorbance (red line) tracking profiles for a thin film (A+B) under 6 cycles of UV/Vis irradiation of 1 hour duration are displayed in Figure 65. Note that the absorbance tracking profile has been thoughtfully commented in previous chapter with the main results being:

- Photoreversion process described by a mono exponential function with a average characteristic time of 27.2 min and a slight decreasing trend upon successive irradiations explained in term of non-converted CF (reversion illumination period too short)
- Photocyclization process described by a bi-exponential function with an average short time of 2 min and an average longer time of 26.2 min; the statistical weight of the former decreasing, cycle after cycle, in benefit to the later. This result is attemptability explained in term of structural modifications around the photochromic core or AP/P equilibrium affecting the overall kinetic of AP species.

At first glance, it is striking to observe the similar trends for both displacement and absorbance tracking profiles. Under successive cycle, the non-color OF thin Film (A+B) induces a shift to the right (light direction) under UV irradiation and to the left under Visible irradiation. As seen in figure 63 if the magnitude of the displacement is constant for visible excitation with an average around ~480 µm, the situation is

more complex for the UV excitation. The displacement increases for the first two cycle up to 600 μm and then continuously decrease down to 390 μm.
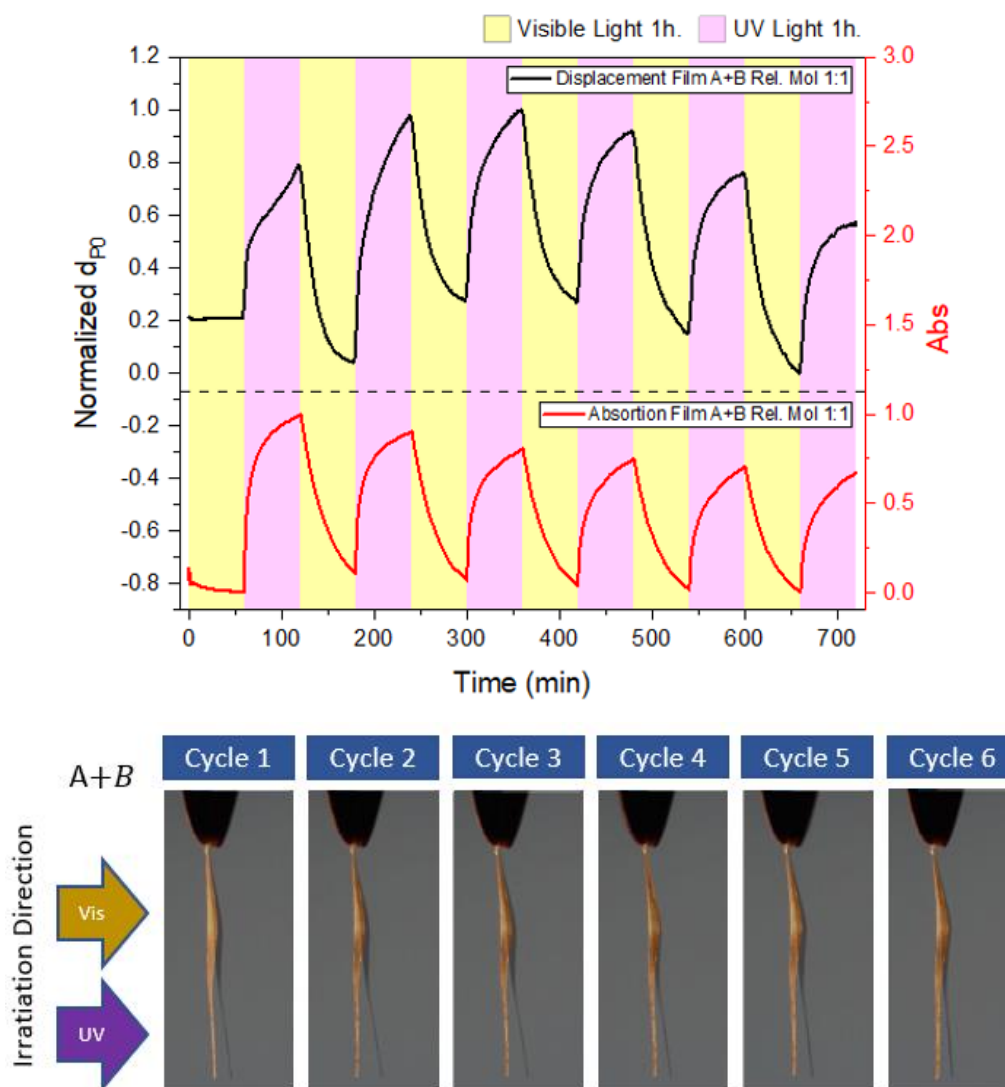
Figure 65. Normalized displacement shown by an film (A+B) under UV/Vis cycling irradiation (310 nm, 590 nm at 796 μW), black line. Absorbance of film (A+B) @ 635 nm, with UV/Vis cycles of irradiation, red line. Bottom, snapshots of each end of irradiation cycle. (2 x 8 x 0.02 mm)
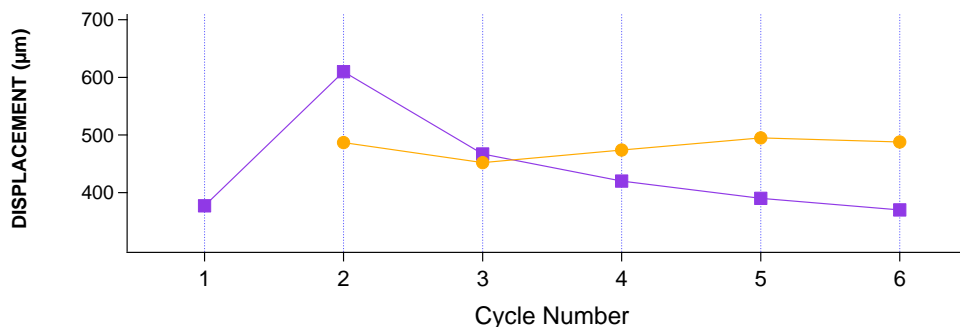
Figure 66. Magnitude of the displacement for each UV (purple) and Visible (orange) cycle.

IV.C.2. Kinetic analysis

As explained in the previous chapter, the absorbance tracking profiles, i.e. $A_{CF} = f(t)$, were fitted using mono-exponential and bi-exponential for UV and visible irradiation respectably. After several tests, we have found that the displacement tracking profiles i.e. $d_{P_0} = f(t)$ are best fitted with the same trends.

Consequently, we have fitted the displacement tracking profiles for photocyclization under UV irradiation,

$$d_{P_0}(t)_{UV} = D_1 e^{-\left(\frac{t}{\tau_{D1}}\right)} + D_2 e^{-\left(\frac{t}{\tau_{D2}}\right)} \tag{32}$$

The statistical weight of each exponential term is defined as

$$x_i = \frac{D_i}{D_1 + D_2} \text{ with i} = 1,2 \tag{33}$$

While for photoreversion induced by VISIBLE irradiation a mono-exponential function is enough

$$d_{P_0}(t)_{visible} = D_3 e^{-\left(\frac{t}{\tau_{D3}}\right)} \tag{34}$$

The fitting results are gathered on Table 5 and correlation graphics are presented as well.

	Absorbance profile						Displacement profile					
	UV				VIS		UV				VIS	
Cycle	x_1	$\tau_{A1}(min)$	x_2	$\tau_{A2}(min)$	A_3	$\tau_{A3}(min)$	x_1	$\tau_{D1}(min)$	x_2	$\tau_{D2}(min)$	A_3	$\tau_{D3}(min)$
1	0.44	1.2	0.56	17.9				-				
2	0.43	1.3	0.57	18.5	0.195	28.8	0.35	4.4	0.65	50	0.47	16.1
3	0.4	2.1	0.6	26	0.181	28.3	0.39	4.9	0.61	47	0.34	17.4
4	0.35	2.2	0.65	28	0.166	26.9	0.42	5.3	0.58	36	0.50	19.5
5	0.32	2.4	0.68	32	0.154	26.1	0.49	6.2	0.51	39	0.56	21.0
6	0.31	2.8	0.69	35	0.146	25.9	0.51	5.6	0.49	23	0.47	21.9

Table 5. Characteristic times pre-exponential factor or statistical weight from the fitting by mono or biexponential of Absorbance /displacement profile displayed on Figure 65.
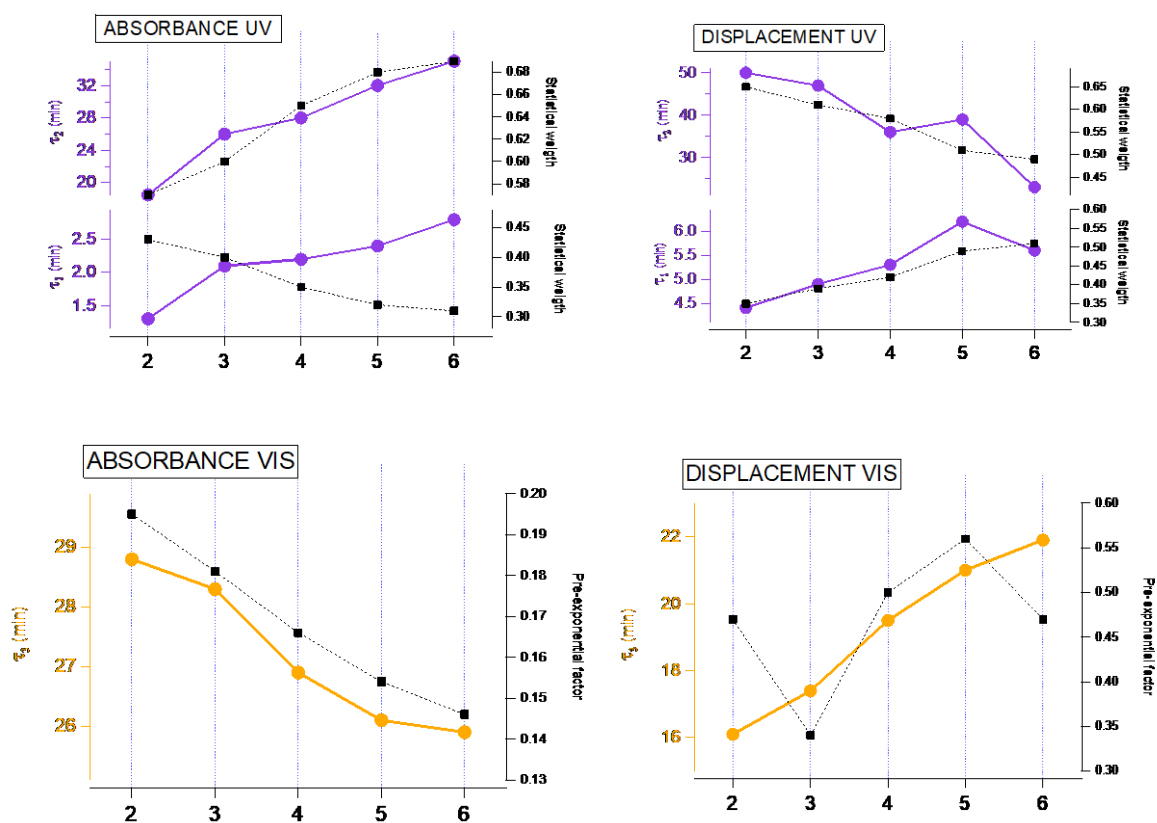
Figure 67. Evolution of the characteristic times along cycle numbers- deduced from the fit of the displacement (right) or absorbance tracking profiles (left). Mono or bi-exponential function was used for Visible and UV excitation respectively.
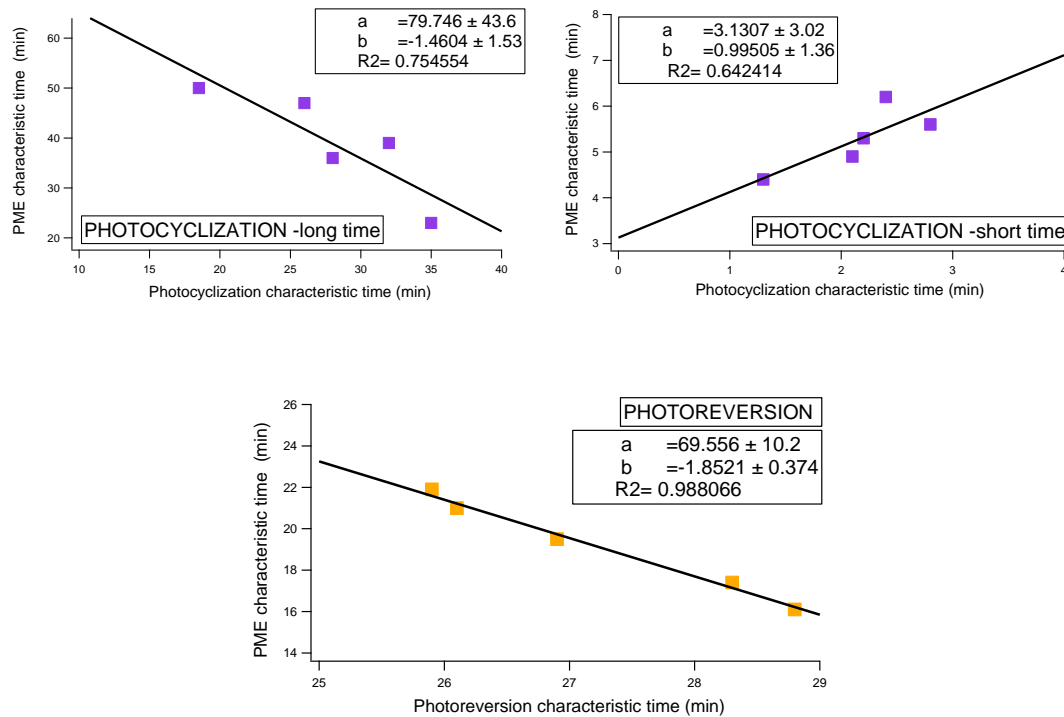
Figure 68. Correlation between PME and photochromic characteristic times for UV (left) and Visible (right).

Let us first analyze the photoreversion case. From cycle #1 to cycle #6, the characteristic time for the discoloration kinetic is decreasing (from 29 to 26 min), while the characteristic time for displacement is increasing (from 16 to 22 min), i.e. the bending back motion velocity is slowing. Note that, the photomechanical effect under visible irradiation is somewhat faster than the discoloration kinetic. The linear correlation between the two times are excellent (R^2=0.988) with the following equation:

$$\tau_{PME}^{VIS} = 70 - 1.8 \times \tau_{REV} \tag{35}$$

To the best of our knowledge, this kind of linear relations has never been reported for polymeric system including photochromic units. The strength of such a relation relies on the ability of the elastomeric system to behave like a photochromic crystal with macroscopic dimension.

Concerning photocyclization, the situation is more complex because two characteristic times are required to describe either the coloration kinetic (see

previous chapter) or displacement tracking profile. The coloration kinetic requires a short time τ_1 ~2 min and a longer time τ_2 ~28 min while the displacement is slower with a characteristic time of τ_1 ~5 min and τ_2 ~40 min. Both times evolves along the cycles numbers: i) both shorter times τ_1 increase in a similar way (slope of unity for the correlation curve); ii) for τ_2, while the time is increasing for the coloration kinetic, this time is decreasing for the PME meaning that the film bend faster in the last cycle, surprisingly. The linear correlation equation (R^2=0.75) for this longer time

$$\tau_{PME}^{UV} = 80 - 1.5 \times \tau_{CYC} \qquad (36)$$

is very close in comparison with the previous one. It may suggest that among τ_1 and τ_2, only the longer time will be affected by the processes affecting the photochromic units (% conversion or evolving structural surroundings or AP/P equilibrium). It may also suggest that the shorter time will be more related to the elastomer itself.

IV.C.3. Reversibility and cumulative effect

In this section, we are interested with the mechanical reversibility or the cumulative effect when the PME during UV irradiation is not compensated by the analog during visible irradiation.

The displacement tracking profile obtained for a thin film (A+B) submitted to 12 similar UV/Vis irradiation cycles with an exposure time of 1 hour is displayed in Figure 69. As previously reported, the film showed a back-and-forth uniform periodic behavior throughout the 12 irradiations cycles. Except to the two first cycles, the maximum displacement experienced by the film was 125 µm for UV while the displacements for the visible irradiations were higher than 160 µm. Note that some mutual oscillations are suspected probably due to some geometrical factor (shape of the film, angle of irradiation, etc.). Anyhow, because of this unbalanced displacement, at the end of the 12 irradiations cycles, an overall displacement of 850 µm toward the left (reverse light direction) was obtained.

Anyhow, besides the fact that VISIBLE PME was more efficient than UV PME, as reported above, the most important points are: i) the well-known fatigue resistance of the DTE molecules [81] is still observed in the supramolecular network; ii) with a judicious choice of the irradiation time, a cumulative effect can be obtained.
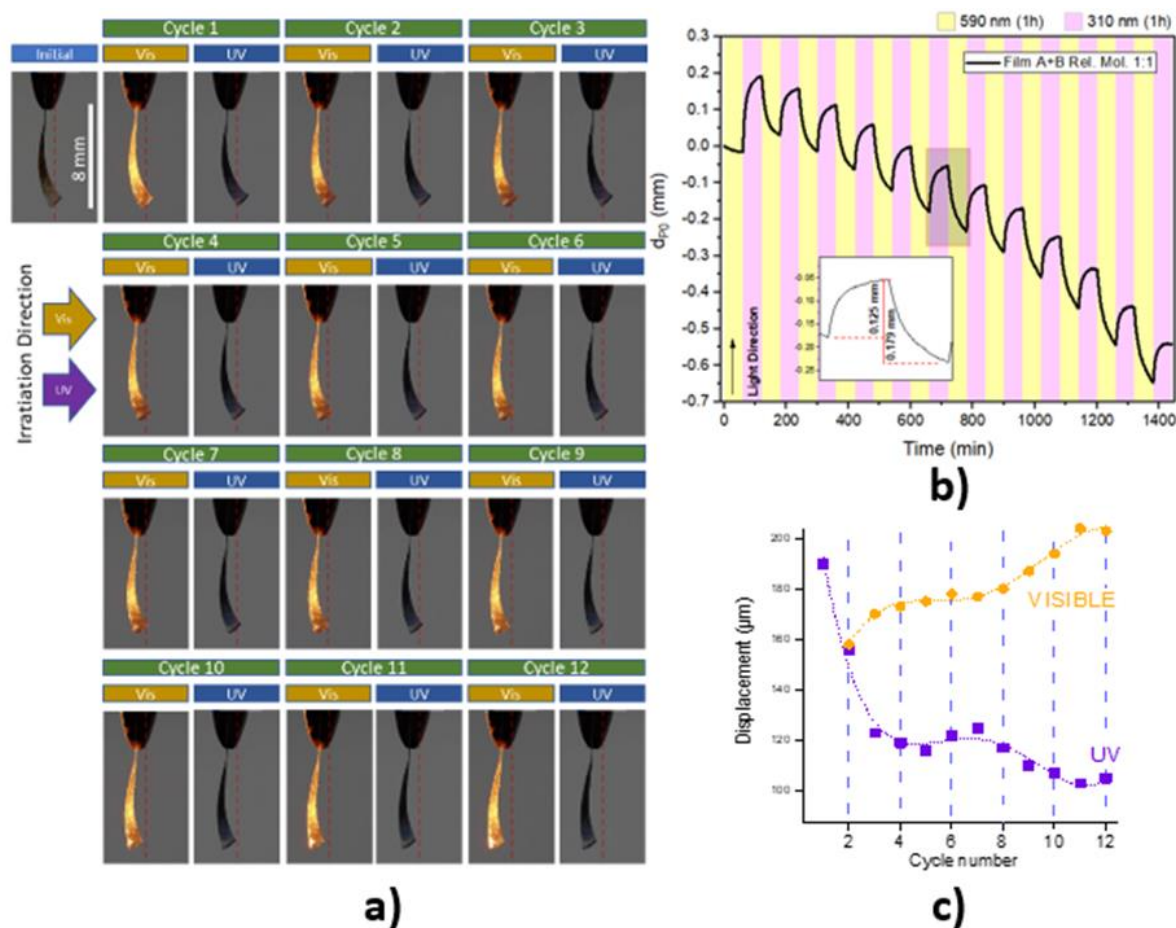
Figure 69 a) Photograms of each of the cycles of the irradiated film (A+B). b) Displacement graph of film (A+B) which was irradiated with UV/Vis light for 12 cycles. c) Magnitude of the displacement in the visible and in the UV for each of the cycles.

To illustrate this last point, a similar video has been registered for a novel thin film (from the same batch) with similar dimensions but reducing the irradiation time to 20 min and the corresponding displacement profile is shown on Figure 70. Paying attention to the absorbance curve, this irradiation time has been carefully chosen to ensure a total reversion. The thin film displacements were exactly the same compared to the previous case but with regular displacements of 0.180 mm per

cycle. If the displacement gap in each cycle is the same as that experienced for one-hour irradiation cycles (Figure 69b smaller overall deformation was obtained: displacement of 850 μm for 1-hour exposure times compared to a displacement of 375 μm for 20-minute exposure times. Similarly, the behavior of the overall displacement changes from a curved shape to a linear shape as the exposure time is reduced.
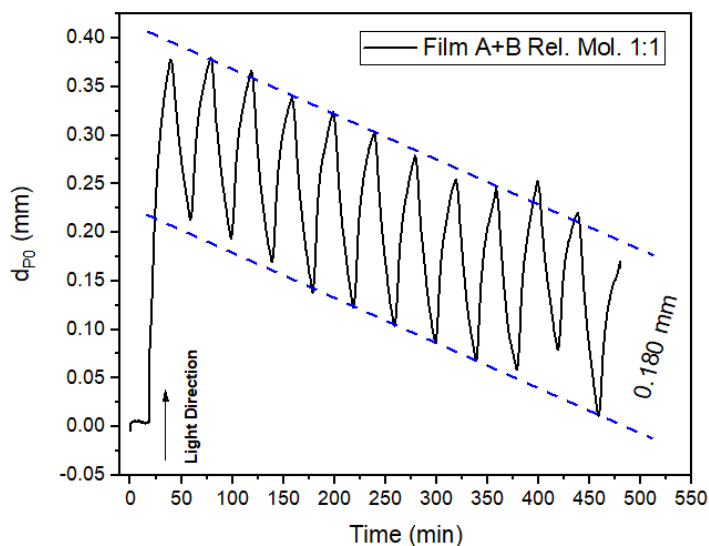
Figure 70. Displacement was obtained for a Film (A+B) exposed to 12 cycles of UV/Vis radiation (310 nm, 590 nm at 796 μW) with an exposure time of 20 minutes per wavelength.

IV.D. Comparison with other photoactuators

A comparison with others photactuators found in the literature is now relevant. The task is not so trivial because the researchers' groups have chosen to track the photoinduced bending with different variables: displacement of the tip, the bending angle θ or sophisticate evaluation of the curvature [82]. Furthermore, it has been demonstrated that the bending velocity is proportional to the irradiation power and a normalization is required.

Let's consider a strip with length l and width L (surface section S= l x L) irradiated during Δt with an irradiation power P. The maximum displacement is d_{max}. The bending (displacement) velocity will be given by:

$$v_{bend} = \frac{d_{max}}{\Delta t} \tag{37}$$

And taking into account the irradiation power (and assuming the entire strip is illuminated), the normalize bending velocity will be defined as

$$v_{bend}P^{-1} = \frac{v_{bend}}{P \times S} \tag{38}$$

We will compare the present results with the bending of DTE crystals form Irie group [37], and the recent study of Ikeda with LCE based on polyurethane (Figure 12 in chapter 1) [51]. The present results coming from the analysis of the thin film (A+B). DTE crystal, PU-LCE-AZOs are gather together in Table 6. Note that, unfortunately, the actual power used to illuminate the crystal with the visible light is not precise.

Clearly, by inspecting the $v_{bend}P^{-1}$ values, the elastomeric photoactuators cannot compete with the DTE monocrystal. However, it worth to remind that monocrystals will be dedicated for the academic world with no possibility to rise their dimensions up to few millimeters. In contrast, the comparison with IKEDA system show that the performances are of the same order of magnitude for the UV excitation but with better performance for the LC system: 7.5 mm.J^{-1} vs ~1 mm. J^{-1} for our thin film. In contrast, we improve the performance by a factor of 3 for the visible excitation.

In summary, with a very basic preparation, our supramolecular approach can compete and even give better performances compare to the Liquid Crystal Elastomer systems. In the future, investigation of PME at higher light power –few tens of mW.cm^{-2} regime- will be of crucial importance to confirm the comparable or better performances of our system.

Materials	Thickness (μm)	Length (cm)	width (cm)	Surface (cm²)	UV				VISIBLE			
					Power (mW/cm²)	Energy (mJ/cm²)	Bending velocity (μm.s^{-1})	Normalized velocity (mm.J^{-1})	Power (mW/cm²)	Energy (mJ.s^{-1})	Bending velocity (μm.s^{-1})	Normalized velocity (mm.J^{-1})
DTE crystals[a]	10	0.17	0.02	0.0034	30	0.102	59	578	-	-	5	-
PU-AZOs[b]	16	1	0.2	0.2	10	10	15	7.5	0.04	0.008	2	0.25
This work	17.5	0.8	0.2	0.16	0.0008	0.128	0 .173	1.35	0.0008	0.000128	0.113	0.88
							0.110	0.86				

Table 6. Comparison for Photomechanical performances with other studies in the literature.
a= [83], b = [51].

IV.E. Chemical and Physical factors influencing PME

IV.E.1. Effects of photochromic unit concentration

As observed in section IV.2, the variation of the concentration of molecule A0 in a supramolecular network formed by elastomer B directly affects the magnitude of the PME. In this section, the proportionality of the photomechanical effect with respect to the concentration of A molecules immersed in the supramolecular network formed by the mixture of A and B will be explored. Therefore, four films were fabricated from (A+B) solutions in OF form, each with different molar ratio $A:B$. (1:1, 1:2, 1:3 and 1:5). Each film was irradiated with UV and Visible light (310 nm, 590 nm at 796 µW) for 6 cycles of one hour each.
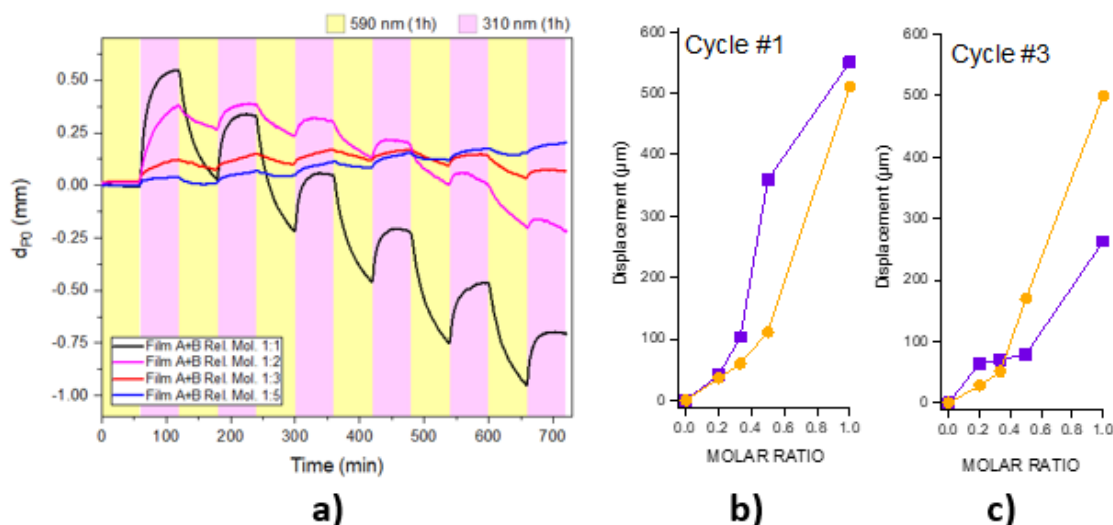
Figure 71. a) Displacement tracking profile obtained for (A+B) thin films with different molar ratio: 1:1, black line. 1:2, magenta line. 1:3, red line. 1:5, blue line. All films were irradiated in alternating one-hour cycles of UV/Vis illumination (310 nm, 590 nm at 796 µW). b) Displacement magnitude for cycle 1. c) Displacement magnitude for the cycle 3.

The displacements tracking profiles for the 4 films are displayed in Figure 71. For each films a similar back and forth displacements were reported as the previously except that theses displacements amplitudes were directly proportional to the concentration of the A. Additionally, the cumulative effect is different with the increasing quantity of A. Taking the algebraic difference between the first and the

106

last position of the thin film, the following trend is observed function of the molar ratio ($A:B$):

(1,5)	(1,3)	(1,2)	(1,1)
+ 200 µm	+ 50 µm	- 20 µm	- 700 µm

Let's analyze those two aspects, amplitude, and cumulative effect.

Tuning the amplitude. For the cycle #1 and #3, the maximum displacement reached during UV or VIS irradiation of each film is plotted function to the molar ratio in the Figure 71b and Figure 71c. The first cycle is always different from the successive one: whatever the molar ratio used, the first bending toward the right induced by UV is of higher amplitude compared to back motion induced by visible. Then, as shown by Cycle #3, increasing the quantity of photochromic units allow the visible back motion to be of higher amplitude compared to UV motion amplitude. Those effects are easily rationalized: during the first UV illumination, 100% of the UV absorbed are engaged within the photocyclization process while for the successive cycles, part of the UV photons are absorbed by the CF molecules that relaxes photophysically or even induced a photoreversion. This kind of "screening effect" [84] will increase with the increasing quantity of A.

Tuning the global displacement. To address the question of the cumulative effect, the total displacement of each film was fitted by a linear function, (Figure 72a). The slope of each function is a robust representation of the global deformation experienced in each film. Figure 72b plots the slopes of the fitted functions with respect to the molar ratio of each respective film. This plot shows a quite linear relationship between the ratio of A-isomers and the global strain. Thus, it is possible to determine that the recovery processes of the (A+B) system is highly influenced by the amount of A-isomers immersed in the supramolecular network. Indeed, as just explained above, the magnitude of the displacement induced by the UV is damped by the UV absorption of CF molecule and this effect prevails for molar ratio higher than (1:3). In contrast, such screening effect does not exist during the visible radiation, the PME being consequently directly proportional to the quantity of photochromic units. In brief, for low content of DTE,

the PME induced by UV light is stronger than PME induced by visible. For high content of DTE, the situation is reversed. This is the reason why, after 6 irradiations cycles, a global displacement of the thin film is observed toward the right (+200µm) for ratio (1:5) and toward the left (-700µm) for ratio (1:1).
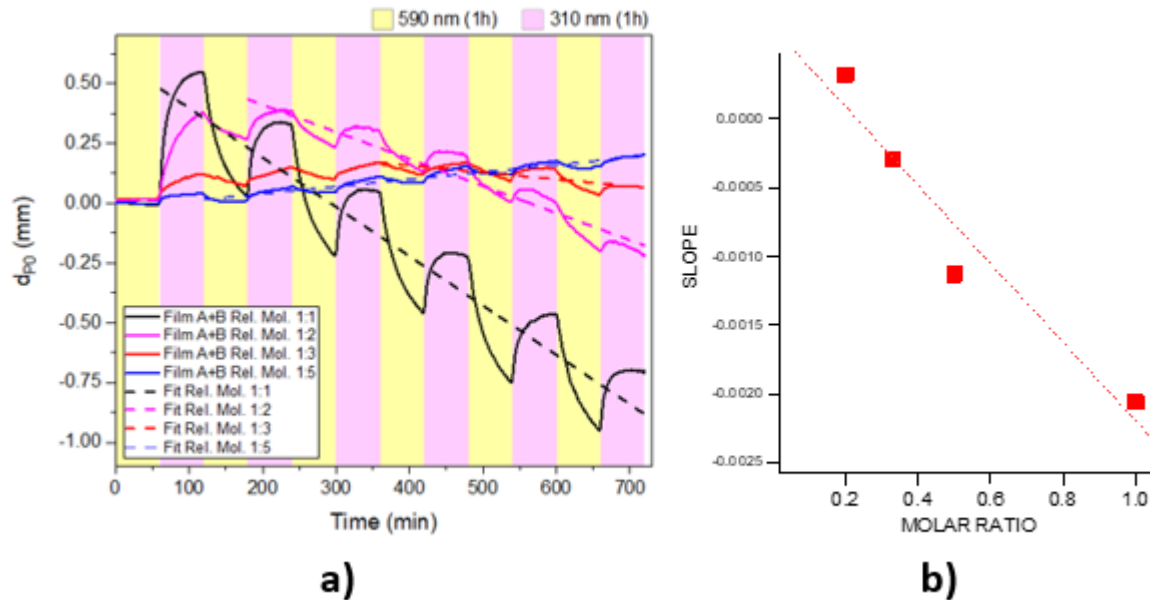
Figure 72. a) Fitting of linear functions to the displacements obtained with films of different molar ratios. b) Slope values of the fitted functions vs. molar ratio.
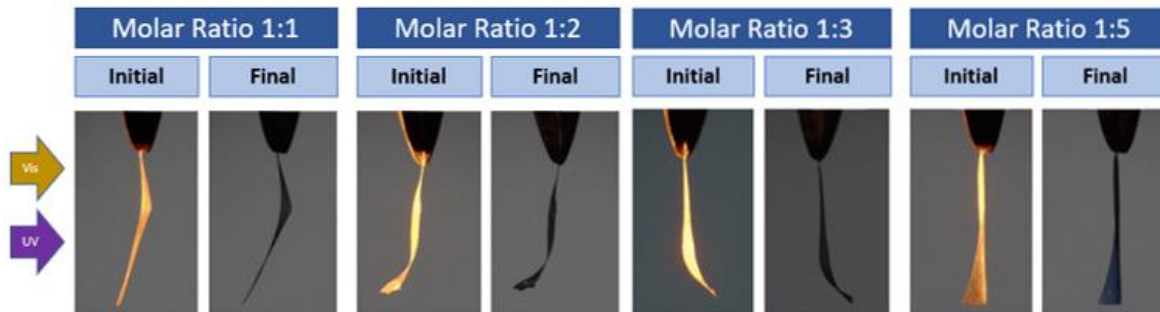
Figure 73. Initial and final frames in the displacement analysis for films (A+B) with molar ratios 1:1 to 1:5.

Geometrical factor? The shape and position of the film is another factor that could affect the performance of the photomechanical effect, the images in Figure 73 show the frames taken at the beginning and at the end of the displacement

analysis. This comparison is intended to try to find if there is a relationship between the initial shape or position of the films and the deformation of the films in the irradiation cycles or the final overall deformation. In the films presented, only the 1:3 molar ratio film shows a significant difference in its initial shape compared to the other films with different molar ratios. The films with molar ratios 1:1, 1:2 and 1:5 initially had a slight concave curvature in the opposite direction to that of irradiation; this shape was maintained during the irradiation cycles despite the deformation presented. Although there is a difference in the initial shape of the films, the graphs in Figure 73 in addition to the images in Figure 69a do not provide any clear evidence of a connection between the initial shape of the films and the deformation produced by the photomechanical effect.

IV.E.1.1. The importance of UPy hydrogen bonding networks

General presentation. In this section, we aim to assess the role played by the UPy-UPy hydrogen bonding network for the PME effect reported above. To do so, we will compare the displacement tracking profile for two thin films elaborated with the same photochromic unit DTE-UPy (A) but with two different elastomers: i) the regular elastomer PEB-UPy (B) studied so far; ii) a mixture of UPy functionalized elastomer from the commercial diol with an average of 50% of the OH group being substituted by the UPy units, (B$_{50}$).
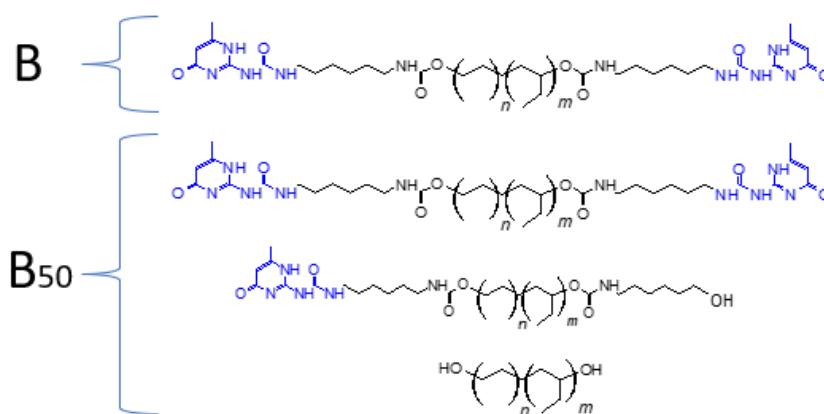
Figure 74. Schematics of thermoplastic elastomeric molecules functionalized at 100 percent and 50 percent.

The displacement tracking profiles for the two thin films (A+B) and (A+B$_{50}$) with molar ratio (1:1) are presented in the Figure 74 with the same scale. A comparison table is also displayed on the Table 7. Clearly, the first striking results concerns the drastic decrease for the PME amplitudes for both UV and Visible excitations. Suppressing half of UPy units divides the PME amplitudes by an average factor of 14.8 for UV and 12.3 for visible excitation. Concerning the dynamics analysis (see above), it is surprising to observe a quite similar behavior for the cycle #2 followed by a drastic decrease of τ_2 for (A+B$_{50}$) (50 to 16 min). In contrast, the characteristic times for visible excitation are of the same order of magnitude.
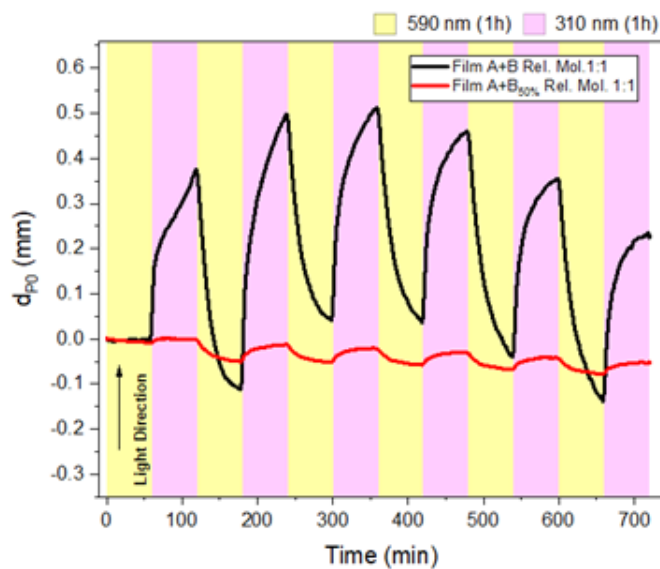
Figure 75. Comparison of the displacement presented between the film (A+B) (black line) and film (A+B$_{50}$) (red line).

Cycle	UV						VIS			
	(A+B)			(A+B$_{50}$)			(A+B)		(A+B$_{50}$)	
	τ_1 (min)	τ_2 (min)	d_{P0} max (µm)	τ_1 (min)	τ_2 (min)	d_{P0} max (µm)	τ_3 (min)	d_{P0} max (µm)	τ_3 (min)	d_{P0} max (µm)
2	4.4	50	610	5.4	50	38	16.1	487	18.7	50
3	4.9	47	470	3.2	16	31	17.4	450	17.3	40
4	5.3	36	420	3.0	15	31	19.5	475	16.1	36
5	6.2	39	390	2.5	16	27	21.0	495	16.2	37
6	5.6	23	370	3.2	17	25	21.9	488	16.8	36

Table 7. Comparison of values Characteristic times pre-exponential factor or statistical weight from the fitting by mono or biexponential of displacement between (A+B) and (A+B$_{50}$) films.

110

Mechanical results (summary). To better understand those results, it worth to summarize here the mechanical tests perform by our collaborators @ *Laboratoire de Mecanique de Lille* for the thin film B, B_{50} and (A+B). Note that the thin films were elaborated with hydraulic press [47] resulting in thicker films. The main results are summarized on Table 8.

First, stress relaxations experiments (σ=f(t) under constant deformation) has been conducted to deduced visco-elastic dynamical parameters but fitting the relaxation curve with a stretch-exponential

$$\frac{\sigma(t)}{\sigma_0} = k_2 \exp\left(-\frac{t}{\tau_0}\right)^{\beta} \beta \tag{39}$$

Where τ_{σ} is the stress relaxation characteristic time while k_2 and β are dimensionless parameters. Then, tensile test have been performed σ=f(ε) under constant strain rate) for deducing the well-known Young Modulus E.

	τ_{σ} (s)	k_2	β	E(MPa)
B_{50}	331.5	0.21	0.30	21.1
B	3.2	0.60	0.15	21.8
$(A+B)_{50}$ (OF)	-	-	-	20.6
$(A+B)_{50}$ (CF)	-	-	-	24.7

Table 8. Stress relaxation characteristic time τ_{σ}, while k_2 and β are dimensionless parameters and Young Modulus E.

First, the very similar Young Modulus for B_{50} and B indicate that both elastomers have a similar ability to propagate the PME coming from the photochromic units. Indeed, the rigidity (stiffness) is conferred by the crystalline domains coming from the initial PEB elastomer [47] common for the two samples. The main difference between the two samples is the very slow response time for B_{50} compared to B for more than two orders of magnitude! In other words, the poor performance for B_{50} is due to the poor ability for the UPy-PEB-OH chains to reorganize fastly enough during the (de)coloration kinetic. The Photomechanical effect characteristic time

being initiated by the photoswitching process (through the gradient effect) and propagated by the thermoplastic elastomer, a kind of convolution product can be express

$$d_{P_0}(t) \propto e^{-\frac{t}{\tau_{PME}}} \propto e^{-\frac{t}{\tau_{photochromism}}} \otimes e^{-\frac{t}{\tau_\sigma}}$$

To get an efficient photoactuator, one needs: $\tau_{photochromism} \gg \tau_\sigma$ which is not the case for $A + B_{50}$.

> **Clearly, a good UPy-UPy network connecting both DTE-UPy and PEB-UPy is the most fundamental key parameter to obtain good PME performances.**

Then, paying attention to film (A+B) in OF vs CF, the sight difference for the Young Modulus indicates than CF thin film (blue) is more brittle than the OF thin film (colorless). As explained by the bimetallic model presented in chapter I this is the key to transduce the change in mechanical properties into mechanical forces.

IV.E.2. The importance of elastomer crystallinity

In order to investigate the role played by the crystallinity of the PEB elastomer, we undertake the comparison for the displacement tracking profile for the previous thin film (A+B) with an analog changing the semi-crystalline elastomer PEB-UPy with an amorphous PEB-UPy (see chapter 2 for details). The comparison is displayed on Figure 76 and Table 6. For the amorphous thin film, a similar back and forth displacement is observed under successive UV/Visible irradiation compared to the previous case; however, some significant differences are noticed:

- Amplitudes are divided by an average factor of 2.7 for UV and 2.5 for Visible.

- Although characteristic times τ_3 for photoreversion are of the same order of magnitude (~20 min), throughout cycles, one observes a decreasing trend for the amorphous film.

- Similarly, for photocyclization, a drastic decreasing trend is also observed for τ_2 but not for τ_1.

- For the visible illumination periods, a clear thermal relaxation (film bending forward to the light direction) occurs after 20 min of irradiation. The displacement tracking profile were fitted with linear functions and the slope are indicated into Table 8.

- Unlike thin film (A+B), a dumping effect is noticed for the amplitudes of the PME induced by the visible performances (-25% between cycle #1 and cycle #6).
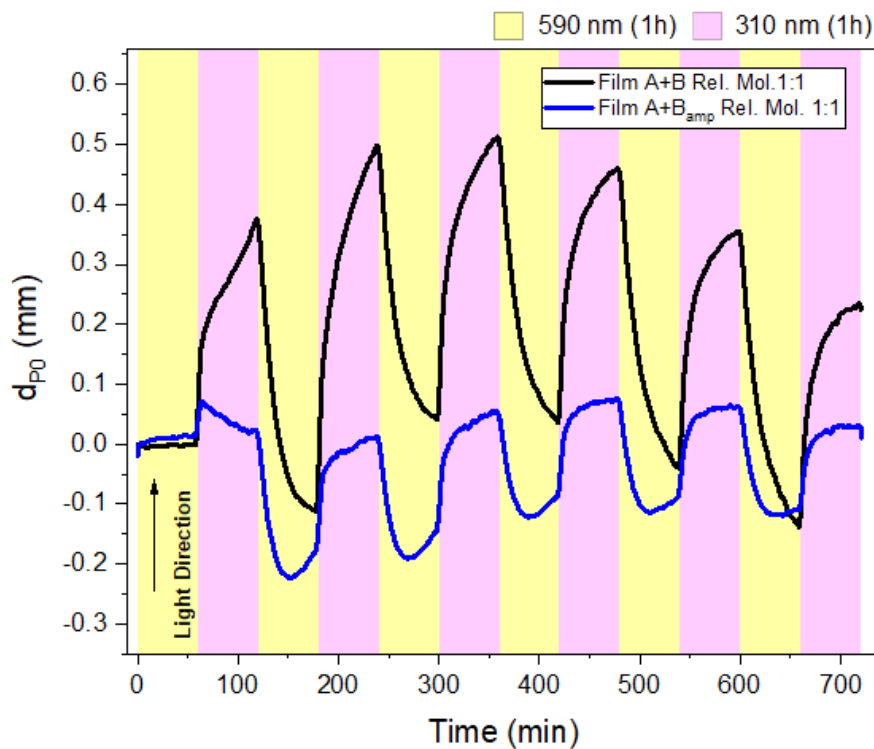
Figure 76. Displacement tracking profile for thin film (A+B) in black and thin film (A+B$_{amp}$) in blue. (amp=amorphous)

Cycle	UV						VIS				
	(A+B)			(A+B) amorph.			(A+B)		(A+B) amorph.		
	τ_1 (min)	τ_2 (min)	d_{P0} max (μm)	τ_1 (min)	τ_2 (min)	d_{P0} max (μm)	τ_3 (min)	d_{P0} max (μm)	τ_3 (min)	d_{P0} max (μm)	Slope (mm.min-1)
2	4.4	50	610	3.5	200	190	16.1	487	20	240	0.004
3	4.9	47	470	3.8	60	195	17.4	450	16	200	0.003
4	5.3	36	420	4.1	20	160	19.5	475	21	175	0.003
5	6.2	39	390	4.7	16	150	21.0	495	16	185	0.002
6	5.6	23	370	5	21	140	21.9	488	12	180	0.0004

Table 9. Values were obtained by fitting the graph to the displacement of the film (A+B)$_{amp}$. Irradiated for 6 cycles of UV/Vis light.

The elastomer PEB-UPy (B) being semi-crystalline the reticulation is brought by both UPy-UPy aggregate and crystalline domains of Polyethylene branch. In contrast, the amorphous analog is only reticulated by the UPy-UPy aggregate, simple evidence being the liquid aspect of the polyethylene-butylene precursor prior UPy telechelic functionalization. By consequence, the comparison for the two samples allows to conclude that:

Even if semi-Crystalline domains of the elastomers are not required to get PME, they magnify the amplitude of the collective effect probably through the rise of the Young Modulus. The presence of semi-crystalline domains prevents the dumping throughout the successive illuminations.

IV.F. Conclusions

In this chapter, we present for the first time, photomechanical effect for the novel system that blend a photochromic DTE and a thermoplastic elastomer in supramolecular interaction via UPy units.

We have presented the results obtain with the novel displacement tracking profile set up. For a thin film (A+B), with typical dimension 8 x 2 x 0.017 mm, the film bend to the right toward the UV light and revert back to the left with visible light. The displacements amplitude rises up to 500 µm and the UV and Visible amplitude are not similar for a given irradiation time (1h) and LED power (700µW). The visible displacement amplitude is directly proportional to the DTE quantity, while for the UV case, the situation is more complex due to screening effect (both OF and CF absorb UV). Due to this difference, the global displacement (additive displacement for each irradiation cycle) can be control by the quantity of DTE or b the irradiation period. The kinetic analysis of the displacement tracking profile show that the PME is totally control by the propagation of OF/CF gradient along the material. The forward backward characteristic times are fully correlated with the kinetic of coloration or discoloration of the film. Indeed, the mono or biexponential trend reported for the discoloration and coloration kinetic respectively is strictly reflected during the PME.

A comparison of our system with very recent study dealing with PU-AZOs LCE system indicate that our system is competitive for UV excitation, and even feature better performances for Visible excitation. Clearly, our novel system –easy to prepare and reusable- pave the way for a new paradigm –allowing to explore the centimetric scale not reachable for DTE crystal.

After preliminary tests engaging systems without (A0+B0) or partial (A0+B) UPy network, it has been concluded that the good supramolecular connection via quadruple hydrogen bonding is the most important parameter to obtain an efficient PME. Indeed, with a fast visco-elastic response of the elastomeric network, the good UPy connection between A and B units will better propagate the mechanical stress at the molecular level (difference of Young Modulus between OF and CF). Otherwise, the PME would be blurred out by a slow viscoelastic response case of (A+B$_{50}$). The semi-crystalline properties of the elastomer seems to be fundamental to maintain good reversibility.

CHAPTER V

Structural and Morphological Analysis of

DTE-UPy/PEB-UPy Thin Films

In the previous sections, the photomechanical effect produced by irradiating thin films made from a mixture of A and B with UV/Vis light has been analyzed. These analyses focused on the dynamics of the films during the irradiation processes, leaving aside the study of the structural and morphological processes involved in this phenomenon.

However, the study of the surface and structure provides essential information on the conformation of the material and its properties, both optical and mechanical. Concerning supramolecular networks based on the combination of elastomers with UPy units, the study of their structure and morphology shows the correlation of their mechanical properties with the organization of the supramolecular assembly [85].

On the other hand, it is well known that the deformation direction (towards or away from the light) of crystals formed from diarylethene derivatives depends strongly on the wavelength at which they are irradiated [40], the irradiated face [86], irradiation angle [87], light polarization [88] and combination with other molecules [89]. In this context, the study of the structure, surface and morphology of materials made from a mixture of diarylethene derivatives and polymers, such as liquid crystal

elastomers [54], provides important information on the behavior and performance of the photomechanical effect present in these materials. It is important to note that the study of these materials often presents a higher complexity due to the random organization of the photoactive molecules and chains, while the phase difference and the organization of the domains in addition to the crystallinity play a crucial role in the performance of the photomechanical effect [90].

In this section, we will analyze the results obtained from the use of scanning electron microscopy (SEM) and atomic force microscopy (AFM) techniques, which provide information on the changes produced on the surface. On the other hand, Wide Angle X-ray Scattering (WAXS) and Small Angle X-ray Scattering (SAXS) techniques provide information on the crystalline conformation and its distribution, as well as the distribution of macromolecules, size, shape, and characteristic distances.

V.A. Surface Topographic Analysis Using SEM

SEM analysis was performed on two samples of the same film (A+B). Each sample was brought to a different state by exposing each piece to UV light at 310 nm (CF) and Visible light at 590 nm (OF) for a period of 3h. Subsequently, each sample was coated with a thin layer of carbon to enhance the secondary electron signal and protect the samples from thermal damage.

The OF sample analyzed by SEM is shown in Figure 77a. It shows an inhomogeneous topography with irregular shaped domains with well-defined boundaries. The domain size analysis showed an average diameter distribution of 163 nm and a standard deviation of 43 nm (see Figure 78). On the other hand, Figure 77b corresponds to the image of the sample in the CF state. The sample presented a more rugged irregular topography compared to that observed in the OF sample, with irregularly shaped domains with poorly defined boundaries. The distribution of domain diameters for this sample was larger with an average diameter of 250 nm with a standard deviation of 96 nm.

The diameter distribution analysis in Figure 78 and the SEM photographs in Figure 77 demonstrate a significant difference in the surface morphology of the samples. In particular, the diameter analysis showed statistically that the size of the domains in the CF state is 53% larger compared to the OF state. In addition, the topography appears more rugged in the CF state.
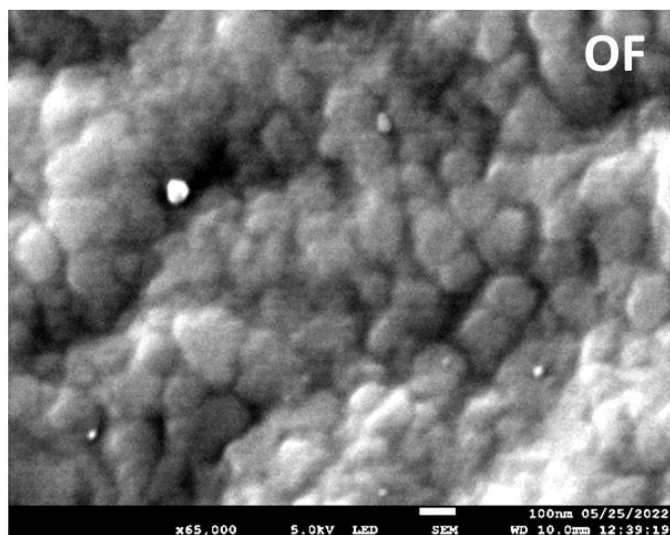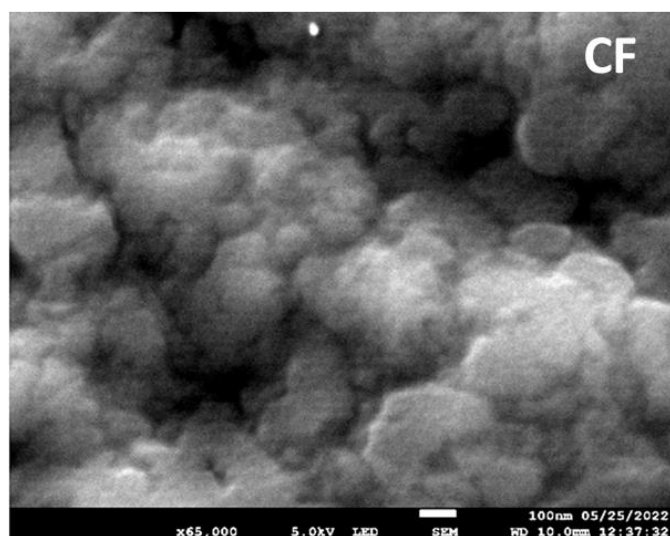
Figure 77. SEM images of two samples of a film (A+B) in a) Open Form and b) Close Form.

This first study shows a significant change in the size of the domains between the OF and CF states, however, it is necessary to corroborate with other studies to verify that the changes are produced by photomechanical effects and not only by the difference in the scanned areas.
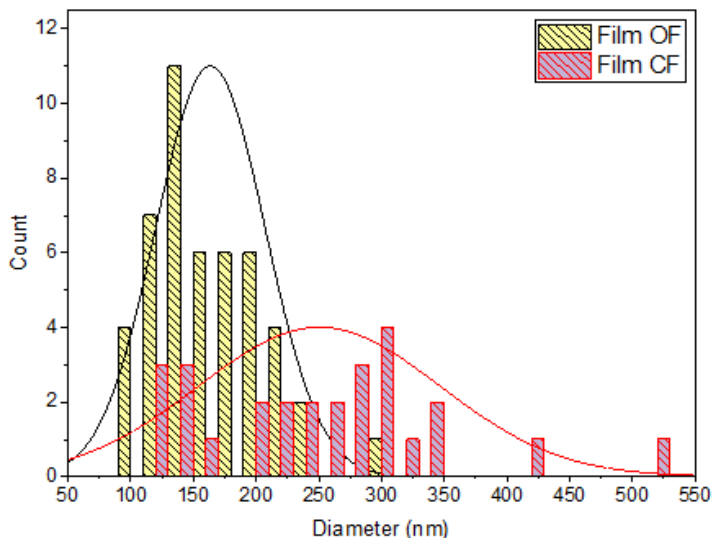
Figure 78. Distribution of domain sizes for films (A+B) in Open Form and Close Form state.

V.B. Photomechanical Effect on the Surface of Thin Films

The SEM images showed a difference in the surface in two samples each in a different state (OF or CF), this difference showed an increase in the surface size of the domains as well as a change in the relief. However, it cannot be fully stated that this change is induced by the isomerization of molecule A since the samples could present surface defects inherent to the manufacturing process and the observed changes could be due only to the observation of different zones, even if the two samples belong to the same film. The solution to the above problem was to make observations on a fixed region of the sample by Atomic Force Microscope (AFM). Three comparative measurements were made: the first measurement was made without any preliminary irradiation on the sample (initial), the second measurement was made after irradiation with UV light at 310 nm for one hour, and the last measurement was made after irradiation with visible light at 590 nm for one hour.
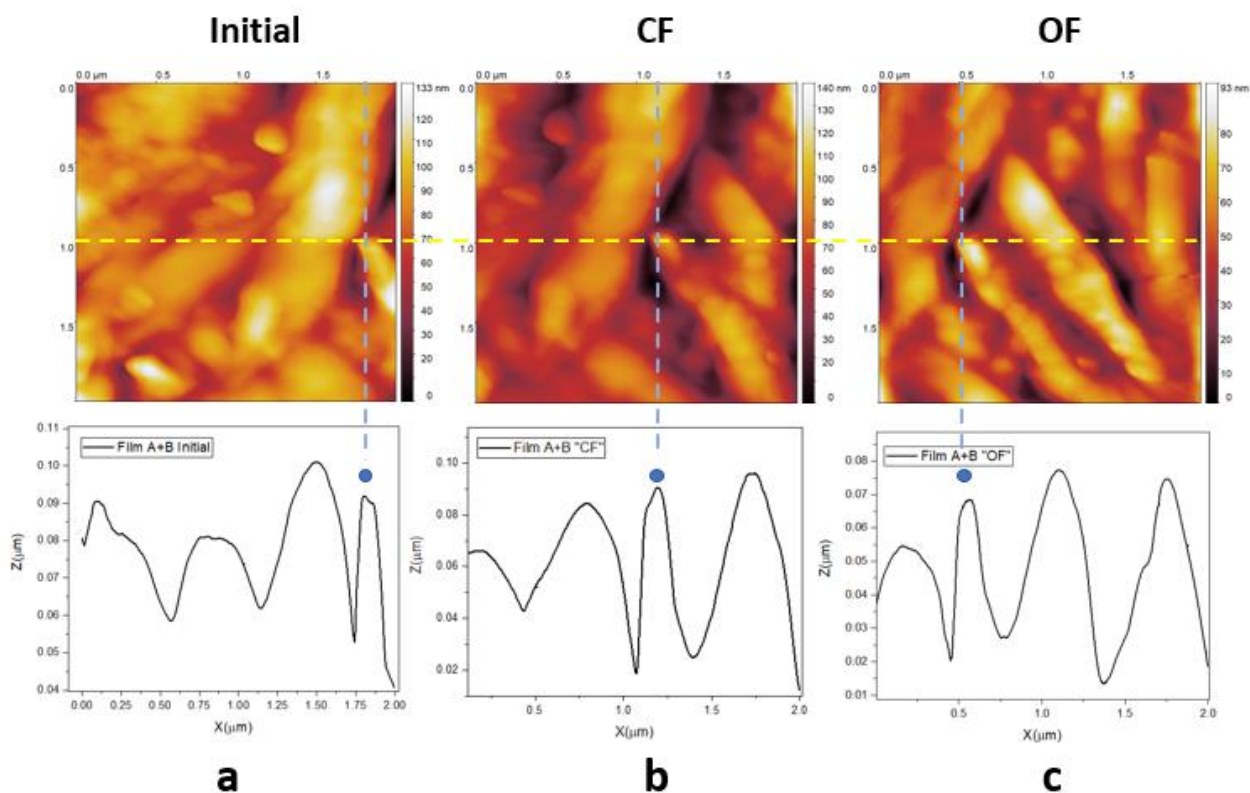
Figure 79. AFM images, a) non-irradiated film (A+B), b) film irradiated with UV light at 310 nm for one hour, c) film irradiated with visible light at 590 nm for one hour. For each image, a height profile plot was made following the yellow line. The blue lines and dots are for reference only.

The AFM images (the size of the analyzed region was 2 µm x 2 µm) are illustrated in Figure 79. A rough surface with irregular domains and no defined structures was observed. The insufficiency of detail (sharpness) in the images can be attributed to the strong electrostatic interaction between the sample and the cantilever of the microscope.

On the other hand, within the analyzed region, an arbitrary reference point was taken, which would facilitate the analysis of the three measurements as well as being easy to recognize. The analyzed point was taken in the left lateral zone in the initial measurement and moved to the left side as the measurements were taken. This translation is possibly due to the programming of the initial coordinates of the microscope itself.

A line (dotted yellow line) was drawn on the Y-axis on the reference point where the height profiles of each of the measurements were extracted. The blue dotted

line represents the reference point on the X-axis on which the height profiles were compared. The blue dot in the lower images of Figure 79, shows graphically the reference point corresponding to the peak of the height profile used in the comparison of profiles in Figure 80.

The analysis was performed by matching the minimum point of each of the profiles by moving them on the X and Y axis, as illustrated in Figure 80, left side. Then the area under the curve was integrated taking as limits the lateral peaks and as baseline the minimum value of the curves. The area obtained is shown on the right side of Figure 80, while the calculated values are shown in Table 10.
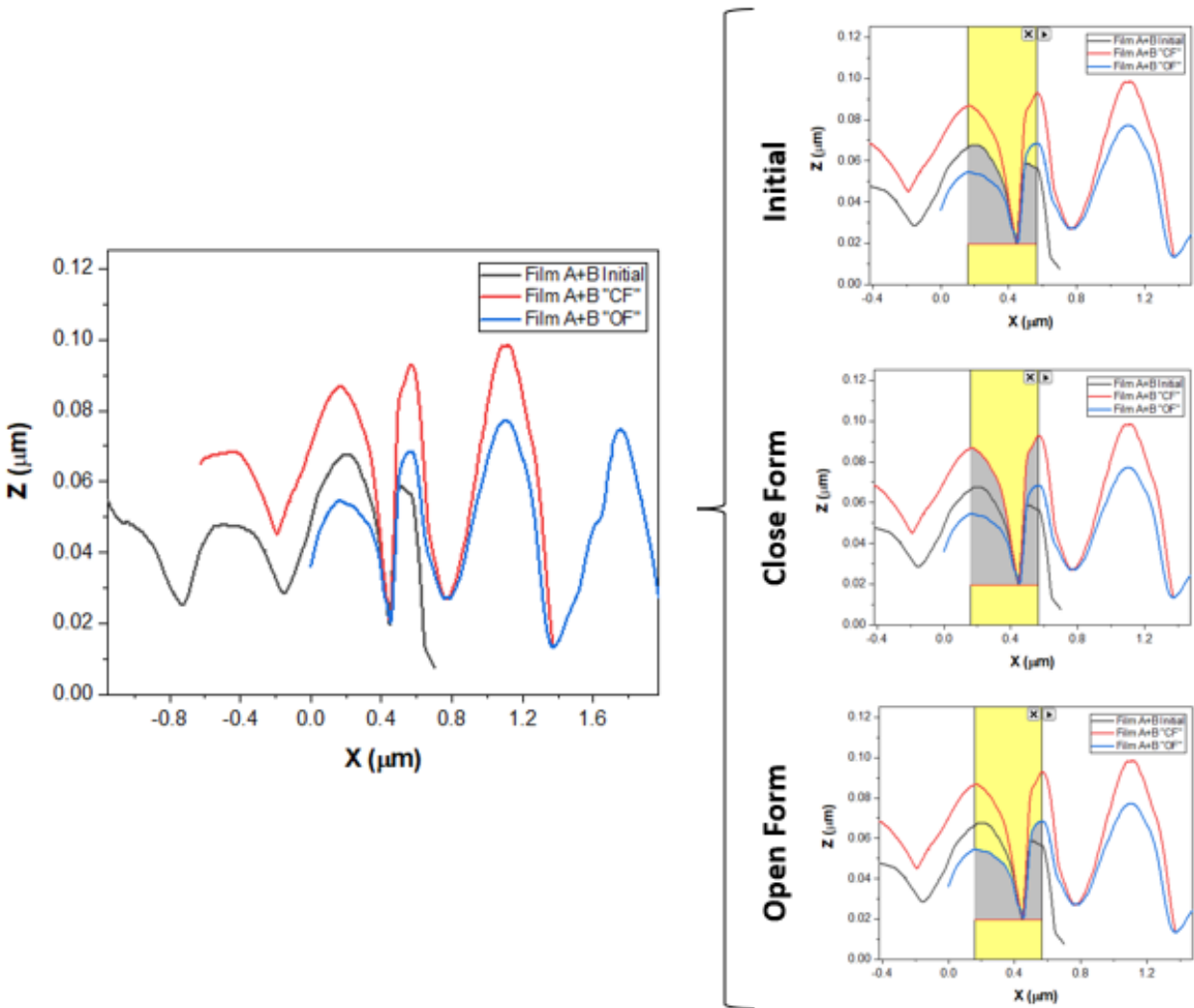
Figure 80. Left side, comparison of height profiles of SEM images. Right side, the integration of curves for the profiles obtained in the initial state, Close Form, and open Form.

State	Area (nm^2)
Initial (OF)	1391
Close Form	1976
Open Form	1152

Table 10. Calculated area values of height profiles obtained from AFM images for a film (A+B) sample.

As can be seen in the height profiles, there is a change in the surface of the film when passing from the initial state to the CF state, which translates into an increase in the height of the peaks, while the analysis of the profiles showed an increase of 42% of the area of the curves. On switching the sample back from the CF state to the OF state by visible light irradiation, a noticeable decrease in peak height was seen, representing a reduction of about 58 % of the curve area.

Clearly, considering the transition from OF to CF, the variation of the height profiles in AFM (+58%) corroborate nicely the change in the size of the domains (+53%) reported from the SEM analysis

As mentioned above, diarylethene, when passing from the OF to the CF state, elongates in the short axis, while it contracts in the long axis. In the case of crystals, the change in their length directly affects the molecular packing around them inducing deformation. The direction of deformation in the case of crystals depends on factors such as: type of derivative, the wavelength of light, irradiated face, and polarization. However, in the case of diarylethene and thermoplastic elastomer blends there are no publications that verify whether these conditions affect the intensity and direction of deformation in the same way.

In the particular case of this thesis, the films (A+B) in Chapter IV show a bending in the direction of irradiation when exposed to ultraviolet (UV) light at 310 nm. This bending does not change direction over several irradiation cycles. SEM and AFM results confirm that this bending is caused by the approximately 50% increase in

the size of the domains formed by A/B, Figure 81. Indeed, this effect schematized together with the interpretation of Morimoto *et al.* for DTEs cocrystals. The analogy between our two systems is relevant: the elongation of the b-axis crystallographic parameter for the crystalline case is corroborated by the swelling of the CF domain.

This structural effect – the reversible swelling of the CF domains under UV/Visible irradiation- is the key to rationalize the PMEs reported in this manuscript so far.
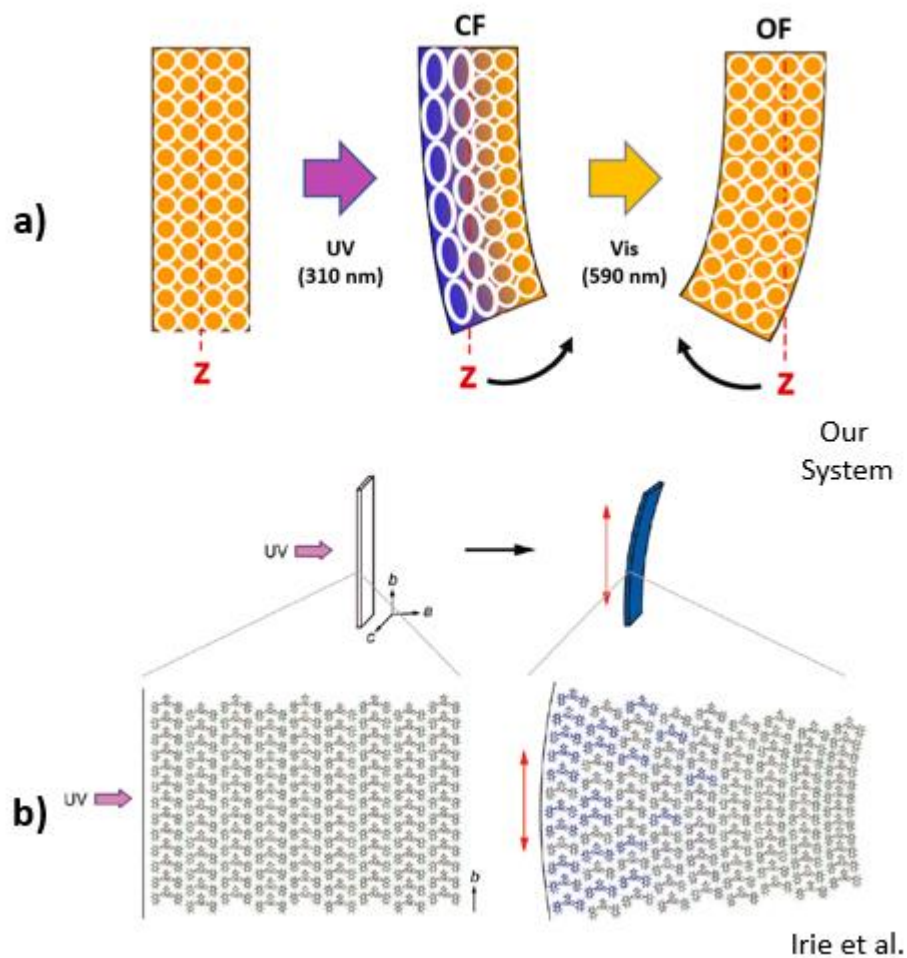
Figure 81. a) Bending of a thin film (A+B) in the direction of light by increasing the size of the domains from OF to CF. b) Crystallographic interpretation for the PME of diarylethene crystal [91].

V.C. Structural Analysis Using X-Ray

In the past chapters and sections, the behavior of films that present photomechanical effect when irradiated by alternating cycles of UV/Vis light was exposed. The behavior of the films when varying the exposure time, as well as their manufacture, was analyzed in the last chapter, while in the past sections, the change in the topography of the film was observed as a first approximation in the rationalization of the structural and morphological change induced by the photomechanical effect on the material. In this subsection, two studies focused on X-ray scattering and diffraction were carried out. Firstly, Wide Angle X-ray (WAXS) analyses were carried out in order to analyze the semicrystalline structure of thermoplastic elastomer B, photoisomer A (both functionalized with UPy units) as well as the films (A+B). Subsequently, analyses were performed with the Small Angle X-ray Scattering (SAXS) technique. This technique allows seeing the changes in the microphase separation between amorphous and ordered zones within the polymer matrix, as well as changes in the volume fractions [92], [93].

V.C.1. Crystal phase analysis of thin films DTE-UPy/PEB-UPy

Thermo elastomer B_0 (Poly(ethylene-co-butylene) is a copolymer whose degree of crystallinity depends strongly on the ratio between ethylene and butylene moieties. When the ratio of butylene is greater than 50% the copolymer remains amorphous, while below this value the copolymer is semi-crystalline [60].

The degree of crystallinity of thermoplastic elastomer B is associated with the ethylene polymer which possesses two main crystalline forms at atmospheric temperature and pressure, the orthorhombic form and the monoclinic form. Of these two crystalline forms, the orthorhombic form is the more stable form, while the monoclinic form is found in smaller proportion and is generated under the alignment of uniaxial stresses such as expansions as well as compressions [94–96].

When the thermoplastic elastomer is functionalized with UPy "B" units, it forms a supramolecular network in which a competition is generated between the intrinsic organization of the elastomer (which depends on the copolymer ratio) and the organization of the macromolecules induced by the self-assembly of the hydrogen bonds.

Organization due to self-organization of the supramolecular network has been reported using WAXS evidencing two characteristic distances: an interplanar distance of 1 nm between UPy near neighbors (dimers) [97] and 0.455 nm between stacked bisurea units [98].

While a comprehensive study on thermoplastic elastomer B (poly(ethylene-co-butylene) copolymer) films was reported by Louati et al [7]. This investigation describes in detail the evolution of the supramolecular network structure with temperature. Additionally, it provides details on the ratio of the crystalline fractions (monoclinic and orthorhombic) strongly influenced by the amount of poly(ethylene-co-butylene) and UPy aggregates.
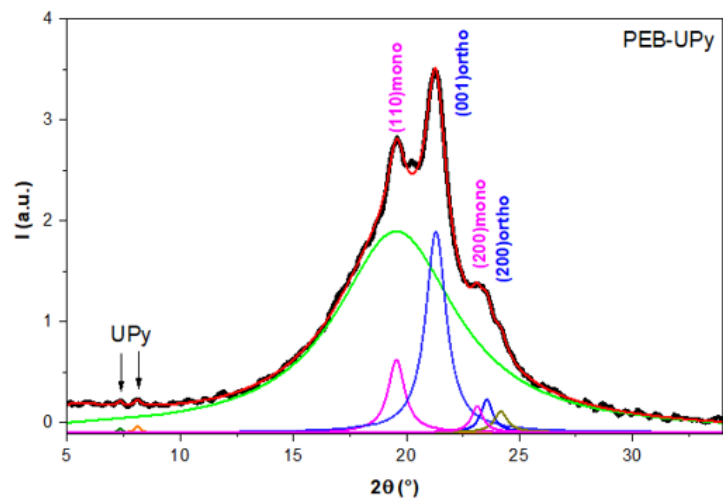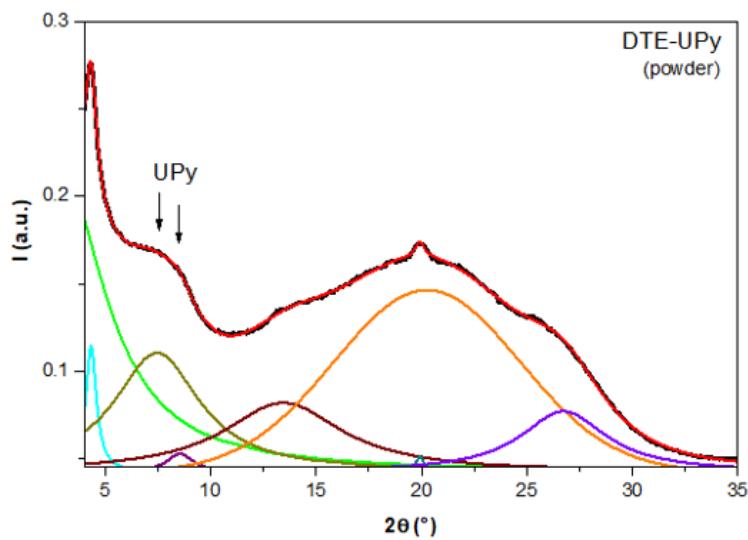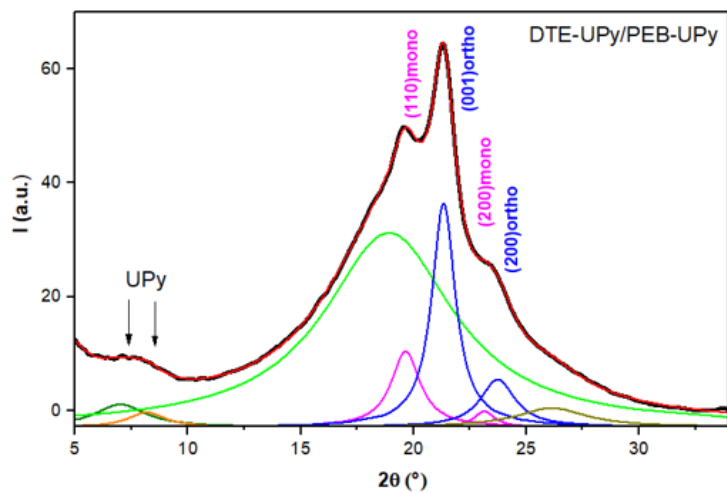
Figure 82. WAXS analysis and deconvolution profiles: a) PEB-UPy film, b) DTE-UPy (powder) and c) DTE-UPy/PEB-UPy film.

In this section, we analyze the changes that occurred in the structure of the B films when the functionalized photoactive molecule A is added. For comparison, WAXS was performed on a film of B (Figure 82a) fabricated with the same process used for the creation of the films (A+B). Also, WAXS was performed on the powder of A (Figure 82b) in order to identify the contributions of the UPy aggregates on the supramolecular network structure.

The WAXS spectrum of a film (A+B) is shown in Figure 82c. The integrated profile was fitted with Lorentzian functions to extract the amorphous and crystalline fractions. This deconvolution exhibits the presence of seven peaks in addition with a large halo corresponding to the amorphous fraction. These peaks are the same as those presented in the WAXS profile of elastomer B, Figure 82a. Four of the seven peaks correspond to the crystalline fractions of polyethylene: two peaks at $2\theta=21.3°$ and 23. 5° correspond to the (110) and (200) planes of the orthorhombic form (a=7.40 Å, b=4.93 Å, and c=2.54 Å), while the peaks at $2\theta=19.5°$ and 23.1° are associated with the (001) and (002) planes of the monoclinic form (a=8.09 Å, b=4.79 Å, c=2.53 Å, and β=107°) [47], [99–101]. The small peak at $2\theta=8.3°$ corresponds to the reflection of the stacked planes of the UPy domains at d=1 nm [59], [102]. The remaining two peaks at $2\theta=7.3°$ and 26.1° are attributed to the contribution of crystalline planes of DTE-UPy. These peaks are observed in the deconvolution performed on the WASX spectrum of the DTE-UPy powder, Figure 82b. Additionally, this deconvolution shows two complementary peaks at $2\theta=13.4°$ and 19.9°, the latter corresponding to the second reflection of the interplanar distance between the UPy motifs. However, they are not visible in the spectra of B and (A+B) due to their low contribution and are therefore overshadowed by the halos of the amorphous contribution.

The crystallinity and relative fractions of the crystalline phases of the B and films (A+B) were calculated from the integrated areas of the corresponding peaks (Table 11). The overall degree of crystallinity of the B film is close to 22%, of which the orthorhombic fraction represents 75% and the monoclinic fraction 25%. For film (A+B) a partial increase in crystallinity was observed, however, this increase in crystallinity cannot be attributed to the addition of DTE-UPy since another film A/B,

128

which will be presented later, showed an overall crystallinity close to 18%. Although. Although the films were prepared in the same way and under the same conditions, the structure tends to be quite sensitive to any external influence, such as the process of separation from the substrate or anchoring to the support. It is important to note that the role of temperature as well as the fabrication process directly affects the overall crystallinity as well as the relative crystalline fractions, as demonstrated in the research of Louati et al [47].

	χ (%)	F_{ortho} (%)	F_{mono} (%)
"B" **PEB-UPy**	22	75	25
"(A+B)" DTE-UPy/PEB-UPy	30	73	27

Table 11. Crystallinity (χ) for films B and (A+B). Relative fraction (F).

V.C.1.1. Effects of the change of state (OF-CF) and irradiation cycles on the crystalline phase

The WAXS intensity profiles for a film (A+B) irradiated with alternating UV/Vis light are shown in Figure 83. The three WAXS spectra were performed in three different states with "in situ" illumination during the data acquisition process. The first spectrum was performed without any irradiation of the film (black line). Subsequently, the film was irradiated with UV light (310 nm at 796 µW) for one hour. After this time, the second spectrum was obtained (red line). Then, the film was irradiated with visible light (590 nm at 796 µW) for one hour to acquire again the WAXS spectrum.
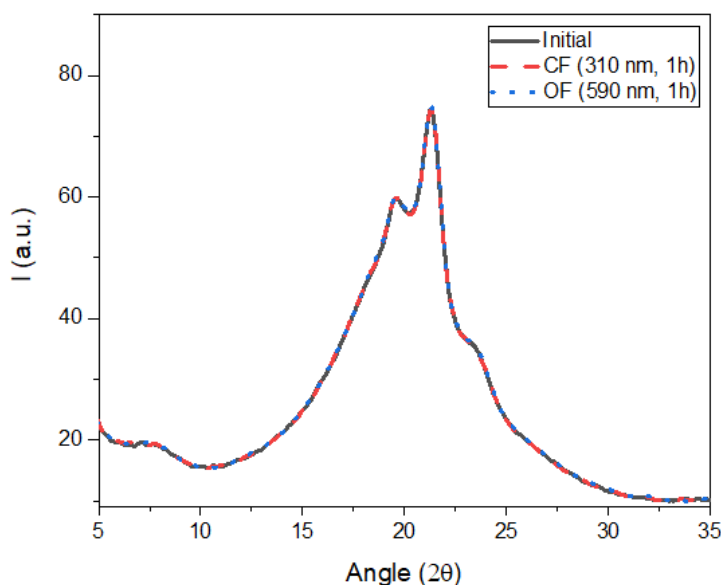
Figure 83. WAXS intensity profiles for a film (A+B) that was exposed to alternating UV/Vis light irradiation (310 nm, 590 nm at 796 µW) for one hour for each wavelength.

The three WAXS spectra for the initial, CF and OF states overlap almost perfectly. As such, no significant change is apparent between the initial state and the OF and CF states. Although it would be expected that there would be changes in peak intensity due to the variation in relative crystal fractions, this was not observed. It is possible that the irradiation time was not long enough to observe any change. As discussed in Chapter III, the time required to obtain a complete photocyclization process is approximately three hours.

On the other hand, to verify if there are changes in the crystallinity, as well as in the relative fractions due to the photocyclization and photoreversion processes, WAXS analysis was performed on a film (A+B) which was exposed to 18 cycles of UV/Vis light irradiation. The WAXS were carried out on two different areas of the same film (A+B). The first analysis was performed on the non-irradiated area, which was covered by the clamps holding the film during the displacement analysis described in Chapter IV. The second analysis was done on the area that was exposed to the 18 UV/Vis light cycles (310 nm, 590 nm at 796 µW). A photograph of a film showing the areas of irradiation and how the area hidden by the clamp is exposed is shown in Figure 53a.
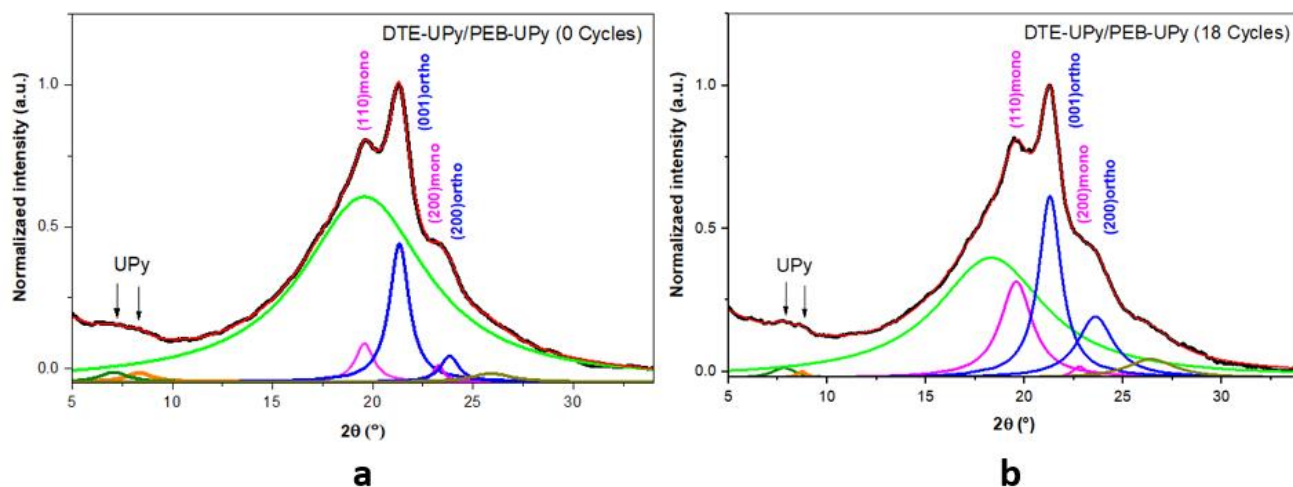
Figure 84. WAXS intensity and deconvolution profiles of a film (A+B) a) not exposed to UV/Vis light irradiation and b) after being exposed to 18 cycles of alternating UV/Vis light irradiation (310nm, 590 nm at 796 µW).

The WAXS profiles for the two areas of the same film (A+B) before and after irradiations are shown in Figure 84. As in the previous subsection, seven peaks incorporated in a halo characteristic of the amorphous fraction are observed.

The four peaks corresponding to the orthorhombic and monoclinic relative fractions are present as in the previous subsection, but with different intensities. The crystallinity and relative fractions corresponding to the deconvolution of the WAXS analyses are shown in Table 12. The overall crystallinity in the non-irradiated zone was close to 18% with a relative orthorhombic fraction of 78% and a relative monoclinic fraction of 22%. Although the crystallinity is lower compared to the film (A+B) in the previous section, the ratio of relative fractions remains almost the same. In the irradiated zone, the overall crystallinity increased to 44%, while the orthorhombic relative share decreased to 66%, which translates into an increase in the monoclinic relative fraction of 50% with respect to the relative fraction of the non-irradiated zone.

This increase in crystallinity is attributed to the reorganization of the polymeric chains induced by the stress gradient along the irradiation cycles of the predominantly amorphous zones. Additionally, the uniaxial tension causes the deformation of the orthorhombic crystalline zones which induces the transformation of a percentage of this fraction to the monoclinic form. Likewise, the interaction

between UPy units within the supramolecular network compresses the chains inciting the monoclinic formation [103].

	χ (%)	F_{ortho} (%)	F_{mono} (%)
(A+B) (0 Cycles)	18	78	22
(A+B) (18 Cycles)	44	66	33

Table 12. Crystallinity (χ) and Relative Fraction (F), for a film (A+B) before being irradiated and after being exposed to 18 cycles of alternating UV/Vis irradiation.

V.C.2. Morphology analysis of thin films DTE-UPy/PEB-UPy

Small Angle X-ray Scattering (SAXS) is a method of characterizing the structure of materials at the atomic and molecular level, which provides information about the shape of aggregates or macromolecules, oligomer state, and the separation distance between crystalline zones [104]. In this sense, SAXS analysis in this subsection aims to identify changes in microphase separation between amorphous zones and crystalline zones associated with functional groups [47], [92], [93].

The SAXS spectra taken on a film (A+B) with "in situ" illumination is shown in Figure 85. Similar to the WAXS analyses in the previous section, three SAXS spectra were performed. The first one was taken on the film without any illumination (initial state, black line). The second spectrum was taken after irradiating the film with 310 nm UV light at 796 µW for a period of one hour (CF state, purple line). The last SAXS profile was taken after illuminating the film for one hour with Visible light at 590 nm at 796 µW (OF state, yellow line).
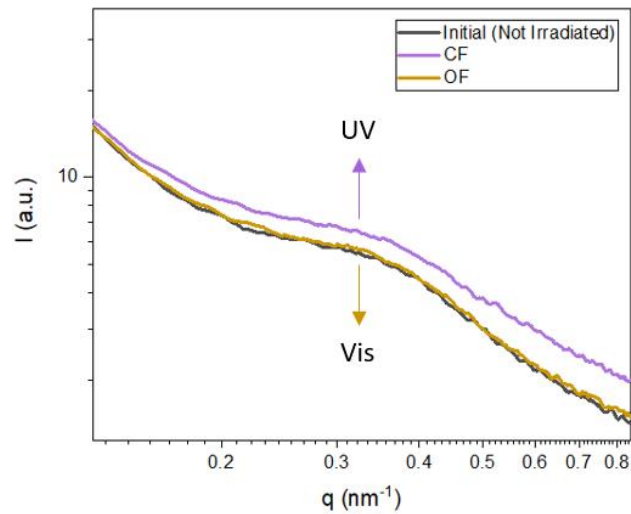
Figure 85. SAXS scattering profiles for a film (A+B), in Initial, CF and OF states. For the CF state, the film was irradiated for one hour with UV light at 310 nm at 796 µW. While the OF state was irradiated with Visible light at 590 nm at 796 µW.
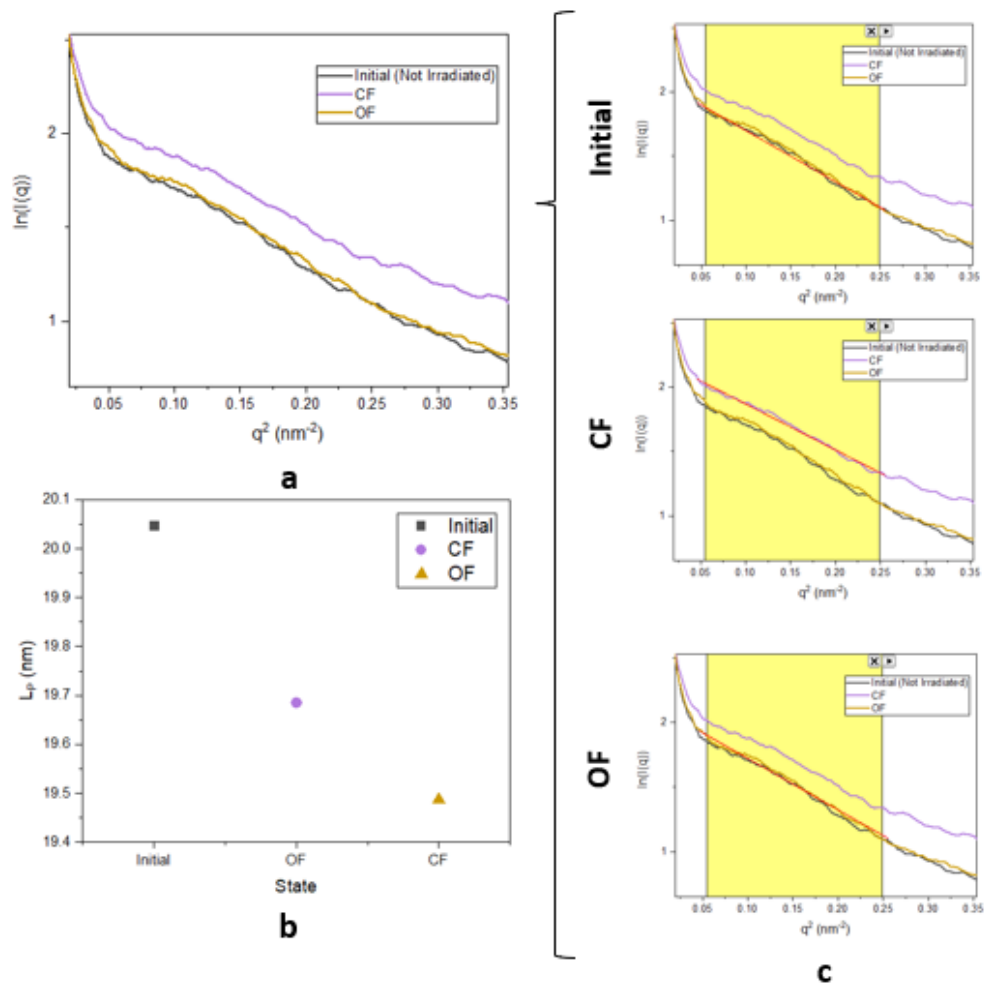
Figure 86. a) Graph of SAXS dispersions following Guinier's approximation. b) long period, L_p, obtained for each state. c) Linear fit of the graphs for Initial, CF and CF states following Guinier's approximation.

133

The SAXS profiles obtained (Figure 85) show a dispersion peak associated with the presence of ordered arrays (regular stacking of crystalline lamellae) immersed in an amorphous matrix. The intensity of the SAXS profile in the initial state (black line) increases when the film is converted to the CF state (photocyclization) and decreases reaching almost the original state when it passes from the CF state to the OF state (photoreversion). This increase and decrease in intensity can be translated as a variation in electron density and thus a change in free volume in the amorphous zones.

The estimation of the distance between amorphous and crystalline fractions can be done by defining the Long-Period (L_p). According to Bragg's law (d=2π/q) it is possible to define the distance between fractions, so that $L_p = 2\pi/q_{max}$, where q_{max} is the position of the maximum peak in the SAXS intensity profile. The L_p values for the SAXS spectra for the initial, CF and OF states are given in Table 13 and Figure 86b. The decrease in the L_p may be due to the interaction of UPy dimer units originated by expansion-contraction in the isomerization of A molecules and the aggregates formed from it. The above can be translated as a variation in the distance between zones with a huge quantity of stacked UPy units as seen in Figure 43c [62]. The value $q_{max} = 0.3 \, nm^{-1}$ agrees with the value reported by Louati et al. [47], representative of UPy aggregates. The above result shows the enormous influence that UPy bonds and in particular A and B aggregates.

On the other hand, the SAXS technique allows to analyze the distribution of distances by different approximations. The gyration radius (R_g) is the root mean square distance between the atoms of the chains and their center of mass (equation (40)), the change in R_g gives information about the average expansion or contraction of the chains [105].

$$R_g = \left(\frac{1}{n} \sum_{i=1}^{n} (r_i - r_{nm})^2 \right)^{\frac{1}{2}} \tag{40}$$
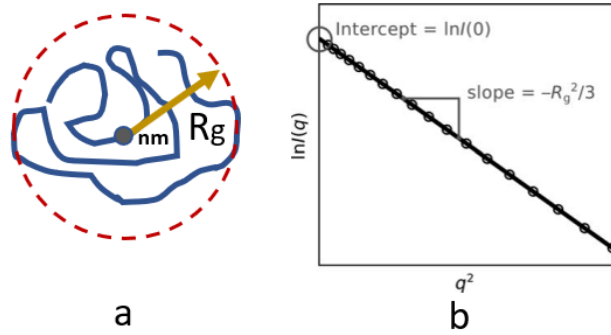
Figure 87. a) Illustration of the gyration radius, which is the root mean square distance between the atoms and the center of mass. b) Schematic of the graph of Guinier's approximation.

Where n is the number of atoms, r_i and r_{nm} correspond to the coordinates of the atoms with respect to the center of mass of the chain, respectively.

Guinier's approximation states that for very small scattering angles, the scattering intensity depends on $I(0)$ and R_g, so that the intensity can be expressed according to equation (41) [106]:

$$I(q) = I(0) \exp\left(-\frac{q^2 R_g^2}{3}\right) \tag{41}$$

Thus, $I(0)$ is the extrapolated dispersion at $q = 0$. This allows plotting the natural logarithm of the intensity $\ln(I(q))$ versus q^2, The obtained curve can be fitted to a linear function (equation (42)), where R_g is related to the slope of the dispersion, slope S (Figure 87b), as shown in equation (43). The dispersion in the graph $\ln(I(q))$ vs q^2 can be the linear fitting from equation (41), obtaining:

$$\ln I(q) = \ln I(0) - \frac{\left(R_g q\right)^2}{3} \tag{42}$$

with slope

$$S = -\frac{\left(R_g q\right)^2}{3} \tag{43}$$

135

	q_{max} (nm^{-1})	L_p (nm)	S (nm^2)	R_g (nm)
Initial	0.313	20.0	-3.99	3.4
CF	0.319	19.6	-3.56	3.2
OF	0.322	19.4	-4.04	3.4

Table 13. Values obtained from SAXS analysis for film A/B, Maximum scattering vector scattering (q_{max}). Long period (L_p), Slopes of fitted linear functions (S) and gyration radius (R_g).

The graph following Guinier's approximation is shown in Figure 86a, while the linear fit for each state (Initial, CF and CF) is shown in Figure 86c. The values obtained for the slopes and gyration radii are shown in Table 13.

The R_g obtained varies depending on the state of the film, such that the gyration radius of the initial state decreases 0.2 nm when the film passes to the CF state, i.e., when the film is irradiated with UV light. When passing from the CF state to the OF state by irradiation with visible light, the gyration radius increases 0.2 nm returning to the same value as that presented in the initial state.

This change can be attributed to the modification of the distance between the stacked UPy units or the variation of the distances between subsequent chains containing A molecules.

V.D. Conclusions

This chapter focused on the rationalization of the photomechanical effect present in films (A+B) from a structural, morphological and surface point of view.

SEM analyses provided a first view of the changes presented on the surface when films (A+B) are in different states (OF and CF). In particular, in the OF state, a higher number of domains was observed, with an approximate size of 163 nm, while in the CF state, the domains present are larger (47%), with an average size of 250 nm. Those results were corroborated by AFM analysis reporting for a reversible domains change (+53%) upon illumination. Another confirmation was achieved by the SAXS experiment with the additional information that the volume changes are related to The UPy domains.

With these morphological/structural studies, we obtain microscopic interpretation of the PME. The PME that bend the thin film (A+B) toward the light under UV irradiation is explain in term of the swelling CF domain inside the blue fraction of the sample. When the visible light is irradiated inducing the photoreversion reaction, the domain return to their initial size which induce the displacement of the film in the backward direction. A clear analogy between our system and pure DTE crystal is suggested.

CHAPTER VI

General Conclusions

Organic Photoactuators are a class of smart material that allow controlling the matter with a remote control, the light. Apart the photothermal systems that are not of the scope of the present manuscript, the organic photoactuators that display bending/flattening upon UV/vis irradiation, that include a photochromic unit are dominated by two distinct fields:

- the dynamic crystals including monocrystals of DTE that display very good performances, fast response, good reversibility, and fatigue resistance but with the major drawback to be limited to subcentrimetric dimensions.
- the cross-Linked LCE including photochromic AZOs molecule with excellent performances (especially on UV) and no size limitations but with the major problem inherent to azobenzene compounds– lack of bistablity and the preparation is complex (Photopolymerization and alignment of the mesogen).

As a new alternative, we have elaborated and characterized a novel system that blend a photochromic DTE A and a thermoplastic polyethylene-co-butylene elastomer B both functionalized with the efficient supramolecular UPy units. The solvent route protocol is basic (blending the two components 1h @ 80°C in chloroform) and the thin film elaboration is a very simple spin coating process.

To achieve a thoughtful understanding of the photoactuating properties of the thin film (A+B), we have combined a series of technic dealing with the photochemistry (Absorbance tracking profile), mechanics (displacement tracking profile) and material science approaches (AFM, SEM, X-Ray).

Concerning the performances, it was found that the system operates solely according to the DTE photochromic response as long as the relaxation of the elastomeric matrix is avoided. To do so, a careful choice of the irradiation times is required. The judicious time to avoid such contribution was chosen as 1h but, a shorter time of 10 minutes will be enough in the future. For sake of simplicity, we have chosen irradiation parameters identical for both UV and Visible light (Power and illumination period) and such parameters must be optimized in the future as well. Anyhow, with the present conditions, for a thin film (A+B) with (8 x 2 x 0.017 mm) dimension, for very low power regime (796 µW) the photoactuation observed under 6 cycles of irradiation are:

- under UV excitation: bending toward the light direction with a speed slighting decreasing throughout the cycles -from 23.8 $\mu m.s^{-1}$.
- under Visible excitation: bending backward the light direction with a constant speed of 0.1 $\mu m.s^{-1}$.

It has been found that the photo actuation characteristic times follow the kinetic of photoconversion along the film with linear correlation at least for the Visible case. Indeed, both displacement and absorbance tracking profile follow a simple mono exponential characteristic time that represents the progression of the photoreversion reaction along the thickness of the system and variation of the movement with respect to the exposure time. Reversely, the photocyclization step is more complicated due to a double-exponential trend which is explained according different hypothesis: i) a screening effect due to the first photoconverted layers of CF that absorb the UV light as well, decreasing the absorption efficiency for the subsequent layers ;ii) supramolecular rearrangement between the different UPy units affecting AP/P equilibrium; iii) possible evolving photochemical pathway (branching ratio between Singlet and triplet manifold); iv) structural evolution of the

140

different fraction of crystallinity (monoclinic, orthorhombic) of the PEB domains that trapped the photochromic units. Furthermore, this structural evolution is probably related with the appearance of a white light emission (WLE) that is noticed only for UV excitation. This WLE is tentatively interpreted in term of photoenolization of the UPy units or Aggregation Induced Emission due to UPy stacking that influence the emission properties of A molecule.

To compare different system and size object, we have introduced the normalized bending velocity that take into account the power of the irradiation light (considering a full object illumination). Although our system cannot compete with the DTE crystals (those objects being limited to academic studies), we reach a same order of magnitude compared to LCE-AZOs system for UV irradiation and better performances by a factor of 10 for visible excitation.

Clearly our system mimics the DTE monocrystal photoactuator: when the thin film (A+B) receives the light, the A units acts like the trigger by controlling the progress of the OF/CF gradient while the elastomeric matrix propagate the photomechanical effect to macroscopic scale. By the way, the key structural parameter is the UPy-UPy quadruple hydrogen bonding between A and B in two ways:

a. A good and mutual hydrogen bonding network including both A and B will better propagate the PME resulting in high amplitude displacement.
b. The better the UPy network, the higher the viscoelasticity properties of the elastomeric part, the faster the response of the elastomeric matrix around the photochromic unit.

Note that even if the crystallinity fraction of the elastomer reinforces the PME to be efficiently propagated, this is not a decisive parameter. However, the crystallinity fraction is probably a crucial factor for the fatigue resistance. Indeed, after 6 cycles of UV/Vis irradiation, the part of orthorhombic fraction is increasing in favor to the monoclinic system this evolution being an additional manifestation of the dynamic

properties of the supramolecular components. In the future, we need to figure out if this is an advantage or drawback for the applications.

From a structural point of view, SEM, AFM and SAXS results indicate the films (A+B) in the CF (blue color) is defined by larger domain in the CF compared to the OF (colorless). This change of morphology in the surface or in the bulk are reversible.

Those results totally rationalize the bending toward the light under UV irradiation which is explain in term of positive expansion coefficient inside the Timoshenko bimetallic model equation which is a model apply for DTE crystal photoactuators.

Clearly, the novel photoactuator DTE-UPy/PEB-UPy paves the way for a new paradigm taking benefit of the flexibility confer by the supramolecular chemistry opening a large field for future perspectives.
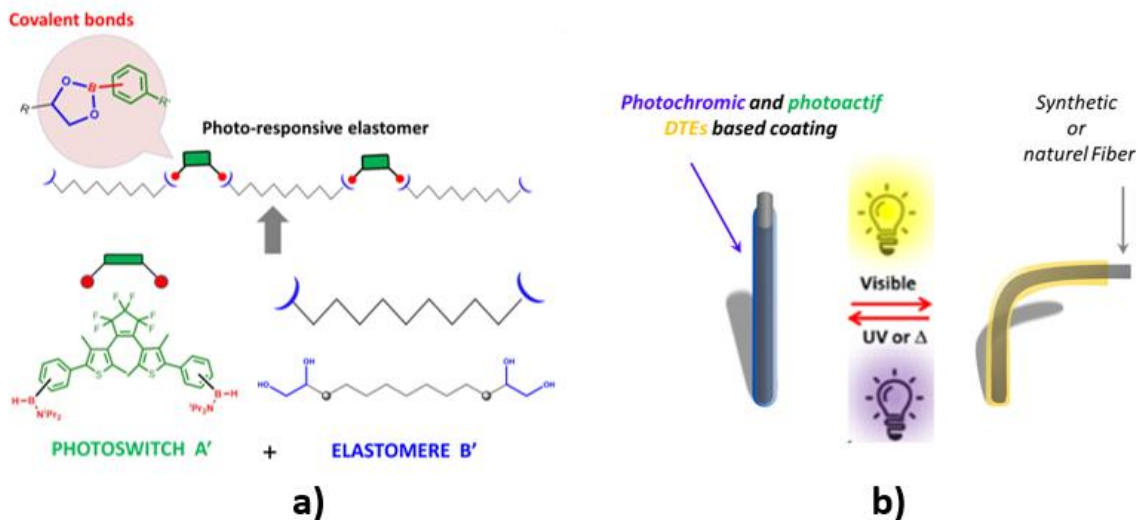
Figure 88. a) blend of DTE (photoswitch) and thermoplastic elastomer sticked through covalent bonding (aminoborane with 1,2-diol); (right) illustration of photoactuating/photochromic textile fiber.

At short term, additional experiments based on Displacement/absorbance tracking profile will be undertake with a priority for further optimization of the PME: i) shortening drastically the irradiation periods (not especially equals) with a special

142

care to return to the initial absorbance ii) increasing substantially the power using advanced Xe lamp with wheel filters. By this way, the irradiation will be at normal incidence, which will probably increase the amplitude of PME. Note that the quantum yield in the thin film will required an exact determination of the extinction coefficient.

At long term, the fields to explore are wild with the possibility to investigate other thermoplastic elastomers (Polyurethane-UPy elastomers are under investigation in our laboratories) or other fabrication protocols (confidentiality required). Besides the UPy supramolecular chemistry, we will investigate a covalent approach. It is derived from the reactivity of an aminoborane end groups containing DTE (A') with an elastomeric telechelic di-diol (Figure 88a) allowing the straightforward connection of the elastomer and the DTE subunits through boronate ligation

From an application point of view, we envision to use the system (A+B) to coat synthetic or natural fiber to get smart photoresponsive textiles (Figure 88b). Because the UPy-UPy crosslinks are still present above the melting temperature of the PEB crystals [47], we envision to adapt our supramolecular approach to 3D printer to explore the promising domain of the 4D printing [107].

References

[1]   W. A. Phillip, "Thermal-energy conversion: Under pressure," *Nat. Energy*, vol. 1, no. 7, p. 16101, Jun. 2016, doi: 10.1038/nenergy.2016.101.

[2]   M. R. Islam, X. Li, K. Smyth, and M. J. Serpe, "Polymer-Based Muscle Expansion and Contraction," *Angew. Chem. Int. Ed.*, vol. 52, no. 39, pp. 10330–10333, Sep. 2013, doi: 10.1002/anie.201303475.

[3]   C. Cheng and A. H. W. Ngan, "Reversible Electrochemical Actuation of Metallic Nanohoneycombs Induced by Pseudocapacitive Redox Processes," *ACS Nano*, vol. 9, no. 4, pp. 3984–3995, Apr. 2015, doi: 10.1021/nn507466n.

[4]   Y. Hu, Z. Li, T. Lan, and W. Chen, "Photoactuators for Direct Optical-to-Mechanical Energy Conversion: From Nanocomponent Assembly to Macroscopic Deformation," *Adv. Mater.*, vol. 28, no. 47, pp. 10548–10556, Dec. 2016, doi: 10.1002/adma.201602685.

[5]   J. Deng *et al.*, "Tunable Photothermal Actuators Based on a Pre-programmed Aligned Nanostructure," *J. Am. Chem. Soc.*, vol. 138, no. 1, pp. 225–230, Jan. 2016, doi: 10.1021/jacs.5b10131.

[6]   M. W. Urban, "Handbook of Stimuli-responsive Materials," p. 298.

[7]   P. M. Mendes, "Stimuli-responsive surfaces for bio-applications," *Chem Soc Rev*, vol. 37, no. 11, pp. 2512–2529, 2008, doi: 10.1039/B714635N.

[8]   M. Ma, L. Guo, D. G. Anderson, and R. Langer, "Bio-Inspired Polymer Composite Actuator and Generator Driven by Water Gradients," *Science*, vol. 339, no. 6116, pp. 186–189, Jan. 2013, doi: 10.1126/science.1230262.

[9]   D. Rus and M. T. Tolley, "Design, fabrication and control of soft robots," *Nature*, vol. 521, pp. 467–475, 2015.

[10]   Y. Yu, M. Nakano, and T. Ikeda, "Directed bending of a polymer film by light," *Nature*, vol. 425, no. 6954, pp. 145–145, Sep. 2003, doi: 10.1038/425145a.

[11]   K. Uchino, "Photostrictive actuators using piezoelectric materials," *Adv. Piezoelectric Mater. Sci. Technol.*, pp. 599–627, Sep. 2010, doi: 10.1533/9781845699758.3.599.

[12]   P. S. Brody, "Optomechanical bimorph actuator," *Ferroelectrics*, vol. 50, no. 1, pp. 27–32, Nov. 1983, doi: 10.1080/00150198308014428.

[13]   K. Uchino, "Micro walking machine using piezoelectric actuators," *J Rob Mech*, vol. 124, pp. 44–47, Jan. 1989.

[14]   H. M. D. Bandara and S. C. Burdette, "Photoisomerization in different classes of azobenzene," *Chem Soc Rev*, vol. 41, no. 5, pp. 1809–1825, 2012, doi: 10.1039/C1CS15179G.

[15]   F. Tong and D.-H. Qu, "Engineering Shapes and Sizes of Molecular Crystals to Achieve Versatile Photomechanical Behaviors," *Langmuir*, vol. 38, no. 16, pp. 4793–4801, Apr. 2022, doi: 10.1021/acs.langmuir.2c00414.

[16]   J. Li, X. Zhou, and Z. Liu, "Recent Advances in Photoactuators and Their Applications in Intelligent Bionic Movements," *Adv. Opt. Mater.*, vol. 8, no. 18, p. 2000886, Sep. 2020, doi: 10.1002/adom.202000886.

[17]   H. Bouas-Laurent and H. Dürr, "Organic photochromism (IUPAC Technical Report)," *Pure Appl. Chem. - PURE APPL CHEM*, vol. 73, pp. 639–665, Jan. 2001, doi: 10.1351/pac200173040639.

[18] M. Irie and D. Kungwatchakun, "Photoresponsive polymers. Mechanochemistry of polyacrylamide gels having triphenylmethane leuco derivatives," *Makromol. Chem. Rapid Commun.*, vol. 5, no. 12, pp. 829–832, Dec. 1984, doi: 10.1002/marc.1984.030051209.

[19] H. G. Heller and S. Oliver, "Photochromic heterocyclic fulgides. Part 1. Rearrangement reactions of (E)-α-3-furylethylidene(isopropylidene)succinic anhydride," *J Chem Soc Perkin Trans 1*, no. 0, pp. 197–201, 1981, doi: 10.1039/P19810000197.

[20] M. Irie, "Diarylethenes for Memories and Switches.," *Chem. Rev.*, vol. 100, no. 5, pp. 1685–1716, May 2000, doi: 10.1021/cr980069d.

[21] E. Barrez, G. Laurent, C. Pavageau, M. Sliwa, and R. Métivier, "Comparative photophysical investigation of doubly-emissive photochromic-fluorescent diarylethenes," *Phys Chem Chem Phys*, vol. 20, no. 4, pp. 2470–2479, 2018, doi: 10.1039/C7CP06541H.

[22] M. Irie, T. Lifka, S. Kobatake, and N. Kato, "Photochromism of 1,2-Bis(2-methyl-5-phenyl-3-thienyl)perfluorocyclopentene in a Single-Crystalline Phase," *J. Am. Chem. Soc.*, vol. 122, no. 20, pp. 4871–4876, May 2000, doi: 10.1021/ja993181h.

[23] I. Hamdi *et al.*, "Excited-State Dynamics of Dithienylethenes Functionalized for Self-Supramolecular Assembly," *J. Phys. Chem. A*, vol. 122, no. 14, pp. 3572–3582, Apr. 2018, doi: 10.1021/acs.jpca.7b10767.

[24] I. Hamdi *et al.*, "New insights into the photoswitching mechanisms of normal dithienylethenes," *Phys Chem Chem Phys*, vol. 18, no. 40, pp. 28091–28100, 2016, doi: 10.1039/C6CP03471C.

[25] M. Irie and M. Mohri, "Thermally irreversible photochromic systems. Reversible photocyclization of diarylethene derivatives," *J. Org. Chem.*, vol. 53, no. 4, pp. 803–808, Feb. 1988, doi: 10.1021/jo00239a022.

[26] A. Spangenberg *et al.*, "Multiscale Approach of Photochromism: Synthesis and Photochromic Properties of a Diarylethene in Solution, in Nanoparticles, and in Bulk Crystals," *Adv. Mater.*, vol. 21, pp. 309–313, Jan. 2009, doi: 10.1002/adma.200801578.

[27] G. S. HARTLEY, "The Cis-form of Azobenzene," *Nature*, vol. 140, no. 3537, pp. 281–281, Aug. 1937, doi: 10.1038/140281a0.

[28] H. Koerner, G. Price, N. A. Pearce, M. Alexander, and R. A. Vaia, "Remotely actuated polymer nanocomposites—stress-recovery of carbon-nanotube-filled thermoplastic elastomers," *Nat. Mater.*, vol. 3, no. 2, pp. 115–120, Feb. 2004, doi: 10.1038/nmat1059.

[29] M. Irie, "Photochromism of diarylethene molecules and crystals," *Proc. Jpn. Acad. Ser. B Phys. Biol. Sci.*, vol. 86, no. 5, pp. 472–483, 2010, doi: 10.2183/pjab.86.472.

[30] A. Suzuki and T. Tanaka, "Phase transition in polymer gels induced by visible light," *Nature*, vol. 346, no. 6282, pp. 345–347, Jul. 1990, doi: 10.1038/346345a0.

[31] P. Naumov *et al.*, "The Rise of the Dynamic Crystals," *J. Am. Chem. Soc.*, vol. 142, no. 31, pp. 13256–13272, Aug. 2020, doi: 10.1021/jacs.0c05440.

[32] P. Naumov, S. Chizhik, M. K. Panda, N. K. Nath, and E. Boldyreva, "Mechanically Responsive Molecular Crystals," *Chem. Rev.*, vol. 115, no. 22, pp. 12440–12490, Nov. 2015, doi: 10.1021/acs.chemrev.5b00398.

[33] T. Kim, L. Zhu, R. O. Al-Kaysi, and C. J. Bardeen, "Organic Photomechanical Materials," *ChemPhysChem*, vol. 15, no. 3, pp. 400–414, Feb. 2014, doi: 10.1002/cphc.201300906.

[34] T. Taniguchi, T. Asahi, and H. Koshima, "Photomechanical Azobenzene Crystals," *Crystals*, vol. 9, no. 9, 2019, doi: 10.3390/cryst9090437.

[35] H. G. Schild, "Poly(N-isopropylacrylamide): experiment, theory and application," *Prog. Polym. Sci.*, vol. 17, no. 2, pp. 163–249, Jan. 1992, doi: 10.1016/0079-6700(92)90023-R.

[36] F. Terao, M. Morimoto, and M. Irie, "Light-Driven Molecular-Crystal Actuators: Rapid and Reversible Bending of Rodlike Mixed Crystals of Diarylethene Derivatives," *Angew. Chem. Int. Ed.*, vol. 51, no. 4, Art. no. 4, Jan. 2012, doi: 10.1002/anie.201105585.

[37] M. Morimoto and M. Irie, "A Diarylethene Cocrystal that Converts Light into Mechanical Work," *J. Am. Chem. Soc.*, vol. 132, no. 40, pp. 14172–14178, Oct. 2010, doi: 10.1021/ja105356w.

[38] S. Kobatake, S. Takami, H. Muto, T. Ishikawa, and M. Irie, "Rapid and reversible shape changes of molecular crystals on photoirradiation," *Nature*, vol. 446, no. 7137, pp. 778–781, Apr. 2007, doi: 10.1038/nature05669.

[39] S. P. Timoshenko and J. M. Gere, *Theory of Elastic Stability*. in Dover Civil and Mechanical Engineering. Dover Publications, 2012. [Online]. Available: https://books.google.fr/books?id=98B6JOW2HiUC

[40] D. Kitagawa, R. Tanaka, and S. Kobatake, "Dependence of photoinduced bending behavior of diarylethene crystals on irradiation wavelength of ultraviolet light," *Phys Chem Chem Phys*, vol. 17, no. 41, pp. 27300–27305, 2015, doi: 10.1039/C5CP03073K.

[41] E. Merian, "Steric Factors Influencing the Dyeing of Hydrophobic. Fibers," *Text. Res. J.*, vol. 36, no. 7, pp. 612–618, Jul. 1966, doi: 10.1177/004051756603600704.

[42] F. Agolini and F. P. Gay, "Synthesis and Properties of Azoaromatic Polymers," *Macromolecules*, vol. 3, no. 3, Art. no. 3, May 1970, doi: 10.1021/ma60015a015.

[43] C. D. Eisenbach, "Isomerization of aromatic azo chromophores in poly(ethyl acrylate) networks and photomechanical effect," *Polymer*, vol. 21, no. 10, Art. no. 10, Oct. 1980, doi: 10.1016/0032-3861(80)90083-X.

[44] M. Warner and E. M. Terentjev, *Liquid Crystal Elastomers*. in International Series of Monographs on Physics. OUP Oxford, 2007. [Online]. Available: https://books.google.fr/books?id=1i18pOTiNtMC

[45] M. Takeshita, M. Hayashi, S. Kadota, K. H. Mohammed, and T. Yamato, "Photoreversible supramolecular polymer formation," *Chem. Commun.*, no. 6, p. 761, 2005, doi: 10.1039/b415114c.

[46] H. M. Keizer, R. van Kessel, R. P. Sijbesma, and E. W. Meijer, "Scale-up of the synthesis of ureidopyrimidinone functionalized telechelic poly(ethylenebutylene)," *Polymer*, vol. 44, no. 19, pp. 5505–5511, Sep. 2003, doi: 10.1016/S0032-3861(03)00631-1.

[47] M. Louati *et al.*, "In-situ SAXS/WAXS investigations of ureidopyrimidinone functionalized semi-crystalline poly(ethylene-co-butylene) supramolecular polymers," *Polymer*, vol. 228, p. 123875, Jul. 2021, doi: 10.1016/j.polymer.2021.123875.

[48] R. P. Sijbesma and E. W. Meijer, "Quadruple hydrogen bonded systems," *Chem. Commun.*, no. 1, pp. 5–16, Dec. 2003, doi: 10.1039/b205873c.

[49] W. KUHN, B. HARGITAY, A. KATCHALSKY, and H. EISENBERG, "Reversible Dilation and Contraction by Changing the State of Ionization of High-Polymer Acid Networks," *Nature*, vol. 165, no. 4196, pp. 514–516, Apr. 1950, doi: 10.1038/165514a0.

[50] M. Yamada *et al.*, "Photomobile Polymer Materials: Towards Light-Driven Plastic Motors," *Angew. Chem. Int. Ed.*, vol. 47, no. 27, pp. 4986–4988, Jun. 2008, doi: 10.1002/anie.200800760.

[51] T. Ube, R. Nakayama, and T. Ikeda, "Photoinduced Motions of Thermoplastic Polyurethanes Containing Azobenzene Moieties in Main Chains," *Macromolecules*, vol. 55, no. 2, pp. 413–420, Jan. 2022, doi: 10.1021/acs.macromol.1c01827.

[52] T. Ikeda, M. Nakano, Y. Yu, O. Tsutsumi, and A. Kanazawa, "Anisotropic Bending and Unbending Behavior of Azobenzene Liquid-Crystalline Gels by Light Exposure," *Adv. Mater.*, vol. 15, no. 3, pp. 201–205, Feb. 2003, doi: 10.1002/adma.200390045.

[53] M. Lahikainen, K. Kuntze, H. Zeng, S. Helantera, S. Hecht, and A. Priimagi, "Tunable Photomechanics in Diarylethene-Driven Liquid Crystal Network Actuators," *ACS Appl. Mater. Interfaces*, vol. 12, no. 42, pp. 47939–47947, Oct. 2020, doi: 10.1021/acsami.0c12735.

[54] T. S. Hebner, M. Podgórski, S. Mavila, T. J. White, and C. N. Bowman, "Shape Permanence in Diarylethene-Functionalized Liquid-Crystal Elastomers Facilitated by Thiol-Anhydride Dynamic Chemistry," *Angew. Chem. Int. Ed.*, vol. 61, no. 11, p. e202116522, 2022, doi: 10.1002/anie.202116522.

[55] R. P. Sijbesma *et al.*, "Reversible Polymers Formed from Self-Complementary Monomers Using Quadruple Hydrogen Bonding," *Science*, vol. 278, no. 5343, pp. 1601–1604, Nov. 1997, doi: 10.1126/science.278.5343.1601.

[56] J. Liao, M. Yang, Z. Liu, and H. Zhang, "Fast photoinduced deformation of hydrogen-bonded supramolecular polymers containing α-cyanostilbene derivative," *J Mater Chem A*, vol. 7, no. 5, pp. 2002–2008, 2019, doi: 10.1039/C8TA12030G.

[57] J. Chen *et al.*, "Artificial muscle-like function from hierarchical supramolecular assembly of photoresponsive molecular motors," *Nat. Chem.*, vol. 10, no. 2, pp. 132–138, Feb. 2018, doi: 10.1038/nchem.2887.

[58] S. H. M. Söntjens, R. P. Sijbesma, M. H. P. van Genderen, and E. W. Meijer, "Stability and Lifetime of Quadruply Hydrogen Bonded 2-Ureido-4[1 *H*]-pyrimidinone Dimers," *J. Am. Chem. Soc.*, vol. 122, no. 31, pp. 7487–7493, Aug. 2000, doi: 10.1021/ja000435m.

[59] D. K. Hohl, S. Balog, C. Cappelletti, F. Karasu, and C. Weder, "Crystallizable Supramolecular Polymers: Binding Motif and Processing Matter," *Macromolecules*, vol. 53, no. 20, pp. 9086–9096, Oct. 2020, doi: 10.1021/acs.macromol.0c00868.

[60] C. A. Sierra and C. Gal, "Thermal and mechanical properties of poly-(styrene-6-ethylene-co-butylene-6-styrene) triblock copolymers," p. 11.

[61] M. Takeshita, M. Hayashi, and T. Miyazaki, "A Fully Photoreversible Supramolecular Polymer Having a Diarylethene Photoswitch," *Chem. Lett.*, vol. 39, no. 2, pp. 82–83, Feb. 2010, doi: 10.1246/cl.2010.82.

[62] L. Le Bras *et al.*, "Understanding the properties of dithienylethenes functionalized for supramolecular self-assembly: a molecular modeling study," *Phys Chem Chem Phys*, vol. 22, no. 13, pp. 6942–6952, 2020, doi: 10.1039/C9CP06590C.

[63] M. Louati, "Etude multi-échelle de films minces photomécaniques basés sur l'assemblage supramoléculaire de photochromes bistables et d'élastomère thermoplastique," PhD Thesis, 2019. [Online]. Available: http://www.theses.fr/2019LILUR050/document

[64] R. F. Egerton, *Physical Principles of Electron Microscopy: An Introduction to TEM, SEM, and AEM*. Springer International Publishing, 2016. [Online]. Available: https://books.google.fr/books?id=HhWfDAAAQBAJ

[65] B. J. B. Folmer, R. P. Sijbesma, R. M. Versteegen, J. A. J. van der Rijt, and E. W. Meijer, "Supramolecular Polymer Materials: Chain Extension of Telechelic Polymers Using a Reactive Hydrogen-Bonding Synthon," *Adv. Mater.*, vol. 12, no. 12, pp. 874–878, Jun. 2000, doi: 10.1002/1521-4095(200006)12:12<874::AID-ADMA874>3.0.CO;2-C.

[66] J. C. Crano and R. J. Guglielmetti, *Organic Photochromic and Thermochromic Compounds*, vol. 1,2. New York: Plenum, 1999.

[67] M. Maafi and R. G. Brown, "Photophysics and kinetics of naphthopyran derivatives, part 1: General analytical solutions for the kinetics of AB(k,ϕ) and ABC(k,ϕ) systems," *Int. J. Chem. Kinet.*, vol. 37, no. 3, pp. 162–174, Mar. 2005, doi: 10.1002/kin.20061.

[68] M. Maafi, "The potential of AB(1Φ) systems for direct actinometry. Diarylethenes as successful actinometers for the visible range," *Phys Chem Chem Phys*, vol. 12, no. 40, pp. 13248–13254, 2010, doi: 10.1039/C0CP00469C.

[69] G. S. Kumar and D. C. Neckers, "Photochemistry of azobenzene-containing polymers," *Chem. Rev.*, vol. 89, no. 8, pp. 1915–1925, Dec. 1989, doi: 10.1021/cr00098a012.

[70] S. Caron, R. A. Lessard, and P. C. Roberge, "Photodarkening and partial photobleaching: application to dichromated gelatin," *Appl Opt*, vol. 40, no. 5, pp. 707–713, Feb. 2001, doi: 10.1364/AO.40.000707.

[71] A. R. Santos, R. Ballardini, P. Belser, M. T. Gandolfi, V. M. Iyer, and L. Moggi, "Photochemical investigation of a photochromic diarylethene compound that can be used as a wide range actinometer," *Photochem Photobiol Sci*, vol. 8, no. 12, pp. 1734–1742, 2009, doi: 10.1039/B9PP00037B.

[72] G. Pariani, A. Bianco, R. Castagna, and C. Bertarelli, "Kinetics of Photochromic Conversion at the Solid State: Quantum Yield of Dithienylethene-Based Films," *J. Phys. Chem. A*, vol. 115, no. 44, pp. 12184–12193, Nov. 2011, doi: 10.1021/jp207210p.

[73] V. M. Breslin and M. A. Garcia-Garibay, "Transmission Spectroscopy and Kinetics in Crystalline Solids Using Aqueous Nanocrystalline Suspensions: The Spiropyran-Merocyanine Photochromic System," *Cryst. Growth Des.*, vol. 17, no. 2, pp. 637–642, Feb. 2017, doi: 10.1021/acs.cgd.6b01476.

[74] K. Kelm, "C. Capellos and B. H. J. Bielski: Kinetic Systems: Mathematical Description of Chemical Kinetics in Solution. Wiley-Interscience, New York, London, Sidney, Toronto 1972, 138 Seiten, Preis: £ 5,00," *Berichte Bunsenges. Für Phys. Chem.*, vol. 77, no. 6, pp. 470–470, Jun. 1973, doi: 10.1002/bbpc.19730770618.

[75] B. B. Mollet *et al.*, "The effect of irradiation by ultraviolet light on ureido-pyrimidinone based biomaterials," *J. Polym. Sci. Part Polym. Chem.*, vol. 54, no. 1, pp. 81–90, Jan. 2016, doi: 10.1002/pola.27887.

[76] H. Dong, M. Luo, S. Wang, and X. Ma, "Synthesis and properties of tetraphenylethylene derivatived diarylethene with photochromism and aggregation-induced emission," *Dyes Pigments*, vol. 139, pp. 118–128, Apr. 2017, doi: 10.1016/j.dyepig.2016.11.054.

[77] T. Zhang, R. Zhang, Z. Zhang, and Z. Ni, "A series of tetraphenylethene-based benzimidazoles: syntheses, structures, aggregation-induced emission and reversible mechanochromism," *RSC Adv*, vol. 6, no. 83, pp. 79871–79878, 2016, doi: 10.1039/C6RA16514A.

[78] M. M. L. Nieuwenhuizen *et al.*, "Self-Assembly of Ureido-Pyrimidinone Dimers into One-Dimensional Stacks by Lateral Hydrogen Bonding," *Chem. – Eur. J.*, vol. 16, no. 5, pp. 1601–1612, Feb. 2010, doi: 10.1002/chem.200902107.

[79] S. Ahn, T. H. Ware, K. M. Lee, V. P. Tondiglia, and T. J. White, "Photoinduced Topographical Feature Development in Blueprinted Azobenzene-Functionalized Liquid Crystalline Elastomers," *Adv. Funct. Mater.*, vol. 26, no. 32, pp. 5819–5826, Aug. 2016, doi: 10.1002/adfm.201601090.

[80] D. Kitagawa, R. Tanaka, and S. Kobatake, "Photoinduced stepwise bending behavior of photochromic diarylethene crystals," *CrystEngComm*, vol. 18, no. 38, pp. 7236–7240, 2016, doi: 10.1039/C6CE00607H.

[81] T. J. White, *Photomechanical Materials, Composites, and Systems: Wireless Transduction of Light into Work*. Wiley, 2017. [Online]. Available: https://books.google.fr/books?id=nBknDwAAQBAJ

[82] D. Kitagawa, K. Kawasaki, R. Tanaka, and S. Kobatake, "in situ eaction and Reversible Single-Crystal-to-Single-Crystal Phase Transition," *Chem. Mater.*, vol. 29, no. 17, pp. 7524–7532, Sep. 2017, doi: 10.1021/acs.chemmater.7b02558.

[83] M. Irie, "Photochromism of diarylethene single molecules and single crystals," *Photochem. Photobiol. Sci.*, vol. 9, no. 12, pp. 1535–1542, Dec. 2010, doi: 10.1039/c0pp00251h.

[84] P. K. Patel *et al.*, "Visible light-triggered fluorescence and pH modulation using metastable-state photoacids and BODIPY," *Phys Chem Chem Phys*, vol. 20, no. 42, pp. 26804–26808, 2018, doi: 10.1039/C8CP03977A.

[85] L. Kan *et al.*, "Microphase separation of a quadruple hydrogen bonding supramolecular polymer: effect of the steric hindrance of the ureido-pyrimidone on their viscoelasticity," *RSC Adv.*, vol. 9, no. 16, pp. 8905–8911, 2019, doi: 10.1039/C8RA08861F.

[86] D. Kitagawa, C. Iwaihara, H. Nishi, and S. Kobatake, "Quantitative Evaluation of Photoinduced Bending Speed of Diarylethene Crystals," *Crystals*, vol. 5, no. 4, pp. 551–561, 2015, doi: 10.3390/cryst5040551.

[87] D. Kitagawa, H. Tsujioka, F. Tong, X. Dong, C. J. Bardeen, and S. Kobatake, "Control of Photomechanical Crystal Twisting by Illumination Direction," *J. Am. Chem. Soc.*, vol. 140, no. 12, pp. 4208–4212, Mar. 2018, doi: 10.1021/jacs.7b13605.

[88] A. Hirano, D. Kitagawa, and S. Kobatake, "Photomechanical bending behavior of photochromic diarylethene crystals induced under polarized light," *CrystEngComm*, vol. 21, no. 15, pp. 2495–2501, 2019, doi: 10.1039/C9CE00175A.

[89] S. Ohshima, M. Morimoto, and M. Irie, "Light-driven bending of diarylethene mixed crystals," *Chem Sci*, vol. 6, no. 10, pp. 5746–5752, 2015, doi: 10.1039/C5SC01994J.

[90] X. Dong, T. Guo, D. Kitagawa, S. Kobatake, P. Palffy-Muhoray, and C. J. Bardeen, "Performance of Composite Glass–Diarylethene Crystal Photomechanical Actuator Membranes," *ACS Appl. Mater. Interfaces*, vol. 14, no. 23, pp. 27149–27156, Jun. 2022, doi: 10.1021/acsami.2c04112.

[91] M. Morimoto and M. Irie, "A Diarylethene Cocrystal that Converts Light into Mechanical Work," *J. Am. Chem. Soc.*, vol. 132, no. 40, pp. 14172–14178, Oct. 2010, doi: 10.1021/ja105356w.

[92] C. Hilger and R. Stadler, "Cooperative structure formation by directed noncovalent interactions in an unpolar polymer matrix. 7. Differential scanning calorimetry and small-angle x-ray scattering," *Macromolecules*, vol. 25, no. 24, pp. 6670–6680, Nov. 1992, doi: 10.1021/ma00050a042.

[93] C. Hilger and R. Stadler, "New multiphase architecture from statistical copolymers by cooperative hydrogen bond formation," *Macromolecules*, vol. 23, no. 7, pp. 2095–2097, Apr. 1990, doi: 10.1021/ma00209a037.

[94] J. C. Wittmann and B. Lotz, "Epitaxial crystallization of monoclinic and orthorhombic polyethylene phases," *Polymer*, vol. 30, no. 1, pp. 27–34, Jan. 1989, doi: 10.1016/0032-3861(89)90378-9.

[95] L. Fontana *et al.*, "High-pressure crystalline polyethylene studied by x-ray diffraction and ab initio simulations," *Phys Rev B*, vol. 75, no. 17, p. 174112, May 2007, doi: 10.1103/PhysRevB.75.174112.

[96] V. F. Holland, "Dislocations in Polyethylene Single Crystals," *J. Appl. Phys.*, vol. 35, no. 11, pp. 3235–3241, Nov. 1964, doi: 10.1063/1.1713204.

[97] W. P. J. Appel, G. Portale, E. Wisse, P. Y. W. Dankers, and E. W. Meijer, "Aggregation of Ureido-Pyrimidinone Supramolecular Thermoplastic Elastomers into Nanofibers: A Kinetic Analysis," *Macromolecules*, vol. 44, no. 17, pp. 6776–6784, Sep. 2011, doi: 10.1021/ma201303s.

[98] R. A. Koevoets, R. M. Versteegen, H. Kooijman, A. L. Spek, R. P. Sijbesma, and E. W. Meijer, "Molecular Recognition in a Thermoplastic Elastomer," *J. Am. Chem. Soc.*, vol. 127, no. 9, pp. 2999–3003, Mar. 2005, doi: 10.1021/ja0451160.

[99] T. Seto, T. Hara, and K. Tanaka, "Phase Transformation and Deformation Processes in Oriented Polyethylene," *Jpn. J. Appl. Phys.*, vol. 7, no. 1, p. 31, Jan. 1968, doi: 10.1143/JJAP.7.31.

[100] Y. Takahashi, T. Ishida, and M. Furusaka, "Monoclinic-to-orthorhombic transformation in polyethylene," *J. Polym. Sci. Part B Polym. Phys.*, vol. 26, no. 11, pp. 2267–2277, Oct. 1988, doi: 10.1002/polb.1988.090261107.

[101] K. E. Russell, B. K. Hunter, and R. D. Heyding, "Monoclinic polyethylene revisited," p. 6.

[102] J.-L. Wietor, D. J. M. van Beek, G. W. Peters, E. Mendes, and R. P. Sijbesma, "Effects of Branching and Crystallization on Rheology of Polycaprolactone Supramolecular Polymers with Ureidopyrimidinone End Groups," *Macromolecules*, vol. 44, no. 5, pp. 1211–1219, Mar. 2011, doi: 10.1021/ma1026065.

[103] G. Beaucage and D. W. Schaefer, "Structural studies of complex systems using small-angle scattering: a unified Guinier/power-law approach," *Proc. Second Internatinal Discuss. Meet. Relax. Complex Syst.*, vol. 172–174, pp. 797–805, Sep. 1994, doi: 10.1016/0022-3093(94)90581-9.

[104] I. W. Hamley, *Small-Angle Scattering: Theory, Instrumentation, Data, and Applications*. Wiley, 2021. [Online]. Available: https://books.google.fr/books?id=L9ktEAAAQBAJ

[105] E. Rieloff and M. Skepö, "Determining Rg of IDPs from SAXS Data," in *Intrinsically Disordered Proteins: Methods and Protocols*, B. B. Kragelund and K. Skriver, Eds., New York, NY: Springer US, 2020, pp. 271–283. doi: 10.1007/978-1-0716-0524-0_13.

[106] Guinier, André, "La diffraction des rayons X aux très petits angles : application à l'étude de phénomènes ultramicroscopiques," *Ann Phys*, vol. 11, no. 12, pp. 161–237, 1939, doi: 10.1051/anphys/193911120161.

[107] L. Ceamanos, Z. Kahveci, M. López-Valdeolivas, D. Liu, D. J. Broer, and C. Sánchez-Somolinos, "Four-Dimensional Printed Liquid Crystalline Elastomer Actuators with Fast Photoinduced Mechanical Response toward Light-Driven Robotic Functions," *ACS Appl. Mater. Interfaces*, vol. 12, no. 39, pp. 44195–44204, Sep. 2020, doi: 10.1021/acsami.0c13341.